

Identification and Adaptive Control of a Coordinate Measuring Machine

Examensarbete utfört i Reglerteknik
vid Tekniska Högskolan i Linköping
av

Ulf Pettersson

Reg nr: LiTH-ISY-EX-3491
Linköping 2004

Identification and Adaptive Control of a Coordinate Measuring Machine

Examensarbete utfört i Reglerteknik
vid Tekniska Högskolan i Linköping
av

Ulf Pettersson

Reg nr: LiTH-ISY-EX-3491

Supervisor: **Paul Anderson**
Thomas Schön

Examiner: **Svante Gunnarsson**

Linköping 13th April 2004.

Abstract

Important factors in manufacturing are quality and cost. Measuring machines play an important role for these fields. In order to meet higher demands on cost and accuracy, measuring machines can be constructed with weaker materials and increased mechanical flexibilities, and therefore there is a need to include the flexibilities in measuring machine models to obtain good performance.

The core theme in this thesis is modeling and identification of the physical parameters of drive mechanisms of a Brown & Sharpe Inc. Global A coordinate measuring machine. The approximation made is that the drive mechanisms can be described by a mass connected by springs, dampers and gear changes. It has been found that a one-spring model gives a reasonably good description of the studied CMM drive mechanism. The physical parameters of this model are identified using off-line algorithms. The algorithms are based on prediction error methods. For the off-line identification the MATLAB™ System Identification Toolbox and the bond graph representation is used.

The chosen model is then used for control. Traditional control and a Model-reference Adaptive System is derived and studied with the aim to increase the damping of CMM drive mechanisms. It is found that the adaptive system has very good disturbance rejection and can correct for drastic model errors. Another impact is that the damping of the studied drive mechanism can be increased with at least a factor of nine.

Keywords: CMM, physical modeling, bond graphs, identification, MRAS, adaptive control.

Acknowledgments

First of all I would like to thank my supervisor Paul Anderson R&D manager at Brown & Sharpe Inc. for encouraging me to complete my thesis. The work in this thesis would not have been possible without the support from Brown & Sharpe Inc.

I would also like to thank my examiner Professor Svante Gunnarsson for his guidance and my co-supervisor Thomas Schön for all your help.

Furhermore, of my colleges at Brown & Sharpe Inc. I would like to thank Barry Epstein for helping me when research was going slow. Especially I would like to thank Gary W. Russell R&D manager of electronics and Abraham Shapiro for all the discussions and questions you have to put up with. They have also given me valuable help from reading early versions of the thesis. I would like to thank Paul Witkos for helping me set up all the hardware and Brian Delphino for supporting me with CAD-drawings. Then also Dr. Wim Weekers for your support, good advice and for teaching me the basics in metrology.

Finally I would like to thank my family and my girlfriend for all the help and support.

Notation

Physical Model Symbols

r_1, r_2, r_3, r_4	Radii of pulley \mathcal{A} , \mathcal{B} , \mathcal{C} and \mathcal{D} .
$\mathcal{A}, \mathcal{B}, \mathcal{C}, \mathcal{D}$	Pulley drive mechanism.
\mathcal{E}	Bridge.
θ	Motor shaft angle.
θ_1	Motor shaft angle at pulley \mathcal{A} .
ω	Angular velocity of the motor shaft.
$\omega_1, \omega_2, \omega_3$	Angular velocity of pulley \mathcal{A} , \mathcal{B} and \mathcal{C} .
r_1, r_2, r_3	Radii of pulley \mathcal{A} , \mathcal{B} and \mathcal{C} .
k, k_1, k_2, k_3	Spring constants.
d, d_1, d_2, d_3	Damping coefficients in the springs.
F_1, F_2, F_3	Belt tension at pulley \mathcal{A} , \mathcal{B} and \mathcal{C} .
F_k	Force generated by spring k .
$F_{k_1}, F_{k_2}, F_{k_3}$	Force generated by spring k_1 , k_2 and k_3 .
F_d	Force generated by damper d .
$F_{d_1}, F_{d_2}, F_{d_3}$	Force generated by damper d_1 , d_2 and d_3 .
F_m	Force generated by the inertia m .
F_ϕ	Frictional sliding force. Section 3.3.1.
$F_{\phi+d_3}$	Frictional sliding force. Section 3.3.2.
F_m	Force generated by m .
v_1, v_2, v_3	Velocity for pulley \mathcal{A} , \mathcal{B} and \mathcal{C} .
v, v_4	Velocity bridge.
y_b	Position bridge.
$Y_b(s)$	Laplace transformed bridge position.
m	Mass of bridge.
ϕ	Sliding friction bridge.
T_1	Torque generated electrical motor at pulley \mathcal{A} .
$G_{\theta_1 y_b}(s)$	Transfer function from θ_1 to y_b .

Bond Graph Symbols

s	s-junction.
p	p-junction.
e	Effort.
f	Flow.
C	C-element.
I	I-element.
R	R-element.
S_e	Effort source.
S_f	Flow source.
TF	Transformer-element.
GY	Gyrator-element.

Control Symbols

$r(t), u_c(t)$	Reference signal or command signal.
$y(t)$	Output signal.
Φ	Parameter vector for the MRAS.
ζ_1	Desired damping of the DC motor system.
ζ_2	Desired damping of the total system.
$G_{i_a, \theta}(s)$	Transfer function for the DC motor.
$G_{\theta, y_b}(s)$	Transfer function for the drive mechanism.
θ	Motor shaft angle.
ω	Angular velocity of the DC motor.
ω_1	Desired bandwidth of the DC motor system.
ω_2	Desired bandwidth of the total system.
y_b	Bridge position.
\dot{y}_b	Bridge velocity.
y_m	Desired bridge position.
\dot{y}_m	Desired bridge velocity.
$G_{c_1}(s)$	Transfer function, closed-loop system of the DC motor.
$G_{c_{tot}}(s)$	Closed-loop transfer function for the total system.
$G_0(s)$	Transfer function used with the Nyquist criterion.
$V(e, \theta)$	Quadratic function.
K_1, K_2	Observer gains for motor and total system respectively.
L_1, L_2	Feedback gains for motor and total system respectively.
S	Sensitivity function.
T	Complementary sensitivity function.
n, n_{tot}	Measurement noise for motor and total system respectively.
w, w_{tot}	Process noise for motor and total system respectively.
$w_u, w_{u_{tot}}$	Noise affecting input u for motor and total system respectively.

Identification Symbols

$\epsilon(t)$	Prediction error $y(t) - \hat{y}(t, \theta)$.
$\hat{\epsilon}_N(t)$	Residuals associated with model θ_N .
$e(t)$	Noise variable.
$G(q, \theta)$	Model of the system parameterized by θ .
$H(q, \theta)$	Noise model parameterized by θ .
λ_0	Variance of the noise.
$\hat{\sigma}_i(t)$	Estimated standard deviation of the i th parameter.
N	Vector containing polynomial orders for an ARX model.
n_a	Number of poles in an ARX model.
n_b	Number of zeros in an ARX model.
n_k	Time delay of input to an ARX model.
$u(t)$	The input to the system.
$V_N(\theta)$	Loss function or criterion function.
$\hat{y}(t, \theta)$	One-step-ahead predictor.
$\hat{\theta}_N$	Value that minimizes $V_N(\theta)$ with LSE.
R_y^2	Multiple correlation coefficient.
ω_p	Frequency peak of estimated black-box models.
ζ	Identified damping of drive mechanism.
s_1, s_2, s_3, s_4	Zeros and poles of estimated drive mechanism.
$G_{arx2}(s)$	Transfer function of estimated drive mechanism.
$\hat{G}(s)$	Approximation of $G_{arx2}(s)$.
k	Identified spring constant of drive mechanism.
d	Identified damping constant of drive mechanism.

Operators and Functions

q^{-1} Delay operator, $q^{-1}u(t) = u(t - 1)$.

Abbreviations

akf	Auto correlation function.
ARX	AutoRegressive with eXternal input.
ARMA	AutoRegressive Moving Average.
ARMAX	AutoRegressive Moving Average with eXternal input.
BJ	Box-Jenkins.
CMM	Coordinate Measuring Machine.
DC	Direct Current.
DFT	Discrete Fourier Transform.
FIR	Finite Impulse Response.
FFT	Fast Fourier Transform.
FPE	Forward Prediction Error.
IDFT	Inverse Discrete Fourier Transform.
LSE	Least Squares Estimation.
MRAS	Model-Reference Adaptive System.
OE	Output Error.
PID	Proportional Integral Derivative.
SITB	MATLAB [™] System Identification ToolBox, (Ljung, 2000).

Contents

1	Introduction	1
1.1	Background	2
1.2	Problem Description	2
1.3	Contributions	2
1.4	Thesis Outline	3
2	Coordinate Measuring Machine	5
2.1	Understanding the CMM	5
2.2	The CMM System	6
2.3	The Mechanical Structure	7
2.4	The Y-axis Drive Mechanism	8
2.5	The Controller, B3C-LC	11
2.6	The Controller Software	13
2.7	The Control System	14
3	Physical Modeling	15
3.1	Modeling with Bond Graphs	15
3.1.1	Junctions	16
3.1.2	Buffers and Dissipators	18
3.1.3	Sources	18
3.1.4	Transformers and Gytrators	19
3.2	Modeling a Simple Mechanical System	19
3.3	Modeling the Drive Mechanism of the Y-axis	20
3.3.1	One-spring Model	21
3.3.2	Three-spring Model	23
4	Identification Methods	27
4.1	Model Structures	27
4.2	Forming the Predictor	28
4.3	Linear Regression	29
4.4	Residuals and Prediction Errors	29
4.5	Loss Function $V_N(\theta)$	30
4.6	Computing the Estimate $\hat{\theta}_N$	30

4.7	Variance Error	31
4.8	Summary	32
5	Off-line Identification	33
5.1	Data Collection and Pre-processing	33
5.1.1	Data Collection	33
5.1.2	Choice of Input Signal	34
5.1.3	Model and Validation Data	34
5.1.4	Identification of False Frequencies	35
5.2	Estimated Black-box Models	36
5.3	Validation	40
5.4	Identified Parameters	40
5.5	Summary	41
6	Model Reference Adaptive Systems (MRAS)	49
6.1	Introduction	49
6.2	Lyapunov Theory	49
6.2.1	Lyapunov Theory for Time-invariant Systems	50
6.2.2	Finding Lyapunov Functions	51
6.2.3	Lyapunov Theory for Time-variable Systems	52
6.2.4	State Feedback	56
6.2.5	Advantages with Lyapunov Stability Theory	58
6.3	Summary	58
7	Adaptive Control	59
7.1	System Description	59
7.1.1	DC Motor System	60
7.1.2	The Total System	60
7.2	Control of the DC Motor	60
7.3	Control of the Total System	63
7.3.1	Process Observer	67
7.4	Simulations	69
7.4.1	Simulation of the DC Motor System	69
7.4.2	Simulation of the Total System	69
7.5	Stability of the Closed-loop System	70
7.5.1	Closed-loop System of the DC Motor	71
7.5.2	Total Closed-loop System	71
7.6	Sensitivity and Robustness	72
7.6.1	Sensitivity	73
7.6.2	Robustness	73
7.7	Summary	79
8	Conclusions	83
8.1	Summary	83
8.2	Further Work	85

A Physical Models	89
A.1 One-spring Model	89
A.2 Three-spring Model	91

Chapter 1

Introduction

During the last decades measuring robots or measuring machines have become a very important tool to evaluate and monitor the quality of processes. Whenever there is a need for high precision measurement of industrial workpieces measuring machines play an important role. Measuring machines are today used in (for instance) the aviation and the machine-tool industry. However, measuring machines are applied to new areas each year. To be able to go into new markets the measuring machines often require better performance or lower price. A solution to meet these demands is to construct the measuring machines with lighter and weaker materials. Therefore the demands on good control of dynamic structures and accurate models used in the controllers are growing. As real processes are time-varying there is also a need for adaptive control, typically drive mechanisms change their characteristics in measuring machines.

This thesis focus on identification and adaptive control of drive mechanisms in measuring machines. A fundamental property in measuring machine control is that the amount of sensors is limited. It is common practise in control of these drive mechanisms to measure speed of electrical motors and position of the dominating inertia. This thesis presents another approach, to measure position of motors and position of inertia. Still, since the structures are non-rigid, there is a need for accurate models and good control to compensate for the flexibilities in the drive mechanisms. A cornerstone is the building of physical and black-box models that can be used in adaptive control of measuring machines.

In the experiments in this thesis a bridge Coordinate Measuring Machine, Global A, from Brown & Sharpe Inc. is used. Brown & Sharpe Inc. has a long tradition in metrology and has been pioneers many times with new inventions. Founded in the mid 1800s the company has developed and manufactured different kinds of products from classical micrometers to guns. Today their focus is primarily coordinate measuring machines. The facility is located in North Kingstown, Rhode Island, USA.

1.1 Background

In order to obtain good performance and high precision results of a measuring machine, the vibrations in moving machine parts must be minimized. Thus damping of drive mechanisms is very critical to the system. It was common practice in older systems to increase the position loop gain to achieve some limited improvement in position accuracy. This usually resulted in machine instability due to inadequate drive stiffness or the nonlinear effects of gear backlash. Over time these deficiencies ultimately resulted in degraded performance because of excessive wear in the gear mechanisms or because of motor burn-out.

1.2 Problem Description

The goal is to:

- Develop a digital servo loop to increase position damping of the CMM drive mechanisms.
- Use a rotary encoder to obtain position and velocity feedback of the motor shaft.
- The implementation should be an improvement to the existing tachometer feedback, which only provides velocity feedback.
- Determine the transfer function from the motor shaft angle to linear position of the bridge with use of the outputs from the rotary and linear encoder readings.
- Develop a Model-Reference Adaptive System (MRAS) to control the drive mechanism.

1.3 Contributions

The main contributions of the thesis are the following:

- The derived rigid and flexible physical models of the CMM drive mechanisms in Chapter 3 with use of the bond graph representation.
- Identification of false frequencies in the CMM drive mechanisms in Chapter 5 to decrease model order.
- Identification of the drive mechanism of the Y-axis for the CMM with black-box models in Chapter 5.
- The off-line physical parameter identification applied to the physical models and the estimated black-box models of the CMM in Chapter 5.
- Adaptive control with Lyapunov stability theory of CMM drive mechanisms with a Model-Reference Adaptive System in Chapter 7.

1.4 Thesis Outline

The thesis is organized as follows:

Chapter 2, introduces the Coordinate Measuring Machine. It is explained why position damping is important for CMM drive mechanisms. The controller and its software are discussed.

Chapter 3 introduces the concept of physical modeling with bond graphs. A simple example is given and two physical models are derived for CMM drive mechanisms.

In Chapter 4 a short introduction to system identification using the prediction error methods is given.

The identification, using prediction error methods, of CMM drive mechanisms from real data is shown in Chapter 5, both for physical models and for black-box models.

Chapter 6 introduces the concept of Model-Reference Adaptive Systems. It is found that Lyapunov stability theory can be used to construct the MRAS.

In chapter 7, traditional and adaptive control is applied to the CMM drive mechanisms. An MRAS based upon Lyapunov stability theory is derived. Stability and robustness analysis is carried out thoroughly for the derived controllers.

Finally in Chapter 8 some conclusions and pointers to future work are given.

Chapter 2

Coordinate Measuring Machine

What is a bridge Coordinate Measuring Machine (CMM)? Essentially it is a robot which measures the geometry of parts of almost any shape to high precision. During measurements, machine axes are moving with the use of drive mechanisms. In order to obtain good performance and high precision results, vibrations in moving machine axes must be minimized. Thus damping of drive mechanisms is very critical to the system. This chapters presents details of an existing CMM, its machine parts and their purpose.

2.1 Understanding the CMM

A Cartesian coordinate system is used to describe the movements of the measuring machine. The coordinate system allows for location of features relative to other features on workpieces. A coordinate system is a lot like a street map with buildings, see Figure 2.1.

To walk to the apartment on the second floor in the house from the subway station, a person can walk two blocks along 1st Ave, three blocks on 3rd Street and up one floor in the house. This location can also be described by the coordinates 4-D-2 on the map, corresponding to the X, Y and Z axes of the machine. These coordinates describe the apartment location.

A coordinate measuring machine works in much the same way as ones finger when it traces map coordinates; its three axes from the machine's coordinate system. Instead of a finger, the CMM uses a probe to measure points on a workpiece, see Figure 2.2. Each point on the workpiece is unique with respect to the machine's coordinate system. The CMM combines the measured points to form a feature that can be related to all other features.

There are two types of coordinate systems for a CMM. The first is called the *Machine Coordinate System*. In Figure 2.3, the X, Y and Z-axes refer to the

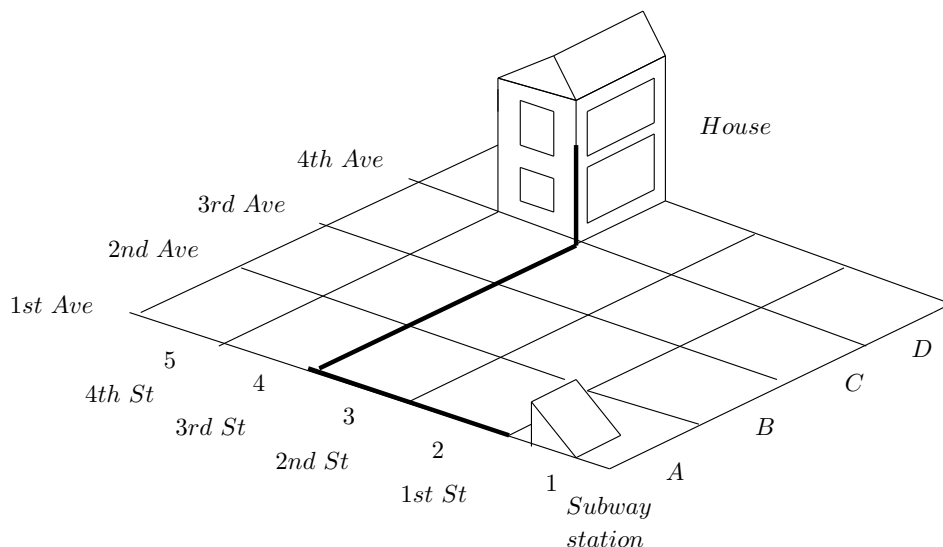


Figure 2.1. The idea of a coordinate system in a coordinate measuring machine. The coordinate system can be interpreted as a street map with unique positions.

machine's motions. When viewed from the front of the machine, the X-axis runs from left to right, the Y-axis runs from front to back, and the Z-axis runs up and down, vertically perpendicular to the other two.

The second coordinate system is called the *Part Coordinate System* where the three axes x , y and z relate to the features of the workpiece.

2.2 The CMM System

The CMM system consists of a controller cabinet, a jog-box, a PC and the mechanical structure. In the cabinet there are driver units for the electrical motors and the computers used for the control. See Figure 2.4 for a picture of the controller, B3C-LC. The cabinet also contains connections to the environment, like I/O ports and a network interface.

The jog-box is used when teaching or manually moving the measuring machine. The jog-box is pictured in Figure 2.4. The PC is used for running measuring software that can communicate with the controller. The mechanical structure basically consists of three linear guideways with drive and scale systems. A picture of the mechanical structure can be seen in Figure 2.5. A very important guideway in the Z-axis direction is the Z-axis drive mechanism. Connected to this drive mechanism is the probe which traces workpieces that are desired to be measured.

In this study only the core of the CMM system is considered and therefore a short presentation of the mechanical structure and the controller is given in the

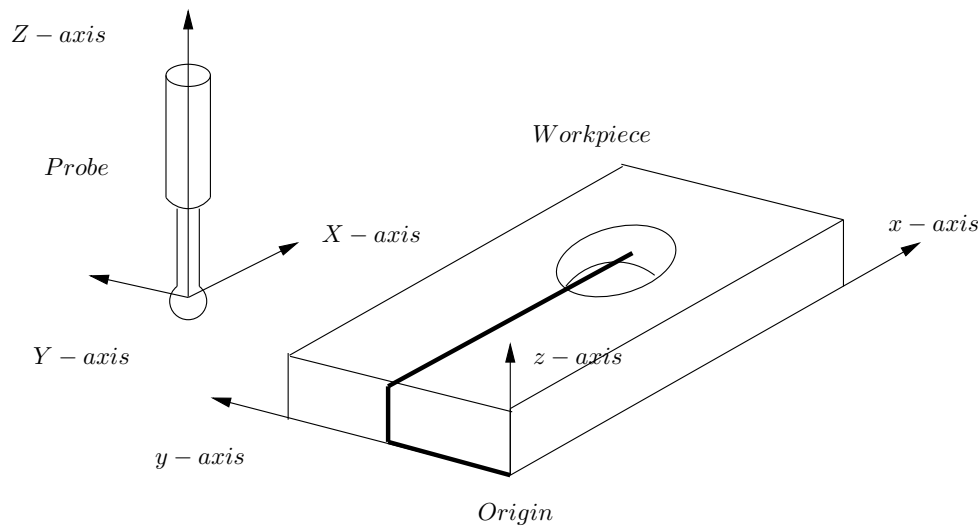


Figure 2.2. The probe and a workpiece. The probe works like a finger when it traces map coordinates.

following sections.

2.3 The Mechanical Structure

In this section the mechanical structure of the Global A is introduced. Furthermore, the Y-axis drive mechanism is discussed and a simplified measuring example is given.

The CMM mechanical structure in Figure 2.5 consists of a workstand, a granite table, a bridge, the Y-axis drive mechanism, the X-beam assembly, the Z-tower, the Z-rail and a probe. All machine coordinates are given in a Cartesian coordinate system. According to Table 2.1, position of machine parts are shown in Figure 2.5.

The granite table is mounted on top of the stable workstand. Parts to be measured are placed and fixed on the table. The bridge is mounted on the Y-axis drive mechanism. The drive mechanism moves the bridge along the Y-axis.

The X-beam assembly consists of a drive mechanism, similar to the Y-axis drive mechanism. The only difference is it makes the Z-tower move along the X-axis. The Z-tower is mounted on top of the X-beam assembly. The Z-tower also has a drive mechanism similar to those above, it moves the Z-rail up and down along the Z-axis. The probe is mounted at the end of the Z-rail. It's purpose is to register contacts with the workpiece surfaces. The probe is basically a very sophisticated switch. To simplify this investigation, only the Y-axis and its drive mechanism are

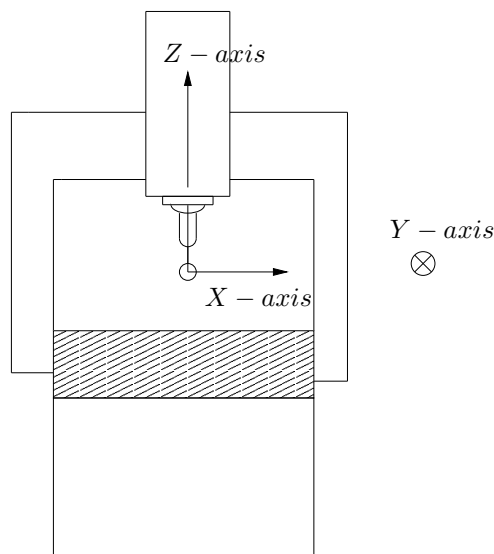


Figure 2.3. The machine coordinate system of a CMM.

Machine Part	Number
Workstand	(1)
Granite Table	(2)
Bridge	(3)
Y-axis Drive Mechanism	(4)
X-Beam Assembly	(5)
Z-Tower	(6)
Z-Rail	(7)
Probe	(8)

Table 2.1. Machine Parts of the studied coordinate measuring machine. The given numbers are used to relate the machine parts to where they are assembled in Figure 2.5.

considered.

2.4 The Y-axis Drive Mechanism

In this section the Y-axis drive mechanism is presented. A simplified measuring example is also given. See Table 2.2 and Figure 2.6 for the system parameters and explanation of symbols. The main part of the drive mechanism is a DC motor which is connected to a pulley (\mathcal{A}). Pulley (\mathcal{B}) is connected to pulley (\mathcal{A}) with a belt. Pulley (\mathcal{C}) is mounted on pulley (\mathcal{B}). Finally, pulley (\mathcal{D}) is connected to

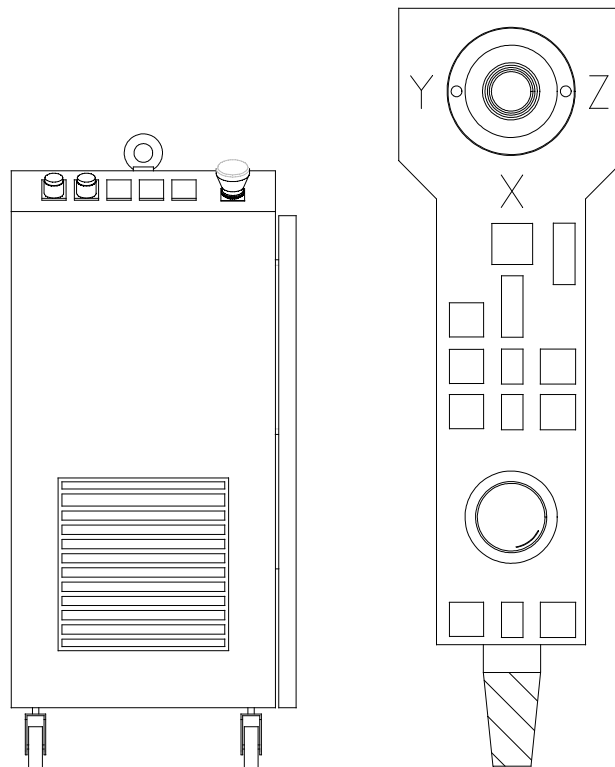


Figure 2.4. The controller, B3C-LC (left). The jog-box (right) used for teaching or manually moving the coordinate measuring machine.

pulley (C) with a belt. The bridge (E) is connected to the belt.

The bridge position y_b in Figure 2.6 and the motor shaft angle θ are derived from linear and rotary encoder readings. The angular velocity ω is measured by a tachometer attached to the motor shaft.

The following example explains what happens when the width of a box is measured, see Figure 2.7 and Figure 2.8.

Example 2.1 *When the width of a box is measured, the following actions take place:*

- *The bridge moves until the probe indicates a hit with the front surface, see Figure 2.7.*
- *The position of the bridge is read by the linear encoder and stored in the controller.*
- *The bridge moves from the opposite side towards the back surface until a hit is registered by the probe, see Figure 2.8.*

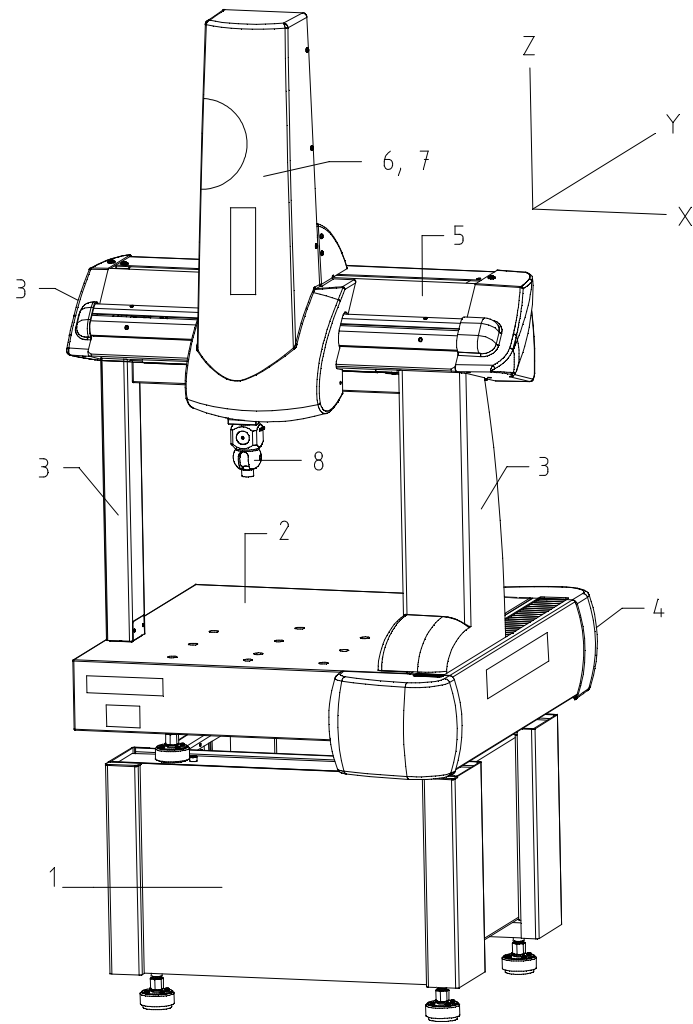


Figure 2.5. The picture shows the mechanical structure of the CMM. The given numbers indicate the machine parts given in Table 2.1.

- *The new position is read by the linear encoder and stored in the controller.*
- *The two position readings are subtracted from one another and the result is the value of the width.*

If the machine vibrates due to lack of damping in the drive mechanism, the probe may not register a true position of the bridge. This explains why damping of drive mechanisms are critical in the system.

Symbol	Explanation	Value
\mathcal{A}	Pulley attached to the motor shaft	
\mathcal{B}	Pulley connected to pulley \mathcal{A} with a belt	
\mathcal{C}	Pulley mounted on pulley \mathcal{B}	
\mathcal{D}	Pulley connected to pulley \mathcal{C}	
\mathcal{E}	The bridge	
r_1	Radius of pulley \mathcal{A}	8.5 mm
r_2	Radius of pulley \mathcal{B}	56 mm
r_3	Radius of pulley \mathcal{C}	13.2 mm
r_4	Radius of pulley \mathcal{D}	13.2 mm
m	Mass of the bridge \mathcal{E}	70kg
y_b	Position of the bridge.	
θ	Motor shaft angle.	
ω	Angular velocity of the motor shaft.	

Table 2.2. System parameters.

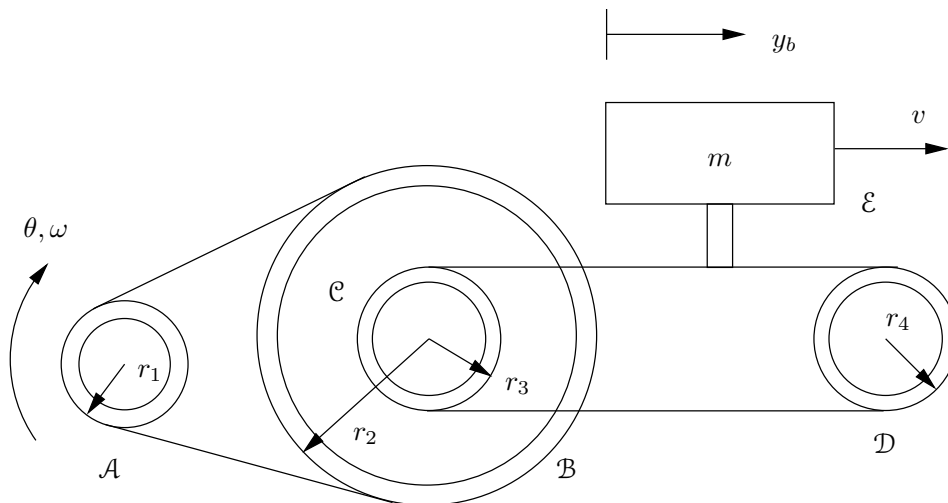


Figure 2.6. The drive mechanism of the Y-axis.

2.5 The Controller, B3C-LC

The main parts of the controller are the cabinet with the contained hardware and the jog-box. In the cabinet the main processor that executes the firmware is an Intel™ 486 processor. The cabinet contains a board with a three axes drive unit for control of the drive mechanisms of the X,Y and Z-axes. Each axis can be individually tuned to optimize the drive characteristics. There are other types

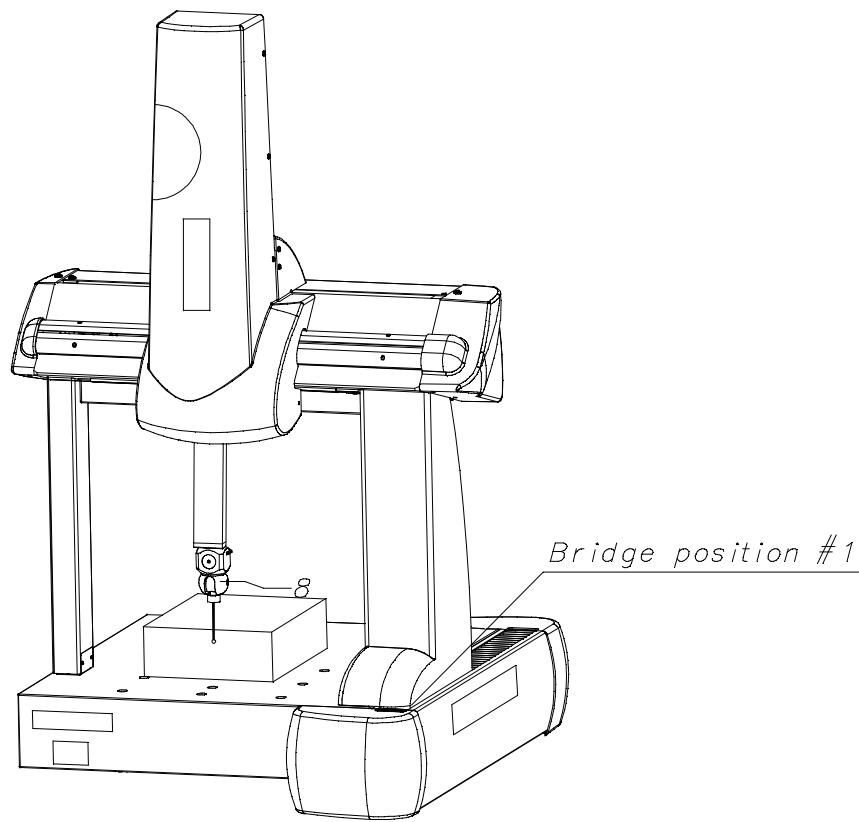


Figure 2.7. Measuring the width of a box. The bridge moves until the probe indicates a hit with the front surface.

of boards that can be inserted to increase performance and functionality. In this investigation a module that allows the user to input analog signals to the hardware servo controller section is used. Furthermore the system has an optional board for Ethernet communication. Inside the cabinet there is also a possibility to connect digital or analog I/O for control.

As mentioned previously the controller, B3C-LC also includes a jog-box shown in Figure 2.4. On the jog-box there is a 3-DOF (Degrees Of Freedom) joystick which can be used in several modes. Essentially the jog-box allows the user to move the bridge in the Y-axis direction, the Z-tower in the X-axis direction and finally the Z-rail in the Z-direction. Hence, since the probe is connected to the Z-rail it is possible to move the probe in the X, Y and Z directions of a Cartesian coordinate system. Typically, the jog-box is used to teach the CMM to trace points on workpieces.

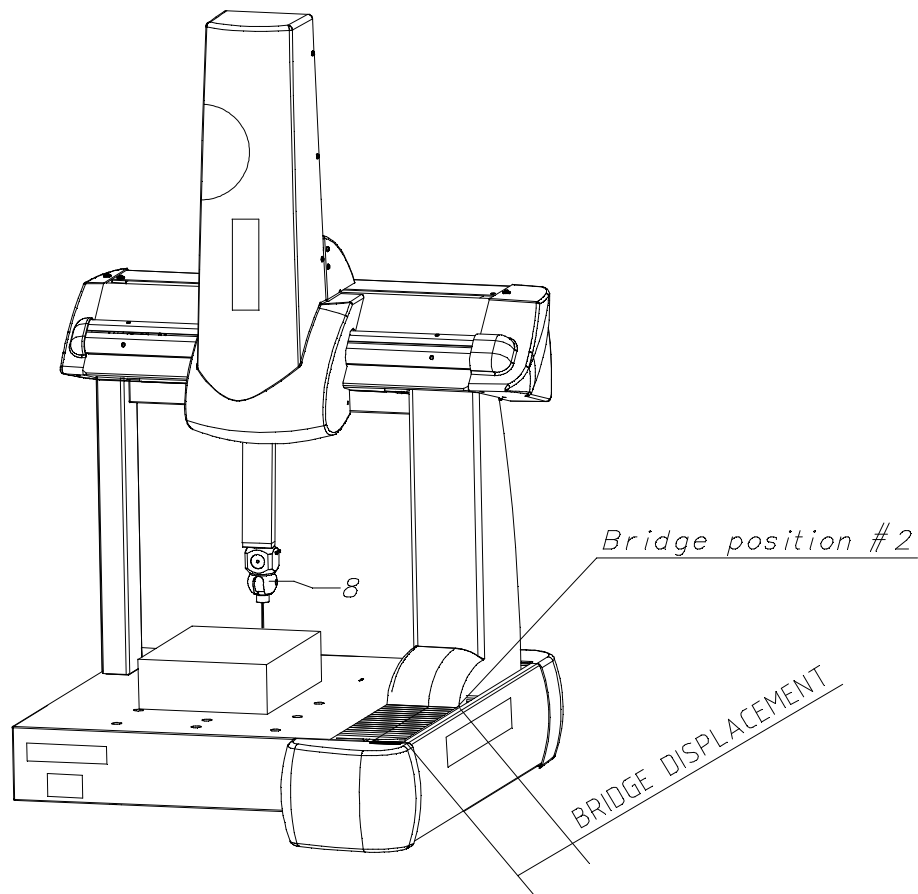


Figure 2.8. Measuring the width of a box. The bridge moves from the opposite side towards the back surface until a hit is registered by the probe.

2.6 The Controller Software

There are a lot of different software programs involved when programming and running the measuring machine. First of all the controller and the control system need to be switched on and booted. This is done using Ethernet because of connection with the measuring software. Mainly, a measuring software product called PC-DIMIS™ (Wilcox, 2001) is used for complex measurements. However, in this work a more simple software called Testsoft™ (B&S, 2000) is used. This software is used for controlling the CMM using simple instructions like:

Example 2.2 A Testsoft™ instructions can look like
movdlt 100,200,50

which makes a relative movement: the bridge moves 200 mm in the Y-axis direction, the Z-tower 100 mm in the X-axis direction and finally the Z-rail 50 mm in the Z-direction.

Example 2.3 Another important Testsoft™ instruction is *autzer*

which moves the bridge, the Z-tower and the Z-rail to a certain known position and initializes the scale systems, in this case, linear encoders.

Both programs are used on a terminal which communicates through Ethernet with the controller.

2.7 The Control System

Here a typical control structure for controlling CMM drive mechanisms is given. A schematic view of the system is given in Figure 2.9. It contains five blocks, F_s , F_p and PID representing the actual controller, and the two other blocks are the DC motor and the drive mechanism. The feedback transfer function F_s is used for angular velocity feedback from the motor with a tachometer. The transfer function F_p is used for position feedback with a linear encoder.

The PID regulator is used to tune system characteristics. Normally the DC

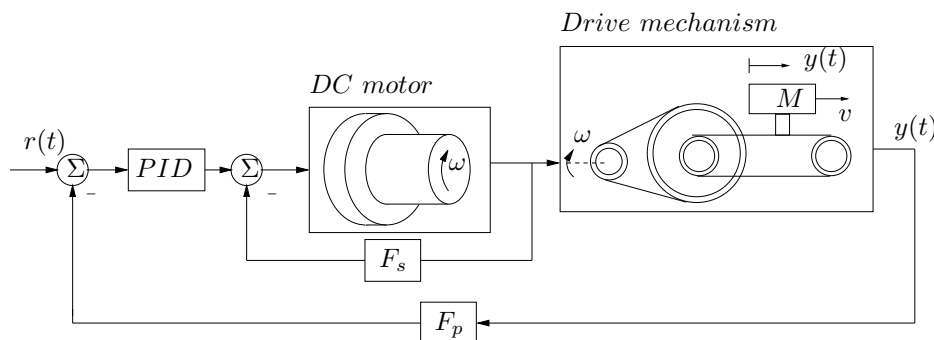


Figure 2.9. An example of a CMM drive mechanism controlled with two feedback controllers and a PID.

motor is treated as a second-order transfer function and the drive mechanism as a static gain depending on the gear ratio of the system. For instance, for the Y-axis drive mechanism the gear ratio can easily be measured by turning the DC motor shaft one revolution and reading the bridge position. However, to increase position accuracy and stiffness of drive mechanisms there is a high demand on accurate models of the system to achieve good performance and better control of the CMM. The input to the system is the armature current reference signal. In the work to be presented the output is normally bridge position.

Chapter 3

Physical Modeling

What is a model? One way to answer the question is to describe how a model can be used. Loosely speaking a model is a tool that can be used to answer questions about characteristics of systems. In this thesis, mathematical models are considered. This means relationships between quantities (length, current, torque, etc.) which can be observed in the system are designated as mathematical relationships in the model.

Example 3.1 *For the system “a particle with mass” Newton’s Law of Acceleration designates a relationship between force and acceleration.*

How are models constructed? In principle there are two approaches. One approach is to construct models using the physical laws of nature. Another approach is to estimate models from collected data. This chapter addresses the first approach.

When describing time-varying physical systems there are some standard methods to use: differential equations, block diagrams and bond graphs¹. In this thesis the bond graph concept in (Glad and Ljung, 2002) is used to determine physical models. The advantage of the bond graph representation is that it makes use of the analogies between electrical, mechanical, hydraulic and thermal systems. Bond graphs make the model building systematic because the flow of energy in the system is followed, moreover the representation guarantees that nothing essential is forgotten in the modeling process.

3.1 Modeling with Bond Graphs

The presented bond graph concept in this section is standard. The fundamentals are presented in, for example (Glad and Ljung, 2002).

Bond graphs describe physical systems by linking the components of the system, under ideal circumstances. By using the bond graph representation it is possible to divide a system into separate parts. Standard symbols are used to identify the

¹Bond graphs were introduced by H. Paynter, MIT.

most common components. The next example shows an electrical system and its corresponding bond graph.

Example 3.2 Consider the electric circuit in Figure 3.1. Each component in the physical model is represented in the bond graph. The bonds between the parts are represented by half arrows, so called harpoons. Furthermore, these bonds describe the ideal energy flow between the parts.

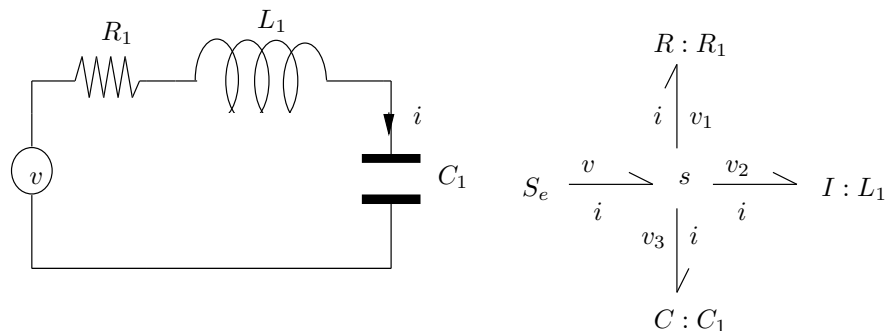


Figure 3.1. An ideal physical model (left) and its corresponding bond graph model (right).

The two variables, *effort* (e) and *flow* (f), determine the energy flow between elements in a system. See Figure 3.2. The product between these variables is always power. The harpoon at the end of a bond is used to denote the direction of positive power, ef . Effort and flow can be positive or negative in the same bond. Normally, the harpoon is put at the same side as the effort variable.



Figure 3.2. Effort (e) and flow (f).

The variables, e and f , in the table below are standard variables in bond graph modeling. Furthermore, Table 3.2 gives examples of standard elements, their notation and explanation.

3.1.1 Junctions

A junction is used to connect the elements in a bond graph. Moreover, junctions cannot store or dissipate energy. For bond graphs there are two types of junctions, s-junctions and p-junctions. Figure 3.3 shows a typical s and p-junction.

In a s-junction the flow is equal for every connected bond. Furthermore, if all efforts are summed the result is always zero. Efforts that are pointing towards the

Domain	Effort (e)	Flow (f)
Electrical	Voltage u [V]	Current i [A]
Mechanical (translation)	Force F [N]	Velocity v [m/s]
Mechanical (rotation)	Torque T [Nm]	Angular velocity ω [rad/s]
Hydraulic	Pressure p [Pa]	Volume flow v [m^3/s]

Table 3.1. The effort and flow variables for typical domains.

Element	Notation	Explanation
Junctions	s, p	Elements that couple energy between various other elements.
Buffers	C, I	Elements that store energy.
Dissipators	R	Elements that dissipate energy.
Sources	S_e, S_f	Elements that generate energy.
Transformers and Gytrators	TF, GY	Elements that convert energy ideally.

Table 3.2. Standard bond graph elements.

s-junction give a positive contribution and efforts pointing from the s-junction give a negative contribution to the sum. See Table 3.3. This rule is equivalent to the Kirchhoff voltage law for electrical systems.

In a p-junction the effort is equal for every connected bond. Moreover, if all flows are summed the result is always zero. Like the s-junction, there is a rule to determine the sign of the flow summation for a p-junction. When a flow is pointing towards the p-junction it gives a positive contribution and if a flow is pointing from the p-junction it gives a negative contribution to the sum, see Table 3.3. This rule is equivalent to Kirchhoff's laws for electrical systems.

Element	Equation	Example
s-junction	$f_1 = f_2 = \dots = f_n$	A fixed connection between two mechanical parts.
	$\sigma_1 e_1 + \sigma_2 e_2 + \dots \sigma_n e_n = 0$	
p-junction	$e_1 = e_2 = \dots = e_n$	A parallel junction in an electrical network.
	$\sigma_1 f_1 + \sigma_2 f_2 + \dots \sigma_n f_n = 0$	

Table 3.3. Junction elements and their corresponding summation rules.

Moreover, σ_i in Table 3.3 becomes

$$\sigma_i = \begin{cases} 1 & \text{if binding points inwards} \\ -1 & \text{if binding points outwards} \end{cases}$$

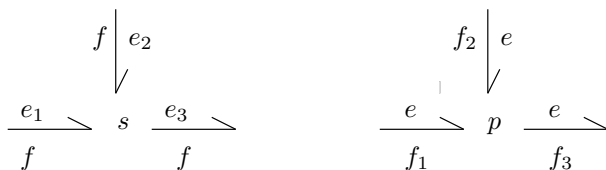


Figure 3.3. The figure shows a typical s and p-junction in bond graph modeling.

3.1.2 Buffers and Dissipators

A buffer is a bond graph element that is able to store energy. In bond graph modeling there are two standard buffer elements, C and I-elements. According to Figure 3.4 these elements have buffer constants, β , α which determine a linear behaviour. Typically for the dissipator, resistor, is that it dissipates free energy. The free energy flows through the system and is finally transformed into thermal energy.

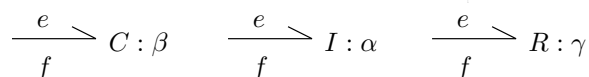


Figure 3.4. C-element, I-element and R-element.

Table 3.4 below shows the linear relationships between effort and flow for the standard elements mentioned above. Application examples are also given.

Element	Equation	Example
C-element	$e(t) = \frac{1}{\beta} \int^t f(\tau) d\tau$	A mechanical spring and an electrical capacitor.
I-element	$f(t) = \frac{1}{\alpha} \int^t e(\tau) d\tau$	A mechanical inertia and an electrical inductance.
R-element	$e(t) = \gamma f(t)$	A mechanical damper and an electrical resistor.

Table 3.4. Relationships for C,I and R-elements.

3.1.3 Sources

A system has to be supplied with energy in order to function properly. A source is a bond graph element that provides a system with energy. In bond graph modeling there are two standard types of sources, effort sources (S_e) and flow sources (S_f). These sources are shown in Figure 3.5.

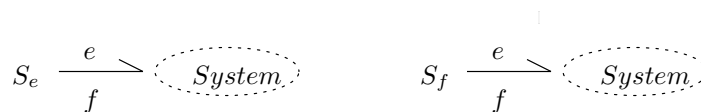


Figure 3.5. Effort source S_e and flow source S_f .

3.1.4 Transformers and Gyrotors

To transform effort and flow from one type of system to another, transformers (TF) and gyrotors (GY) are used. For instance, a gyrotor can be used to explain how the current in a DC motor relates to the generated torque on the motor shaft. Table 3.5 below shows the linear relationships between effort and flow for



Figure 3.6. TF-element, GY-element.

the standard elements above. Application examples are also given.

Element	Equation	Example
TF-element	$e_2 = ne_1$ $f_1 = nf_2$	A mechanical gear.
GY-element	$e_1 = rf_2$ $e_2 = rf_1$	A DC-motor.

Table 3.5. Relationships for TF and GY-elements.

3.2 Modeling a Simple Mechanical System

With the newly obtained knowledge from Section 3.1 it is possible to model rather advanced processes. This section presents one example (Glad and Ljung, 2002) where the bond graph concept is applied to a mechanical system.

Example 3.3 Consider the mechanical system in Figure 3.7. A body with mass m is coupled to a spring with spring constant k . The body is sliding along a surface with a certain friction constant $\phi(v)$. Furthermore, the body is affected by the outer force F .

According to Table 3.4, Newton's Law of Acceleration corresponds to an I-element with the equation

$$m\dot{v} = F_1 \quad (3.1)$$

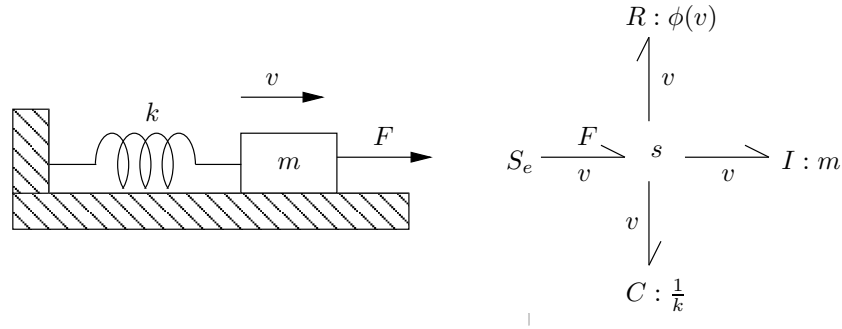


Figure 3.7. A mechanical system and its corresponding bond graph.

where F_1 is the accelerating force. Assume that F_2 is the force acting upon the spring with spring constant k . According to Table 3.4, F_2 is related to the velocity v as

$$\dot{F}_2 = kv \quad (3.2)$$

or in other words, the spring is a C -element with capacitance $1/k$. Table 3.4 gives the following equation for the frictional force F_f

$$F_f = h(v) \quad (3.3)$$

Normally (3.3) is nonlinear. From a bond graph concept point of view, this is an R -element. The outer force F inputs energy to the system, hence this is an effort source S_e . Equations (3.1)-(3.3) depend on the same velocity v . Finally, the accelerating force is the spring and the frictional force subtracted from the total force, that is,

$$F_1 = F - F_2 - F_f$$

Hence, velocity and force fulfil the rules for an s -junction in Table 3.3. The corresponding bond graph to the system is thus given by the bond graph in Figure 3.7.

3.3 Modeling the Drive Mechanism of the Y-axis

This investigation is restricted to the drive mechanism of the y-axis, see Figure 2.6. The model explains how the electrical motor angular velocity affects the position of the bridge. The derivation of the models is based on the following assumptions: the angular velocity generated by the electrical motor is viewed as the angular velocity applied to the system. It is assumed that the only existing friction is the sliding friction of the bridge. All springs are assumed to have linear stiffness.

The drive mechanism can be modeled with different approaches. A first approach can be to assume that the belt between pulley \mathcal{A} and \mathcal{B} is very stiff and that the belt between pulley \mathcal{C} and \mathcal{D} is not stiff. Such a model is investigated in

Section 3.3.1. A more general approach is to assume that none of the belts are stiff. Such an approach is investigated in Section 3.3.2. Intuitively, one may argue that a general approach would give a more accurate model, however, there is a flip-side to that argument. The mathematical relationships become more advanced and thus it will be more cumbersome to derive the model. Another important issue is the risk of over-modeling, that is, that the model may have redundant components. The notation regarding the physical modeling of the drive mechanism is given in Table 3.6. A thorough derivation of the models in Section 3.3 can also be found in Appendix A.

Symbol	Explanation
θ_1	Motor shaft angle at pulley \mathcal{A} .
$\omega_1, \omega_2, \omega_3$	Angular velocity of pulley \mathcal{A} , \mathcal{B} and \mathcal{C} .
r_1, r_2, r_3	Radii of pulley \mathcal{A} , \mathcal{B} and \mathcal{C} .
k, k_1, k_2, k_3	Spring constants.
d, d_1, d_2, d_3	Damping coefficients in the springs.
F_1, F_2, F_3	Belt tension at pulley \mathcal{A} , \mathcal{B} and \mathcal{C} .
F_k	Force generated by spring with constant k .
$F_{k_1}, F_{k_2}, F_{k_3}$	Force generated by spring with constant k_1 , k_2 and k_3 .
F_d	Force generated by damper with constant d .
$F_{d_1}, F_{d_2}, F_{d_3}$	Force generated by damper with constant d_1 , d_2 and d_3 .
F_m	Force generated by the inertia m .
F_ϕ	Frictional sliding force acting on the bridge. Section 3.3.1.
$F_{\phi+d_3}$	Frictional sliding force acting on the bridge. Section 3.3.2.
F_m	Force generated by mechanical inertia m .
v_1, v_2, v_3	Velocity at radius r_1 , r_2 , r_3 for pulley \mathcal{A} , \mathcal{B} and \mathcal{C} .
v_4	Velocity of the bridge.
y_b	Position of the bridge.
m	Inertia, mass of the bridge.
ϕ	Sliding friction of the bridge.
T_1	Torque generated by the electrical motor at pulley \mathcal{A} .

Table 3.6. The notation used for the physical modeling.

3.3.1 One-spring Model

This model is illustrated in Figure 3.8. In this model, the belt between pulley (\mathcal{A}) and (\mathcal{B}) is assumed to be very stiff. The second belt is modeled as a spring connected in parallel with a damper. The spring and the damping constants are given by k and d respectively. The bridge is treated as an inertia with mass m . The bond graph corresponding to the *one-spring model* is illustrated in Figure 3.9. The equations for the one-spring model are derived from the bond graph in Figure 3.9.

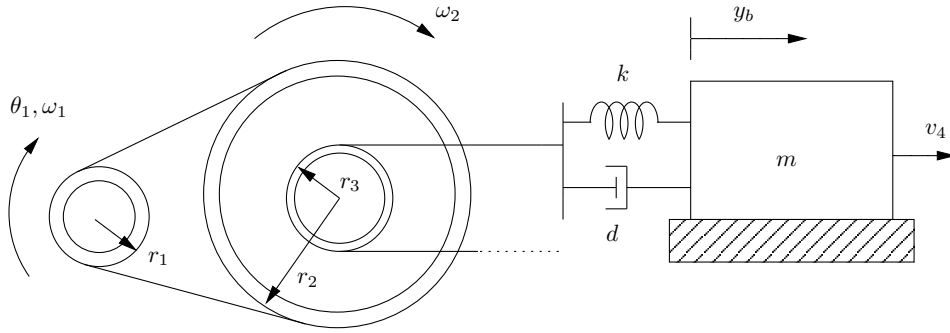


Figure 3.8. One-spring model of the drive mechanism of the y-axis.

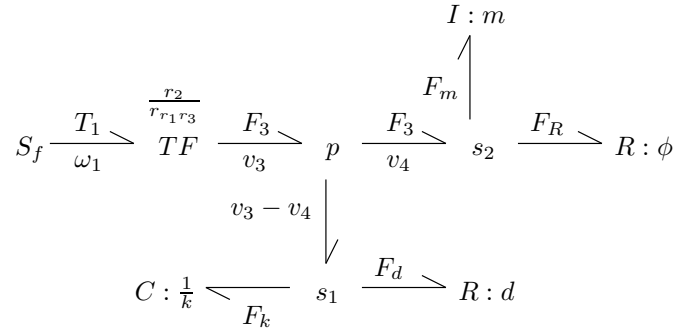


Figure 3.9. Bond graph for the one-spring model of the drive mechanism for the y-axis.

These are given by (Glad and Ljung, 2002)

$$F_3 = F_k + F_d \quad (3.4)$$

$$F_k = k \int^t (v_3(\tau) - v_4(\tau)) d\tau \quad (3.5)$$

$$F_d = d(v_3 - v_4) \quad (3.6)$$

$$F_3 = F_m + F_\phi \quad (3.7)$$

$$v_4 = \frac{1}{m} \int^t F_m(\tau) d\tau \quad (3.8)$$

$$F_\phi = \phi v_4 \quad (3.9)$$

$$v_3 = \frac{r_1 r_3}{r_2} \omega_1 \quad (3.10)$$

These equations can be transformed into state space form. Intuitively, it is practical to use $y = y_b$ as output signal. This choice implies that two state variables can be

used instead of three, which is the case when y_b is used as output. However, since only y_b is measurable, this signal is chosen as the output. The three state model is used for control in Chapter 7. With y_b as output and ω_1 as input (u) the model can be written in state space form as

$$x(t) = \begin{pmatrix} F_k(t) \\ y_b(t) \\ v_4(t) \end{pmatrix} \quad (3.11)$$

$$\dot{x}(t) = Ax(t) + Bu(t) \quad (3.12)$$

$$y(t) = Cx(t) \quad (3.13)$$

$$A = \begin{pmatrix} 0 & 0 & -k \\ 0 & 0 & 1 \\ \frac{1}{m} & 0 & -\frac{d+\phi}{m} \end{pmatrix} \quad (3.14)$$

$$B = \begin{pmatrix} \frac{kr_1r_3}{r_2} \\ 0 \\ \frac{dr_1r_3}{mr_2} \end{pmatrix} \quad C = \begin{pmatrix} 0 & 1 & 0 \end{pmatrix} \quad (3.15)$$

Using Laplace transformation and $\mathcal{L}\{\theta_1(t)\} = \Theta_1(s)$ the relation between angular velocity and position of the bridge can be written as

$$Y_b(s) = G_{\theta_1 y_b}(s)s\Theta_1(s)$$

$$G_{\theta_1 y_b}(s) = \frac{r_1r_3(ds+k)}{r_2(ms^2+(d+\phi)s+k)} \quad (3.16)$$

3.3.2 Three-spring Model

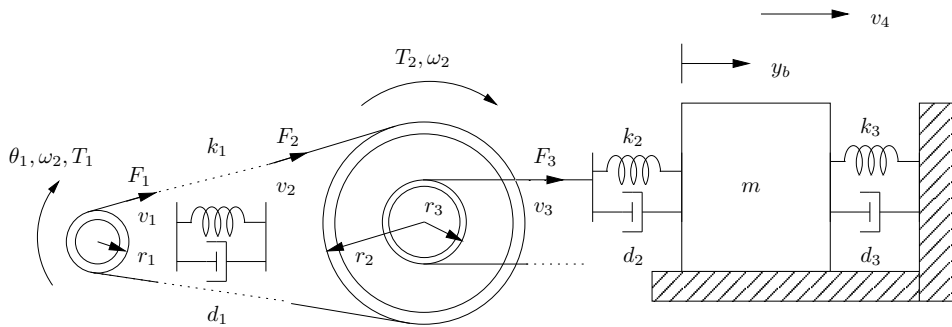


Figure 3.10. Three-spring model of the drive mechanism of the y-axis.

The model is illustrated in Figure 3.10. The two belts are assumed to be flexible. The belt between pulley (A) and (B) is modeled as a spring in parallel

with a damper. The spring and the damping constants are k_1 and d_1 respectively. The belt between pulley (C) and the bridge is modeled as a spring in parallel with a damper. Analogously their constants are given by k_2 and d_2 , respectively. The bridge is treated as an inertia with mass m . Finally, the belt between the bridge and pulley (D) is modeled as a spring in parallel with a damper. Again, their constants are given by k_3 and d_3 respectively. The bond graph corresponding to the *three-spring model* is illustrated in Figure 3.11. The equations for the three-

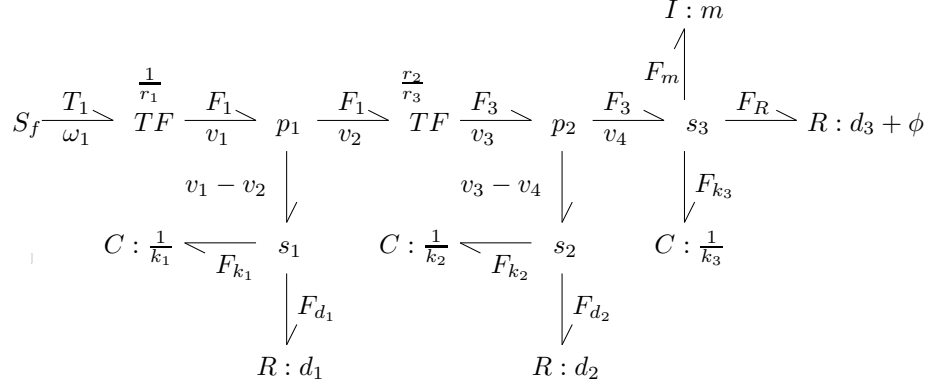


Figure 3.11. Bond graph for the three-spring model of the drive mechanism of the y-axis.

spring model are derived from the bond graph in Figure 3.11. They are given by

$$\begin{aligned} T_1 &= r_1 F_1 \\ v_1 &= r_1 \omega_1 \end{aligned} \quad (3.17)$$

$$F_1 - F_{k_1} - F_{d_1} = 0 \quad (3.18)$$

$$F_{k_1} = k_1 \int^t (v_1(\tau) - v_2(\tau)) d\tau \quad (3.19)$$

$$F_{d_1} = d_1 (v_1 - v_2) \quad (3.20)$$

$$F_3 = \frac{r_2}{r_3} F_1 \quad (3.21)$$

$$v_3 = \frac{r_3}{r_2} v_2$$

$$F_3 - F_{k_2} - F_{d_2} = 0 \quad (3.22)$$

$$F_{k_2} = k_2 \int^t (v_3(\tau) - v_4(\tau)) d\tau \quad (3.23)$$

$$F_{d_2} = d_2 (v_3 - v_4) \quad (3.24)$$

$$F_3 - F_m - F_R - F_{k_3} = 0 \quad (3.25)$$

$$v_4 = \frac{1}{m} \int^t F_m(\tau) d\tau \quad (3.26)$$

$$F_{\phi+d_3} = (\phi + d_3)v_4 \quad (3.27)$$

$$F_{k_3} = k_3 \int^t v_4(\tau) d\tau \quad (3.28)$$

Once again the equations can be transformed into state space form. With y_b as output and ω_1 as input the model can be written in state space form as

$$x(t) = \begin{pmatrix} F_{k_1}(t) \\ F_{k_2}(t) \\ y_b(t) \\ v_4(t) \\ F_{k_3}(t) \end{pmatrix} \quad (3.29)$$

$$\dot{x}(t) = Ax(t) + Bu(t) \quad (3.30)$$

$$y(t) = Cx(t) \quad (3.31)$$

$$A = \begin{pmatrix} -\frac{k_1 r_2^2}{d_1 r_2^2 + d_2 r_3^2} & \frac{k_1 r_2 r_3}{d_1 r_2^2 + d_2 r_3^2} & 0 & -\frac{k_1 d_2 r_2 r_3}{d_1 r_2^2 + d_2 r_3^2} & 0 \\ \frac{k_2 r_2 r_3}{d_1 r_2^2 + d_2 r_3^2} & -\frac{k_2 r_3^2}{d_1 r_2^2 + d_2 r_3^2} & 0 & -\frac{d_1 k_2 r_2^2}{d_1 r_2^2 + d_2 r_3^2} & 0 \\ 0 & 0 & 0 & 1 & 0 \\ \frac{d_2 r_2 r_3}{m(d_1 r_2^2 + d_2 r_3^2)} & \frac{d_1 r_2^2}{m(d_1 r_2^2 + d_2 r_3^2)} & 0 & \frac{d_2^2 r_3^2}{m(d_1 r_2^2 + d_2 r_3^2)} - \frac{d_2 + d_3 + \phi}{m} & -\frac{1}{m} \\ 0 & 0 & 0 & k_3 & 0 \end{pmatrix} \quad (3.32)$$

$$B = \begin{pmatrix} \frac{k_1 r_1 d_2 r_3^2}{d_1 r_2^2 + d_2 r_3^2} \\ \frac{d_1 r_1 k_2 r_2 r_3}{d_1 r_2^2 + d_2 r_3^2} \\ 0 \\ \frac{d_1 r_1 d_2 r_2 r_3}{m(d_1 r_2^2 + d_2 r_3^2)} \\ 0 \end{pmatrix} \quad C = (0 \ 0 \ 1 \ 0 \ 0) \quad (3.33)$$

Using Laplace transformation and $\mathcal{L}\{\theta_1(t)\} = \Theta_1(s)$ the relation between angular velocity and position of the bridge can be written as

$$Y_b(s) = G_{\theta_1 y_b}(s) s \Theta_1(s)$$

$$\begin{aligned} G_{\theta_1 y_b}(s) = & r_1 r_2 r_3 (d_1 d_2 s^2 + (d_1 k_2 + k_1 d_2) s + k_1 k_2) / \\ & \left((d_1 r_2^2 + d_2 r_3^2) m s^3 + \right. \\ & \left. ((d_2 d_3 + m k_2 + d_2 \phi) r_3^2 + (\phi d_1 + m k_1 + d_1 d_2 + d_1 d_3) r_2^2) s^2 + \right. \\ & \left. ((d_1 k_2 + d_1 k_3 + k_1 d_3 + \phi k_1 + k_1 d_2) r_2^2 + (d_2 k_3 + k_2 d_3 + \phi k_2) r_3^2) s + \right. \\ & \left. (k_1 k_2 + k_1 k_3) r_2^2 + k_2 k_3 r_3^2 \right) \end{aligned} \quad (3.34)$$

Chapter 4

Identification Methods

Essentially, the concept of identification is to use measured data to estimate models. This chapter presents the basic principles regarding prediction error identification methods in general and their properties. To begin with some model structures are presented in Section 4.1. Section 4.2 presents a method of forming the predictor. In Section 4.3 linear regression for estimation of parameters is introduced. It is necessary to have standard tools for model validation and such tools are presented in Section 4.4 and Section 4.7. To be able to determine optimal values of model parameters, a *criterion function* is introduced in Section 4.5. A standard method of computing the estimate is given in Section 4.6. The fundamentals of this subject are presented in, for example (Glad and Ljung, 2002).

4.1 Model Structures

Sometimes systems or subsystems cannot be modeled with use of physical principles. The reason for this may be lack of information about the systems function. Another case would be when the physical relationships are too complex to unravel. The remedy for this is to use standard models, which by experience, are able to handle many cases in dynamic systems. The most common class of such standard models is linear systems.

A general time discrete model parameterized by θ can be written as

$$y(t) = G(q, \theta)u(t) + H(q, \theta)e(t) \quad (4.1)$$

The model $G(q, \theta)$ is called the system model and $H(q, \theta)$ the noise model. The delay operator is denoted by q , $qu(t) = u(t+1)$. The noise model is driven by white noise $e(t)$. In many cases it is convenient to use some standard model structure. In black-box modeling with prediction error methods the following general model structure is often used:

$$A(q)y(t) = \frac{B(q)}{F(q)}u(t) + \frac{C(q)}{D(q)}e(t) \quad (4.2)$$

where

$$A(q) = 1 + a_1q^{-1} + \dots + a_{n_a}q^{-n_a}$$

and analogous for the C , D , and F -polynomials, while

$$B(q) = b_1q^{-1} + b_2q^{-2} + \dots + b_{n_b}q^{-n_b}$$

Table 4.1 shows common model structures that are special cases of (4.2).

Polynomials used	Name of the model structure
B	FIR (Finite Impulse Response).
A, B	ARX.
A, B, C	ARMAX.
B, F	OE (Output Error).
B, C, D, F	BJ (Box-Jenkins).

Table 4.1. Common model structures.

4.2 Forming the Predictor

It is possible to predict the output signal $y(t)$ from (4.1), based upon measurements $u(s)$, $y(s)$ with $s \leq t - 1$. This is called the *one-step-ahead* predictor, $\hat{y}(t|\theta)$. For the ARX model the predictor becomes

$$\begin{aligned} \hat{y}(t|\theta) = & -a_1y(t-1) - \dots - a_{n_a}y(t-n_a) + \\ & b_1u(t-nk) + \dots + b_{n_b}u(t-nk-nb+1) \end{aligned} \quad (4.3)$$

It is clear that the predictions for the ARX-model are not only based upon the input $u(t)$ but also on old values of the output signal $y(t)$.

In the general case the predictor can be formed by dividing (4.1) with $H(q, \theta)$, that is

$$H^{-1}(q, \theta)y(t) = H^{-1}(q, \theta)G(q, \theta)u(t) + e(t)$$

or equivalently

$$y(t) = \left(1 - H^{-1}(q, \theta)\right)y(t) + H^{-1}(q, \theta)G(q, \theta)u(t) + e(t)$$

By definition white noise cannot be predicted, and by removing $e(t)$ it can be shown that the predictor can be written as

$$\hat{y}(t|\theta) = (1 - H^{-1}(q, \theta))y(t) + H^{-1}(q, \theta)G(q, \theta)u(t) \quad (4.4)$$

4.3 Linear Regression

In general (4.4) may be a rather complicated function of θ . However, if the predictor $\hat{y}(t | \theta)$ is linear in θ the estimation is easier to carry out. A linear predictor can be written as

$$\hat{y}(t | \theta) = \theta^T \varphi(t), \quad (4.5)$$

where the unknown parameters are put in the column vector θ while old in- and output values are put in the column vector $\varphi(t)$. This model structure is called a linear regression with $\varphi(t)$ being the *regression vector* and its components the *regressors*.

Example 4.1 Consider the parameterization and regression vectors according to

$$\begin{aligned} \theta &= (a_1 \ a_2 \ \dots \ a_{na} \ b_1 \ b_2 \ \dots \ b_{nb})^T \\ \varphi(t) &= (-y(t-1) \ \dots \ -y(t-na) \ u(t-nk) \ \dots \ u(t-nk-nb+1))^T \end{aligned} \quad (4.6)$$

Then (4.6) in (4.5) forms (4.3) or the ARX-model which is the most common case of linear regression.

4.4 Residuals and Prediction Errors

To adjust parameterized models to data systematically some criterion must be used. The most common one is to minimize the *prediction error*. It is possible to evaluate the prediction in (4.4) at time t if the prediction error

$$\epsilon(t, \theta) = y(t) - \hat{y}(t | \theta)$$

is computed. Furthermore, if the predictor $\hat{y}(t | \theta)$ is a linear regression the difference

$$\epsilon(t, \theta) = y(t) - \varphi^T(t)\theta$$

is the error associated with the value θ . This is called the prediction error corresponding to θ .

$$\hat{\epsilon}_N(t) = \epsilon(t, \hat{\theta}_N) \quad (4.7)$$

Equation (4.7) defines the *residuals* ("leftovers") associated with the estimated model $\hat{\theta}_N$. Often it is desired to investigate how well the predicted output $\hat{y}(t | \theta)$ explains the actual output. According to (Ljung, 1987) the ratio

$$R_y^2 = \frac{\sum_{t=1}^N \hat{y}(t | \theta)}{\sum_{t=1}^N y^2(t)} = 1 - \frac{\sum_{t=1}^N \hat{\epsilon}_N^2(t)}{\sum_{t=1}^N y^2(t)} \quad (4.8)$$

measures the proportion of the total variation of y that is explained by the regression. It is called the *multiple correlation coefficient*. Often (4.8) is expressed in percent.

4.5 Loss Function $V_N(\theta)$

With collected in- and output data during a period $t = 1, \dots, N$ it is possible to evaluate how well the model; with parameters θ , describes the characteristics of the system. Usually the scalar function is formed

$$V_N(\theta) = \frac{1}{N} \sum_{t=1}^N \epsilon^2(t, \theta) \quad (4.9)$$

It represents a measure of goodness or a *loss function* for the parameters θ . It is intuitive to choose the value of θ that minimizes (4.9). This value is defined as

$$\hat{\theta}_N = \arg \min_{\theta} V_N(\theta) \quad (4.10)$$

Furthermore, it is often derived to estimate the variance of the white noise $e(t)$. If $\hat{\theta}_N$ is determined, it is possible to estimate the variance as

$$\hat{\lambda}_N = \frac{1}{N} \sum_{t=1}^N \epsilon^2(t, \hat{\theta}_N)$$

4.6 Computing the Estimate $\hat{\theta}_N$

Consider the special case with a linear regression model according to (4.5). If θ is assumed to be a column vector with dimension d the error becomes

$$\epsilon(t, \theta) = y(t) - \theta^T \varphi(t)$$

and the quadratic criterion in (4.10) can be written as

$$\begin{aligned} V_N(\theta) &= \frac{1}{N} \sum_{t=1}^N \left(y(t) - \theta^T \varphi(t) \right)^2 \\ &= \frac{1}{N} \sum_{t=1}^N y^2(t) - \frac{1}{N} \sum_{t=1}^N 2\theta^T \varphi(t) y(t) + \frac{1}{N} \sum_{t=1}^N \theta^T \varphi(t) \varphi^T(t) \theta \\ &= \frac{1}{N} \sum_{t=1}^N y^2(t) - 2\theta^T f_N + \theta^T R_N \theta \end{aligned}$$

where

$$f_N = \frac{1}{N} \sum_{t=1}^N \varphi(t) y(t) \quad (4.11)$$

$$R_N = \frac{1}{N} \sum_{t=1}^N \varphi(t) \varphi^T(t) \quad (4.12)$$

f_N has dimension $(d \times 1)$ and R_N $(d \times d)$. If R_N is non-singular, that is, $\det R_N \neq 0$ then (4.10) can be written as

$$V_N(\theta) = \frac{1}{N} \sum_{t=1}^N y^2(t) - f_N^T R_N^{-1} f_N + (\theta - R_N^{-1} f_N)^T R_N (\theta - R_N^{-1} f_N) \quad (4.13)$$

The last element in (4.13) is always positive, because matrix R_N is positive definite (R_N is assumed to be non-singular). Hence, the minimum value of $V_N(\theta)$ is reached when the last element is zero, that is,

$$\theta = \hat{\theta}_N = R_N^{-1} f_N \quad (4.14)$$

Thus, the Least Squares Estimation (LSE) $\hat{\theta}_N$ is calculated with equations (4.11), (4.12) and (4.14). Notice that for the ARX-model in (4.6), all elements in matrix R_N and vector f_N are of the type

$$\begin{aligned} & \frac{1}{N} \sum_{t=1}^N y(t-j)u(t-k) \\ & \frac{1}{N} \sum_{t=1}^N y(t-j)y(t-k) \\ & \frac{1}{N} \sum_{t=1}^N u(t-j)u(t-k) \end{aligned}$$

Henceforth, the estimate $\hat{\theta}_N$ is formed by the covariance functions of y and u .

4.7 Variance Error

If the bias error is zero, that is, there exist a value θ_0 such as

$$y(t) - \hat{y}(t | \theta_0) = \epsilon(t, \theta_0) = e(t)$$

where $e(t)$ is white noise with variance λ . Then it can be shown that the covariance matrix for $\hat{\theta}_N$ can be estimated from the data as

$$\hat{P}_N = \frac{1}{N} \hat{\lambda}_N \hat{R}_N^{-1}$$

where

$$\begin{aligned} \hat{R}_N &= \frac{1}{N} \sum_{t=1}^N \psi(t, \hat{\theta}_N) \psi^T(t, \hat{\theta}_N) \\ \hat{\lambda}_N &= \frac{1}{N} \sum_{t=1}^N \epsilon^2(t, \hat{\theta}_N) \\ \psi(t, \theta) &= \frac{d}{d\theta} \hat{y}(t | \theta) \end{aligned}$$

4.8 Summary

Chapter 4 introduces the concept of identification and identification methods. The black-box model approach is chosen and investigated. The standard model structures are introduced, the ARX-model is thoroughly investigated. The parameters in such models are derived from linear regression which is well known in the field of statistics. The concept of residuals and prediction errors is introduced, a suggestion to calculate variance of estimated parameters is given.

Chapter 5

Off-line Identification

Identification of systems is a recognized modeling tool in control engineering and the theory applies very well on time-invariant systems. Furthermore, there are powerful software tools available, for instance the System Identification Toolbox (Ljung, 2000) for MATLAB™ (MathWorks, 2003). In this chapter the goal is to identify a rigid or a flexible model of the drive mechanism of the y-axis presented in Section 2.2 by measuring the input signal (the motor shaft angle) and the output signal (measured bridge position). In other words the goal is to identify the stiffnesses and dampings for the mechanical configuration.

This chapter is organized as follows; Before the identification experiments in Section 5.2, data collection and pre-processing is described in Section 5.1. In Section 5.3 another data set, a *validation data set*, is used to determine the quality of the models. The stiffness and dampings of the mechanical configuration is identified in Section 5.4. Finally a summary is given in Section 5.5.

5.1 Data Collection and Pre-processing

According to (Gustafsson et al., 2001), pretreatment of data has to take place before system identification techniques are applied. If there are trends and mean values of a signal that are undesirable to model, they have to be removed. Otherwise, estimation of ARX and ARMAX-models can become totally incorrect.

5.1.1 Data Collection

To collect data, digital encoder outputs are read from the B3C-LC controller in Section 2.2 and are then transmitted with cables to a PC with a data acquisition card. However, the data acquisition card allows for dual communication, that is, it is possible to transmit data from the PC via the card to the controller. The card has a sampling rate of a 1000 Hz. Software called LabVIEW™ (NI, 2002) controls the data acquisition card and allows for data collection. The recorded digital data takes the form of *text-files*. Moreover, it is possible to create signals of many shapes

with LabVIEW™; such as sine, cosine and chirp signals. The data acquisition card can then be used for transmission of signals to the controller.

5.1.2 Choice of Input Signal

To be able to determine an accurate model of a system, it is necessary to excite as much information as possible from the process. The solution is to use an input signal with a vast frequency content. There are several ideas to choose a suitable input signal. However, the choice also depends on hardware implementation, that is, which signals are possible to inject with the current hardware configuration of the system.

- If the characteristic frequencies of a system are known, say f_1, f_2, \dots, f_n , then it is possible to construct a signal with the same frequency content in the discrete frequency domain, the phase can be random. Then the signal can be transformed from the Discrete Fourier Transform (DFT) domain to the time discrete domain with Inverse Discrete Fourier Transform (IDFT). The result can be used as input to the system.
- A popular choice is to use a so called *pseudo random* signal or *telegraph signal*. Essentially it is a square-wave signal with a random period.
- Another choice is to use a *chirp signal*, a sine wave with increasing frequency. Thus all resonance frequencies can be excited.

In the work to be presented here, a chirp signal is used as input signal or reference signal. Normally a chirp signal is defined as

$$y[k] = \sin\left(\left(2\pi\frac{k}{N}\right)k\right), k = 0, 1, \dots, N$$

Unfortunately the chirp signal cannot be injected directly to the motor shaft as a reference signal, but is injected and added in an inner loop. This depends on hardware limitation. However, the signal does not get distorted in the process. Henceforth, the wave characteristics of the measured input signal will still have a chirp pattern.

5.1.3 Model and Validation Data

Estimation and validation of a model should never be based upon the same data set, overly optimistic results may occur. Hence, two data sets are collected from the system, *model* and *validation data*. The model data is used for model estimation. The validation data is only used for comparison with predicted data from an estimated model. The model and validation data are collected in the open-loop system.

The first approach here to identify the model of the drive mechanism of the y-axis is to use a chirp signal with frequencies between 10 and 30 Hz. In MATLAB™

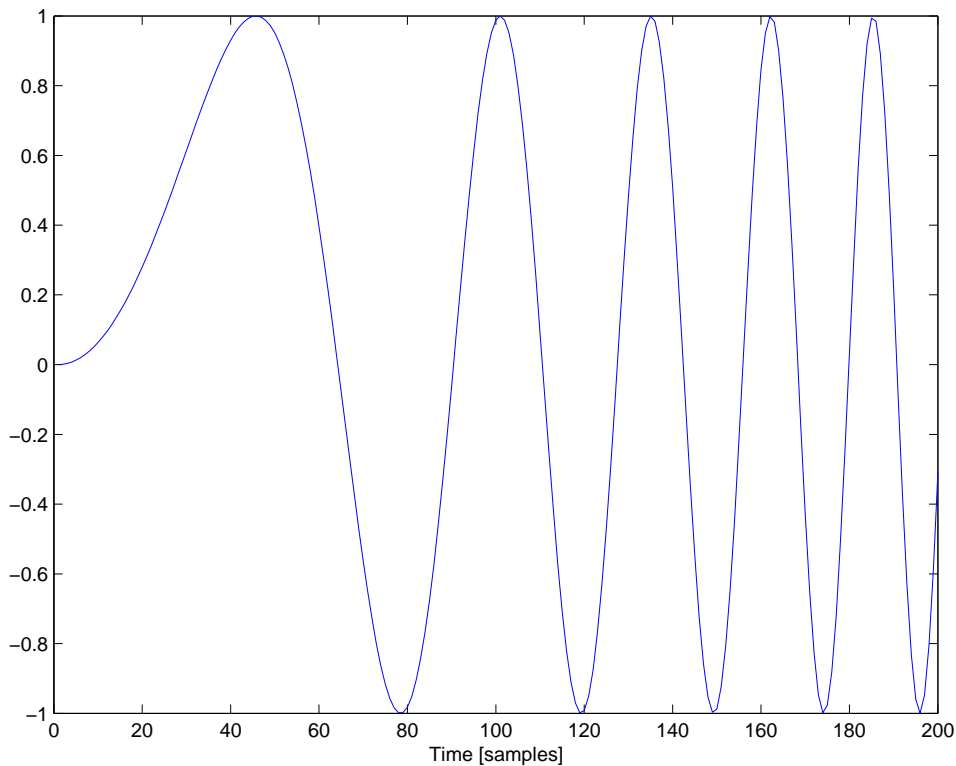


Figure 5.1. Chirp signal with frequencies between 0-5 Hz.

the `fft` function is used to monitor the DFT of the output signal y_b , position of the bridge. The DFT of the output signal is plotted in Figure 5.2. The figure shows two distinct peaks at 15 and 22 Hz. A rather naive way would be to model both of these frequencies and stick with a higher model order and heavier computer computations. However, it is possible to analyze and determine the origin of the frequencies.

5.1.4 Identification of False Frequencies

An accelerometer assembled on the x-beam assembly shown in Figure 5.3 is used for vibration measurements. The vibration signal is amplified with a device and then monitored on a spectrum analyzer. The spectrum analyzer transforms the signal and plots the DFT of the input. The idea with measuring these vibrations is to determine if frequencies originated from the x-beam assembly and/or from the z-tower (see Section 2.5) are transferred to the drive mechanism of the y-axis.

The spectrum analyzer shows differences with the z-rail positioned up versus

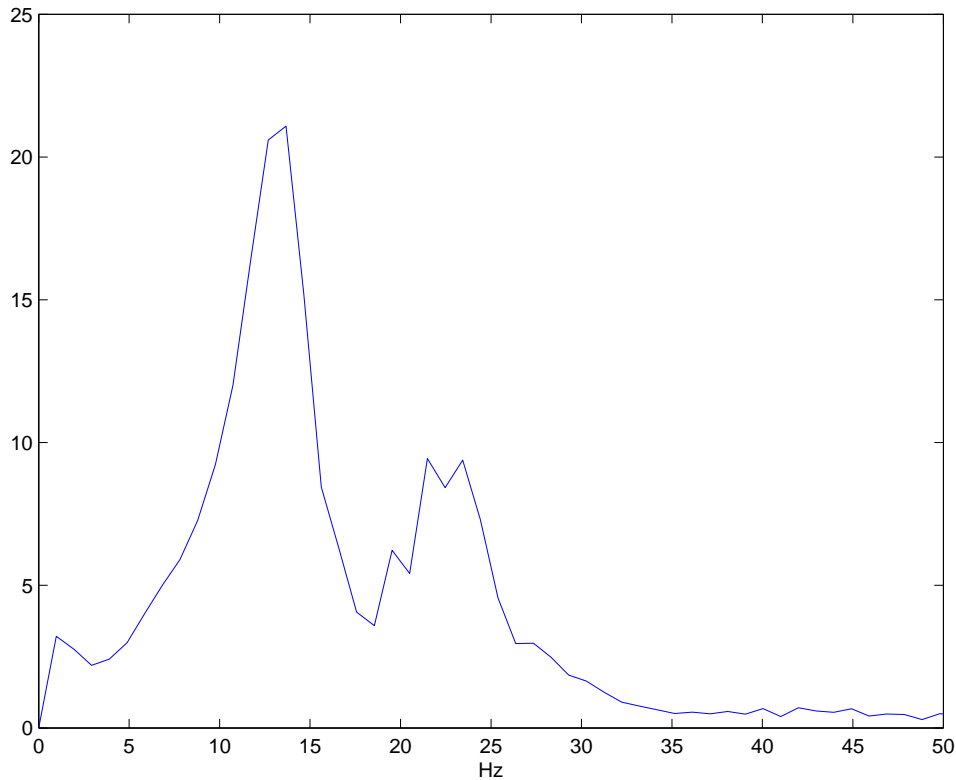


Figure 5.2. Computed DFT of the output y_b , bridge position.

positioned down, see Figure 5.4. In the case with the z-rail up the 22 Hz vibrations are very evident. In the other case with the z-rail down the vibrations are barely visible on the spectrum analyzer. This makes sense because with the z-rail positioned up another system adds, an inverted pendulum. Simply speaking the z-tower acts as a rod with a mass attached on the top. These vibrations are visible when the chirp signal is injected to the system. Hence, frequencies about 22 Hz are to be neglected for the drive mechanism of the y-axis. In other words the drive mechanism has its resonance frequency around 15 Hz. The second approach to identify the system is to use a chirp signal with frequency content between 10 and 16 Hz.

5.2 Estimated Black-box Models

In the work to follow in this section it is found that the system model and the noise model do not necessarily have to be modeled separately, see Section 4.1. As

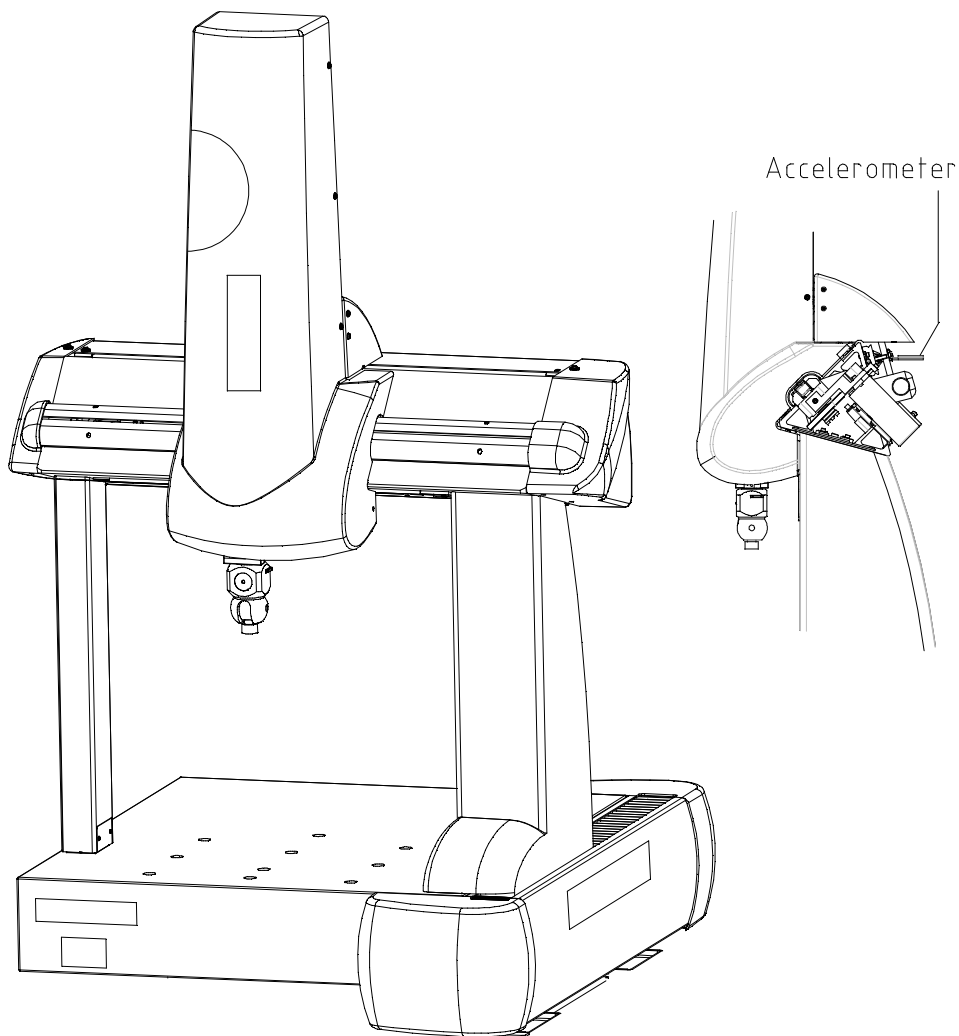


Figure 5.3. Accelerometer attached to the x-beam assembly.

a result, ARX models are used as the model structure in this section. ARX models can be represented, see Chapter 4, by

$$A(q)y(t) = B(q)u(t) + e(t)$$

where A and B are parameterized polynomials, $u(t)$ is the input and $e(t)$ the noise. It is possible to choose the order of the polynomials and the time delay of the input signal. For an ARX model these are often denoted as three numbers in a vector, $\mathcal{N} = [n_a \ n_b \ n_k]$. The two first numbers represent the orders of the polynomials of

the system and the noise model, and the last number represents the time delay.

The following algorithm is used: Remove trends and mean values of the measured motor shaft angle and the measured position of the bridge. Identify with ARX $\mathcal{N} = [2 \ 1 \ 0]$ and $\mathcal{N} = [3 \ 2 \ 0]$. This is done in MATLAB™ code using SITB, see (Ljung, 2000). It has been found that identification with zero time delay gives good results, hence $n_k = 0$. Figure 5.5 shows the input and output signals after their trends and means have been removed.

The Bode plots of the ARX models are shown in Figure 5.6. The model with $\mathcal{N} = [2 \ 1 \ 0]$ corresponds to a one-spring model and is called arx2, that is, it has the same number of poles. The model with $\mathcal{N} = [3 \ 2 \ 0]$ corresponds to a three-spring model (see Section 3.3) and is called arx3. Both models have a peak at $\omega_p = 94$ rad/s. A comparison is given in Table 5.1.

The fit or the multiple correlation coefficient in Section 4.4 is calculated by simulation on the estimation data set. As a reminder the fit is defined as

$$fit \% = \left(1 - \frac{\sum(y(t) - \hat{y}(t))^2}{\sum y^2(t)}\right) \cdot 100$$

It is clear that the fit for the arx3 model is slightly better than the fit for the arx2 model. However, it is common practice to choose the model with the lowest order in such close cases. This is especially acceptable when validation of the models gives very similar results.

	FPE	Loss function	Fit	ω_p
arx2	$1.0 \cdot 10^{-7}$	$1.0 \cdot 10^{-7}$	80.6 %	94 rad/s
arx3	-	$9.3 \cdot 10^{-8}$	85.7 %	94 rad/s

Table 5.1. Fit and frequency comparison of the two ARX models.

Hence, the arx2 model is chosen to represent the drive mechanism of the y-axis. The coefficients of the parameterized polynomials A and B of the arx2 model are given in Table 5.2. The standard deviation σ_i of the polynomial coefficients is also given in Table 5.2.

Parameter	Value	σ_i
a_1	- 1.963	0.002334
a_2	0.9718	0.002187
b_1	0.0118	-

Table 5.2. Coefficients and their standard deviation of the arx2 model.

Bilinear transformation with the MATLAB™ command `d2c` gives the time-continuous arx2 model

$$A(s)y(t) = B(s)u(t) + e(t)$$

$$A(s) = s^2 + a_1s + a_2$$

$$B(s) = b_1s^2 + b_2s + b_3$$

The coefficients of the parameterized polynomials A and B of the time-continuous arx2 model are given in Table 5.3.

Parameter	Value
a_1	28.65
a_2	8931
b_1	0.002998
b_2	11.99
b_3	$1.199 \cdot 10^4$

Table 5.3. Coefficients of parameterized polynomials A and B of the time-continuous arx2 model.

If the white noise $e(t)$ is neglected and using $\mathcal{L}\{\theta_1(t)\} = \Theta_1(s)$, $\mathcal{L}\{y_b(t)\} = Y_b(s)$, the continuous transfer function for the arx2 model becomes

$$Y_b(s) = G_{arx2}(s)\Theta_1(s)$$

$$G_{arx2}(s) = \frac{b_1s^2 + b_2s + b_3}{s^2 + a_1s + a_2} \quad (5.1)$$

The step response for the transfer function in (5.1) is plotted in Figure 5.7. It is clear that the system in (5.1) is fast but very underdamped. The damping of the system is $\zeta \approx 1/10$. The zeros of (5.1) are given by

$$s_1 = (-1.9997 + 0.0258i) \cdot 10^3$$

$$s_2 = (-1.9997 - 0.0258i) \cdot 10^3$$

or in real values 318 Hz. In the same manner, the poles are given by

$$s_3 = (-14.3250 + 93.4120i)$$

$$s_4 = (-14.3250 - 93.4120i)$$

or in real values 15Hz. The Bode magnitude plot in Figure 5.8 of the transfer function in (5.1) shows a peak at 91 rad/sec or 15 Hz.

This implies that the poles at 15 Hz are much more important than the zeros at 318 Hz. Also the very region of interest for the drive mechanism of the y-axis is around 15 Hz as explained above. Thus, with good accuracy the zeros can be neglected. With neglected zeros the approximation of the transfer function in (5.1) becomes

$$G(s) = \frac{a_2}{s^2 + a_1s + a_2} \quad (5.2)$$

where the numerator is chosen for unity gain. The step response and the Bode magnitude plot for the approximated model in (5.2) is plotted in Figure 5.9 and in Figure 5.10 respectively.

5.3 Validation

Figure 5.11 shows a 100 step ahead prediction with the model and compares the output with the validation data. The predicted output data are estimated according to Section 4.3 and Section 4.5. Also, the *multiple correlation coefficient* in Section 4.4 is computed. This is a scalar value in percent describing how well the predicted output explains the actual output. The chosen arx2 model gives a 80.5 % fit with the validation data.

With an ideal model there is no difference between measured and predicted output but white noise, that is, uncorrelated noise with mean zero and variance λ . In other words the residuals in Section 4.4 are to be white in such a case. Thus estimation of the covariance function (akf) of the residuals gives a pulse. Moreover, in that case the cross correlation for input and output residuals is zero. The auto correlation function (akf) of residuals for output y_b and cross correlation for input θ_1 and output y_b residuals is plotted in Figure 5.12. The residuals are very close to white, that is, there is a pulse at time zero. Further, the cross correlation is very small after time zero. This implies the system is almost ideal. The loss function and the forward prediction error given in Table 5.1 are small numbers, which means the difference between the measured output and the predicted output is very small. The standard deviation given in Table 5.2 of estimated parameters is small; 0.1 % and 0.2 %, that is, it is far from the same order as the parameter itself. The model order is low, two poles, one zero and no time delay.

5.4 Identified Parameters

Consider the one-spring model in (3.16). There are obvious similarities between (3.16) and the approximated transfer function in (5.2). The number of poles are two in both cases. Also, if (3.16) is slightly rewritten it becomes

$$G_{\theta_1, y_b}(s) = \frac{\frac{r_1 r_3 d}{r_2 m} \left(s + \frac{k}{d} \right)}{s^2 + \frac{1}{m} (d + \phi) s + \frac{k}{m}} \quad (5.3)$$

If the zero is neglected and it is assumed that $\phi = 0$, then the approximated version of the transfer function in (5.3) becomes

$$G_{\theta_1, y_b}(s) = \frac{\frac{r_1 r_3 k_a}{r_2}}{s^2 + \frac{d}{m} s + \frac{k}{m}} \quad (5.4)$$

Assuming $\phi = 0$ is a good approximation because the bridge has low friction due to the use of air bearings. Finally, it is possible to solve for the unknown parameters in (5.4) with (5.2).

Hence, the one-spring model in Section 3.3.1 describes the drive mechanism of the y-axis very well. However, for a larger machine with longer belts and more mechanical inertia, the system characteristics may change. For such a case the

Parameter	SI Unit
$k_a = 8931$	-
$k = 625170$	N/m
$d = 2005.5$	Ns/m

Table 5.4. Identified parameters.

three-spring model may give better results. It has been noticed that for larger machines the resonance frequency of the belt between pulley \mathcal{C} and \mathcal{D} clearly depends on bridge position. This is not the case for the studied machine.

5.5 Summary

Chapter 5 covers off-line identification. Data collection and pre-processing of data is discussed. The choice of input signal to the system is investigated. Two data sets are presented, model and validation data. False frequencies are identified with use of a spectrum analyzer. The chosen and estimated black-box model $arx2$ is based upon: lowest model order, best prediction compared with validation data, value of loss function, standard deviation of estimated parameters, auto correlation of residuals for the output y_b and finally cross correlation for input θ_1 and output y_b residuals. The chosen discrete model is transformed to a continuous representation. The estimated model is thoroughly validated. The black-box model $arx2$ is compared with the physical one-spring model. Two unknown parameters in the one-spring model are identified, a spring constant and a mechanical damping constant.

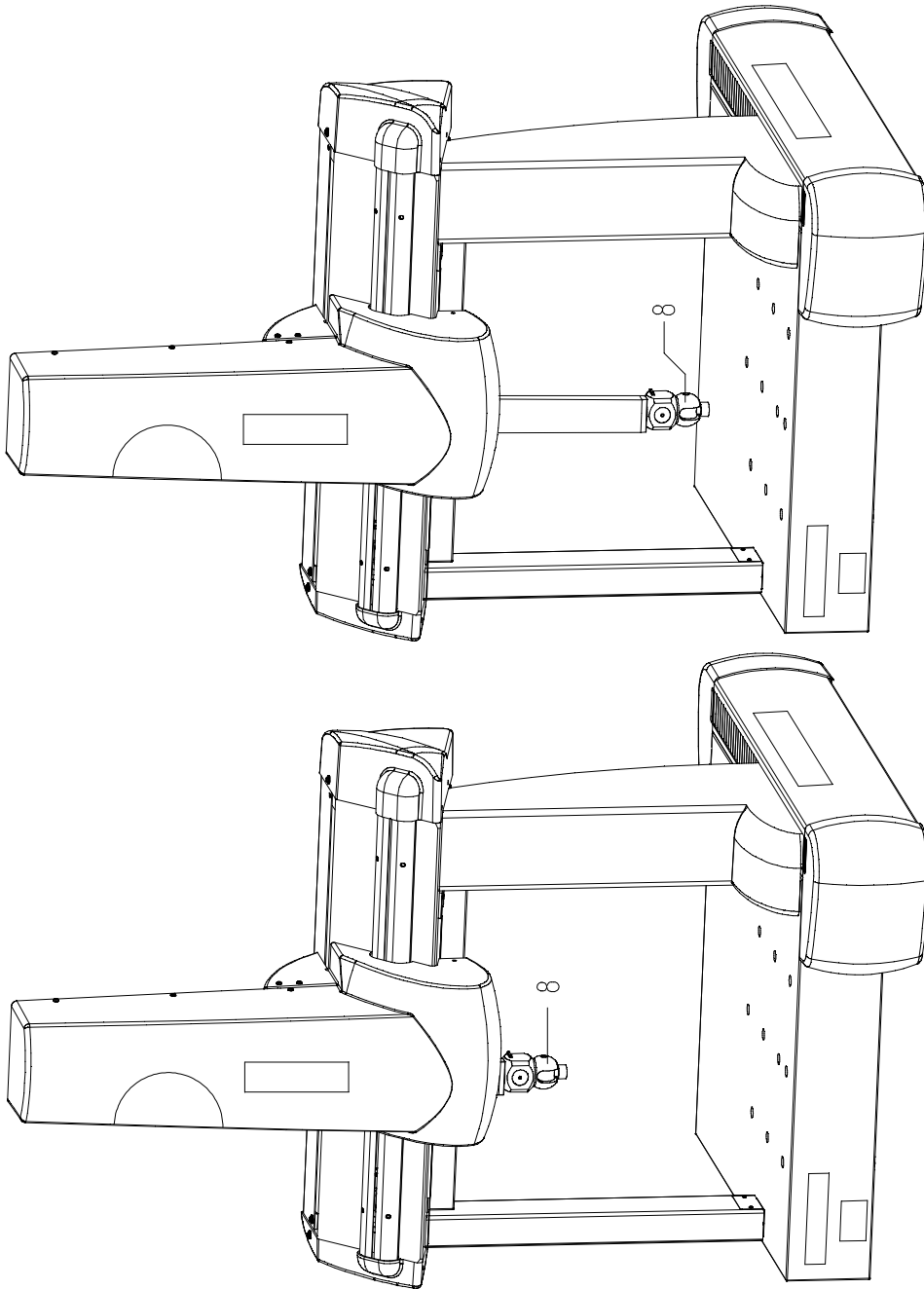


Figure 5.4. Identification of false frequencies. The spectrum analyzer clearly shows the 22 Hz vibrations with the z-rail positioned up (lower figure). With the z-rail positioned down the vibrations are barely visible (upper figure).

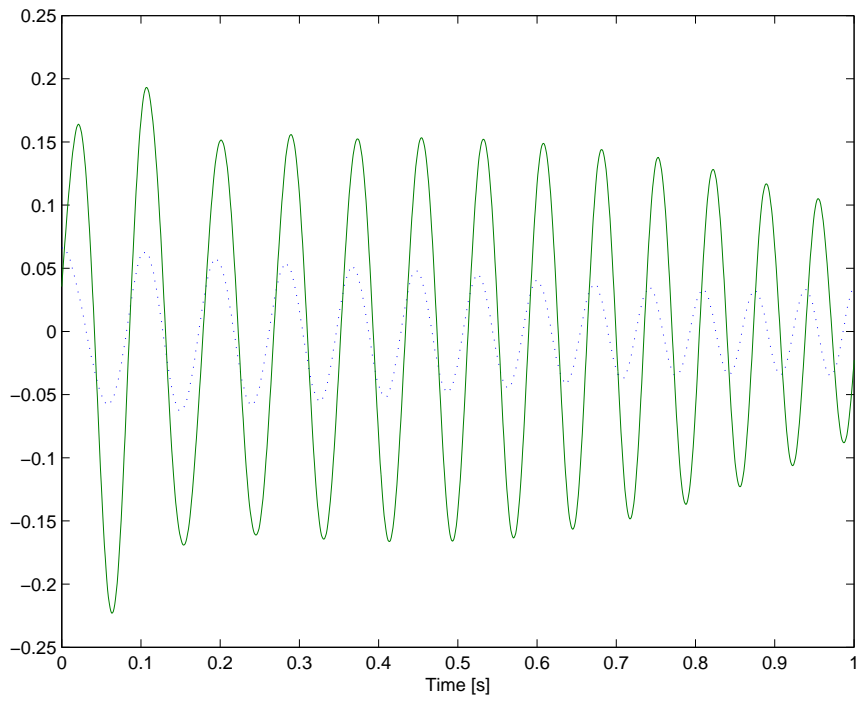


Figure 5.5. Detrended data, θ (dotted) and y_b (solid).

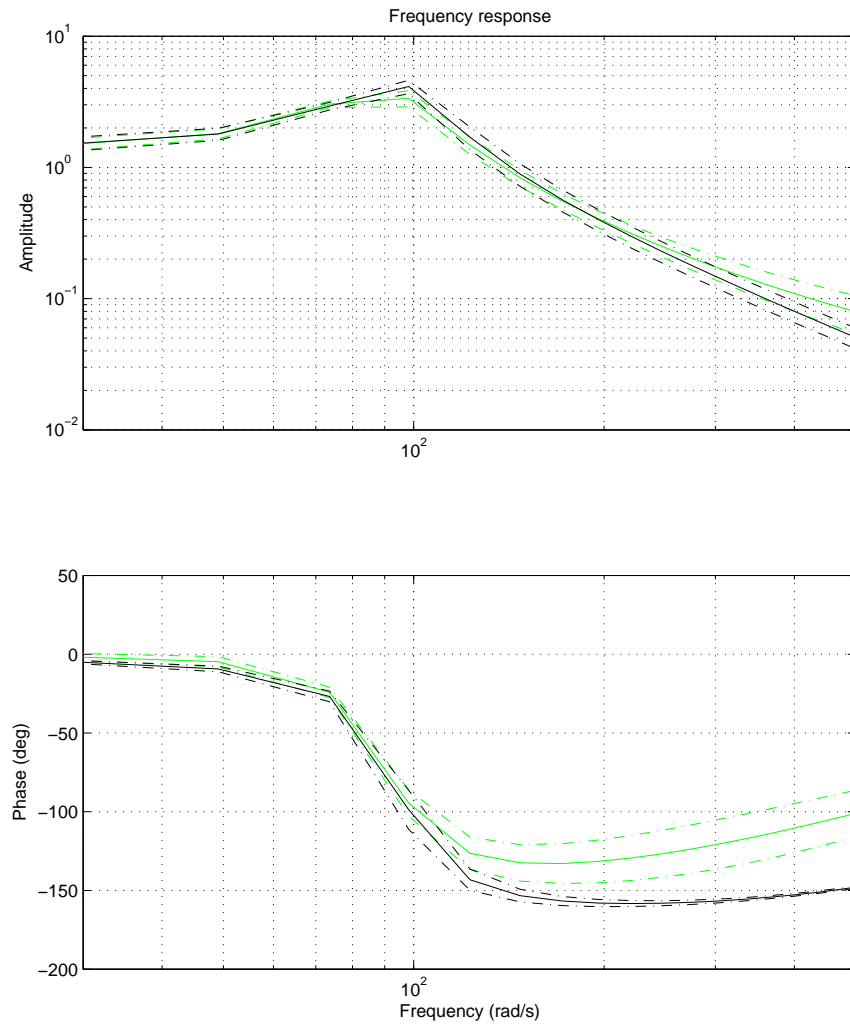


Figure 5.6. Bode plots of the ARX models arx2 (black) and arx3 (green/grey). They are plotted with 99% confidence intervals. Both models have a peak at $\omega_p = 94$ rad/s.

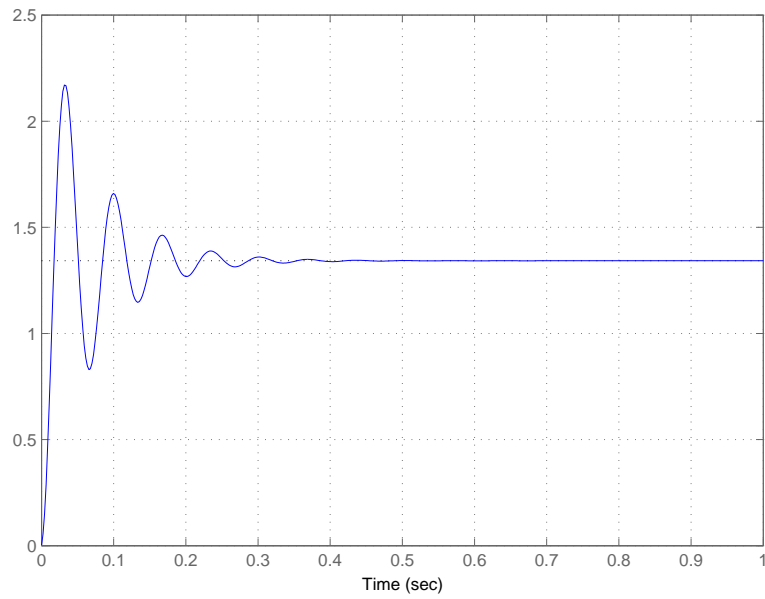


Figure 5.7. Step response for $G_{arx2}(s)$ in (5.1).

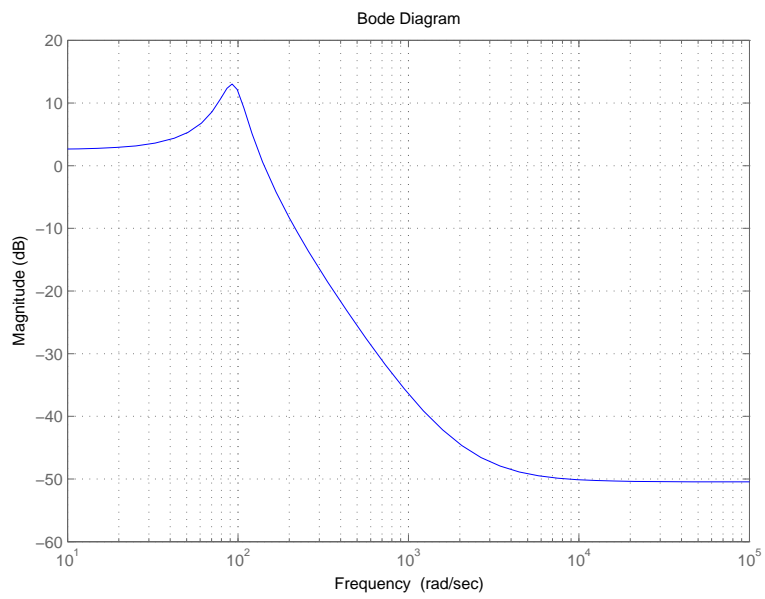


Figure 5.8. Bode magnitude plot for $G_{arx2}(s)$ in (5.1).

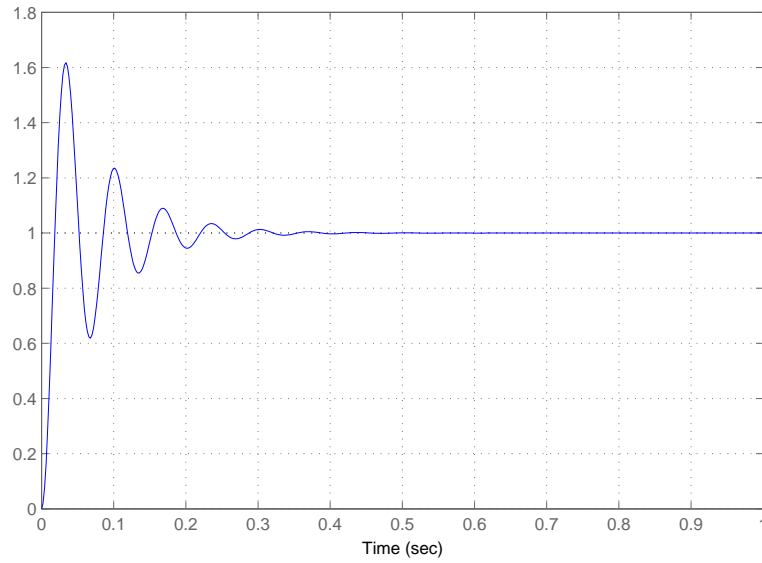


Figure 5.9. Step response for approximated $G(s)$ in (5.2).

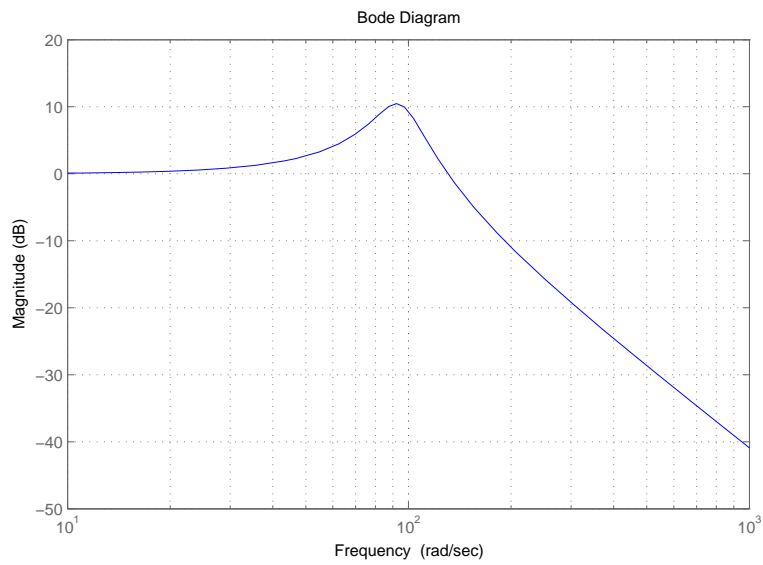


Figure 5.10. Bode magnitude plot for approximated $G(s)$ in (5.2).

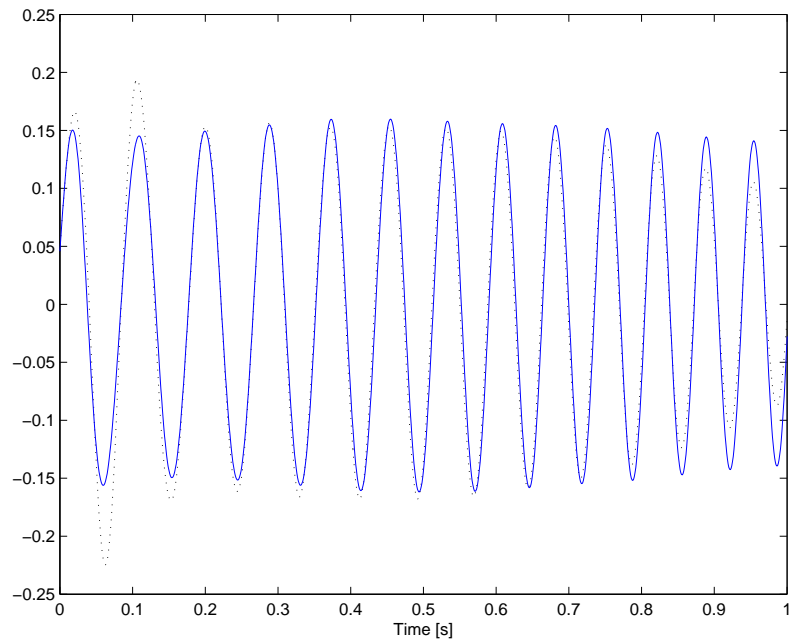


Figure 5.11. Model Prediction. Notation: validation data (dotted), predicted data (solid).

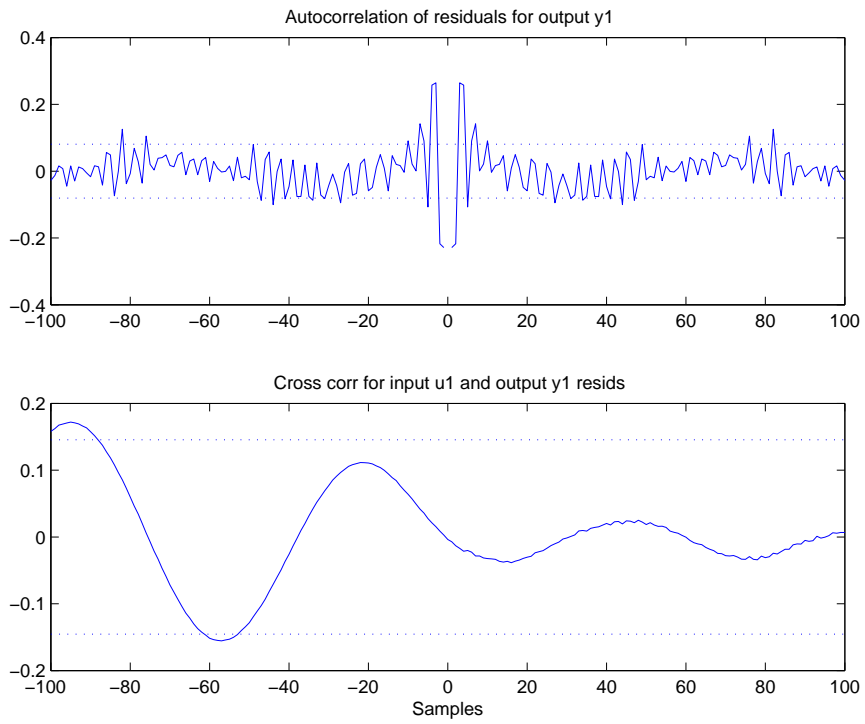


Figure 5.12. Plot with akf and cross correlation of residuals.

Chapter 6

Model Reference Adaptive Systems (MRAS)

In this chapter the model reference adaptive system is presented and discussed. Essentially, one approach to construct MRAS is presented: the Lyapunov stability theory approach.

6.1 Introduction

A model-reference adaptive system, abbreviated MRAS, is an important adaptive controller. What distinguishes an MRAS is that the desired behaviour is defined in a reference model. An advantage with having a reference model is that it makes specifying the behaviour of a servo system straightforward. Figure 6.1 is illustrated in (Wittenmark and Åström, 1995) and shows a block diagram of the system.

In the system the error between the process and the reference model determines how the controller parameters are updated. In this thesis Lyapunov stability theory is used to obtain the parameter update mechanism.

6.2 Lyapunov Theory

An elegant way for designing adaptive controllers that can guarantee stability of a system is Lyapunov stability theory (Glad and Ljung, 1997). Essentially, what Lyapunov theory is all about is transforming one difficult problem to another. Even though initially one may find this concept peculiar it turns out it is an excellent approach. The Lyapunov idea originates from mechanics, with stable and unstable equilibria.

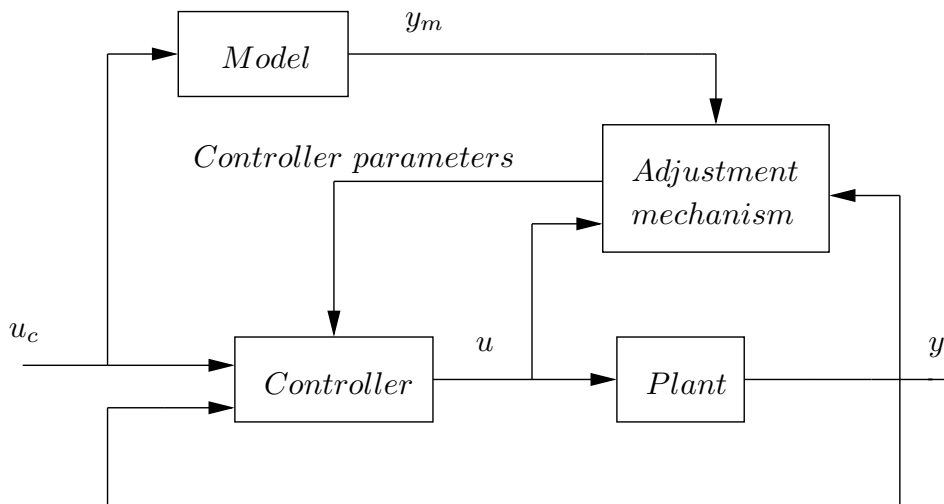


Figure 6.1. Block diagram of a model-reference adaptive system (MRAS).

6.2.1 Lyapunov Theory for Time-invariant Systems

Consider the solution $x(t) = 0$ to the nonlinear differential equation

$$\frac{dx}{dt} = f(x), \quad f(0) = 0 \quad (6.1)$$

where $f(x)$ is nonlinear. Furthermore, $f(x)$ needs to fulfil the Lipschitz conditions locally. To investigate whether the solution $x(t) = 0$ is stable or not with respect to initial conditions and variations in $f(x)$, the following Lyapunov concept is used (Wittenmark and Åström, 1995).

Definition 6.1 *The solution $x(t) = 0$ is called stable if for given $\epsilon > 0$ there exists a number $\delta(\epsilon) > 0$ such that all solutions with initial conditions*

$$\|x(0)\| < \delta$$

have the property

$$\|x(t)\| < \epsilon \quad (6.2)$$

for $0 \leq t < \infty$. The solution is unstable if it is not stable. The solution is asymptotically stable if it is stable and δ can be found such that all solutions with $\|x(0)\| < \delta$ have the property that $\|x(t)\| \rightarrow 0$ as $t \rightarrow \infty$. If the solution is asymptotically stable for any initial value, then it is said to be globally asymptotically stable. Notice that Lyapunov stability refers to stability of a particular solution and not to the differential equation.

□

It is possible to investigate stability by looking at functions with special properties. Positive definite functions can be used to describe these properties (Wittenmark and Åström, 1995).

Definition 6.2 A continuously differentiable function $V : R^n \rightarrow R$ is called positive definite in a region $U \subset R^n$ containing the origin if

$$V(0) = 0$$

$$V(x) > 0, x \in U, x \neq 0$$

A function is called positive semidefinite if the second condition is replaced by $V(x) \geq 0$.

□

An example of a positive definite function in the two-dimensional case is $V(x_1, x_2) = x_1^2 + x_2^2$. The following theorem is used to state whether a solution $x(t) = 0$ is stable or unstable (Wittenmark and Åström, 1995).

Theorem 6.1 If there exists a function $V : R^n \rightarrow R$ that is positive definite such that

$$\frac{dV}{dt} = \frac{\partial V^T}{\partial x} \frac{dx}{dt} = \frac{\partial V^T}{\partial x} f(x) = -W(x) \quad (6.3)$$

is negative semidefinite, then the solution $x(t) = 0$ is stable. If dV/dt is negative definite, then the solution is also asymptotically stable. The function V is called a Lyapunov function for the system (6.1). Moreover if

$$\frac{dV}{dt} < 0$$

$$V(x) \rightarrow \infty, \|x\| \rightarrow \infty$$

then the solution is globally asymptotically stable.

□

6.2.2 Finding Lyapunov Functions

Theoretically, the results from Theorem 6.1 are very promising but in practice there is no general technique for finding suitable Lyapunov functions. However, it turns out that quadratic functions can be used with the following theorem for linear systems (Wittenmark and Åström, 1995).

Theorem 6.2 Let the system

$$\frac{dx}{dt} = Ax \quad (6.4)$$

be stable. Pick Q positive definite. The equation

$$A^T P + PA = -Q \quad (6.5)$$

has always a unique solution with P positive definite and the function

$$V(x) = x^T P x \quad (6.6)$$

is a Lyapunov function. Equation (6.5) is called the Lyapunov equation.

□

The impact of this theorem is that for a stable linear system, it always exists a quadratic Lyapunov function. The next example is illustrated in (Wittenmark and Åström, 1995) and shows how the P matrix in Theorem 6.2 can be derived for a second-order system.

Example 6.1 Consider the system matrix

$$A = \begin{pmatrix} a_1 & a_2 \\ a_3 & a_4 \end{pmatrix}$$

where A is assumed to have all eigenvalues in the left half-plane. Let the matrix Q be

$$Q = \begin{pmatrix} q_1 & 0 \\ 0 & q_2 \end{pmatrix}$$

where q_1 and q_2 are positive. Assume that the matrix P has the form

$$P = \begin{pmatrix} p_1 & p_2 \\ p_2 & p_3 \end{pmatrix}$$

The Lyapunov equation becomes

$$\begin{pmatrix} 2a_1 & 2a_3 & 0 \\ a_2 & a_1 + a_4 & a_3 \\ 0 & 2a_2 & 2a_4 \end{pmatrix} \begin{pmatrix} p_1 \\ p_2 \\ p_3 \end{pmatrix} = \begin{pmatrix} -q_1 \\ 0 \\ -q_2 \end{pmatrix}$$

6.2.3 Lyapunov Theory for Time-variable Systems

Consider the solution $x(t) = 0$ to the nonlinear time-variable differential equation

$$\frac{dx}{dt} = f(x, t) \quad (6.7)$$

where $f(x, t)$ is nonlinear. Furthermore $x(t) = 0$ is called an equilibrium point for (6.7) if $f(0, t) = 0, \forall t \geq 0$. In analogy with previous discussions a guarantee that a solution exists and is unique is that $f(x, t)$ needs to be piecewise continuous in t and locally Lipschitz in x in a neighbourhood of the origin. To investigate whether the solution $x(t) = 0$ is stable with respect to initial conditions and variations in $f(x, t)$, the following Lyapunov concept is used (Wittenmark and Åström, 1995).

Definition 6.3 The solution $x(t) = 0$ is uniformly stable if for $\epsilon > 0$ there exists a number $\delta(\epsilon) > 0$, independent of t_0 , such that

$$\|x(t_0)\| < \delta \Rightarrow \|x(t)\| < \epsilon, \forall t \geq t_0 \geq 0$$

The solution is uniformly asymptotically stable if it is uniformly stable and there is $c > 0$, independent of t_0 , such that $x(t) \rightarrow 0$ as $t \rightarrow \infty$, uniformly in t_0 , for all $\|x(t_0)\| < c$.

□

The class *K functions* are introduced to help state a stability theorem for solutions $x(t) = 0$ to (6.7) (Wittenmark and Åström, 1995).

Definition 6.4 A continuous function $\alpha : [0, a[\rightarrow [0, \infty[$ is said to belong to class *K* if it is strictly increasing and $\alpha(0) = 0$. It is said to belong to class K_∞ if $a = \infty$ and $\alpha(r) \rightarrow \infty$ as $r \rightarrow \infty$.

□

The following stability theorem for time-varying systems is stated with use of the class *K functions* (Wittenmark and Åström, 1995).

Theorem 6.3 Let $x(t) = 0$ be an equilibrium point and $D = \{x \in R^n \mid \|x(t)\| < r\}$. Let V be a continuously differentiable function such that

$$\begin{aligned} \alpha_1(\|x(t)\|) &\leq V(x, t) \leq \alpha_2(\|x(t)\|) \\ \frac{dV}{dt} &= \frac{\partial V}{\partial t} + \frac{\partial V}{\partial x} f(x, t) \leq -\alpha_3(\|x(t)\|) \end{aligned}$$

for $\forall t \geq 0$, where α_1, α_2 and α_3 are class *K functions*. Then $x(t) = 0$ is uniformly asymptotically stable.

□

Quite often when Lyapunov theory is applied on adaptive control problems, dV/dt is only negative semidefinite. This implies that necessary conditions to use Theorem 6.3 are not fulfilled. Nevertheless, *Barbalat's lemma* gives a suitable result (Wittenmark and Åström, 1995).

Lemma 6.1 If g is a real function of a real variable t , defined and uniformly continuous for $t \geq 0$, and if the limit of the integral

$$\int_0^t g(s) ds$$

as $t \rightarrow \infty$ exists and is a finite number, then

$$\lim_{t \rightarrow \infty} g(t) = 0$$

□

It turns out that when Lyapunov theory is applied to adaptive control problems, the time derivative of the Lyapunov function V depends on the control signal and other signals in the system. Barbalat's lemma and its result are used on dV/dt to prove stability with bounded signals (Wittenmark and Åström, 1995).

Theorem 6.4 *Let $D = \{x \in R^n \mid \|x(t)\| < r\}$ and suppose that $f(x, t)$ is locally Lipschitz on $D \times [0, \infty[$. Let V be a continuously differentiable function such that*

$$\alpha_1(\|x(t)\|) \leq V(x, t) \leq \alpha_2(\|x(t)\|)$$

and

$$\frac{dV}{dt} = \frac{\partial V}{\partial t} + \frac{\partial V}{\partial x} f(x, t) \leq -W(x) \leq 0$$

$\forall t \geq 0, \forall x \in D$, where α_1 and α_2 are class K functions defined on $[0, r[$ and $W(x)$ is continuous on D . Further, it is assumed that dV/dt is uniformly continuous in t . Then all solutions $x(t) = 0$ with $\|x(t_0)\| < \alpha_2^{-1}(\alpha_1(r))$ are bounded and satisfy

$$W(x(t)) \rightarrow 0, t \rightarrow \infty$$

Moreover, if all the assumptions hold globally and $\alpha_1 \in K_\infty$, the statement is true for all $x(t_0) \in R^n$.

□

Theorem 6.4 implies bounded states that move towards the set $\{x \in D \mid W(x) = 0\}$. Moreover, the theorem assumes that dV/dt is uniformly continuous. If \dot{V} is bounded it implies that dV/dt is uniformly continuous.

The next example is illustrated in (Wittenmark and Åström, 1995) and shows how Lyapunov stability theory is used to create MRAS. The first step is to derive a differential equation for the error, $e = y - y_m$. A Lyapunov function V and an adaptation mechanism is found such that the error goes towards zero. The time-derivative of V , dV/dt is negative semidefinite, however the Lyapunov function has a bounded second derivative. Finally, Theorem 6.4 is used to show boundedness and that the error goes towards zero.

Example 6.2 *Consider a system described by the model*

$$\frac{dy}{dt} = -ay + bu$$

where u is the control signal and y is the measured output. Assume it is desired to obtain a closed-loop system described by

$$\frac{dy_m}{dt} = -a_m y_m + b_m u_c$$

where $a_m > 0$ and the reference signal u_c is bounded. Let the controller be described by

$$u = \theta_1 u_c - \theta_2 y$$

Introduce the error

$$e = y - y_m$$

The differential equation for the error becomes

$$\frac{de}{dt} = -a_m e - (b\theta_2 + a - a_m)y + (b\theta_1 - b_m)u_c$$

The next attempt is to construct a parameter adjustment mechanism that will drive the parameters θ_1 and θ_2 to their desired values. For this purpose, assume that $b\gamma > 0$ and introduce the following quadratic function

$$V(e, \theta_1, \theta_2) = \frac{1}{2} \left(e^2 + \frac{1}{b\gamma} (b\theta_2 + a - a_m)^2 + \frac{1}{b\gamma} (b\theta_1 - b_m)^2 \right)$$

The function is zero when e is zero and the controller parameters are equal to the correct values. For the function to qualify as a Lyapunov function the derivative dV/dt must be negative. The derivative is

$$\begin{aligned} \frac{dV}{dt} &= e \frac{de}{dt} + \frac{1}{\gamma} (b\theta_2 + a - a_m) \frac{d\theta_2}{dt} + \frac{1}{\gamma} (b\theta_1 - b_m) \frac{d\theta_1}{dt} \\ &= -a_m e^2 + \frac{1}{\gamma} (b\theta_2 + a - a_m) \left(\frac{d\theta_2}{dt} - \gamma y e \right) \\ &\quad + \frac{1}{\gamma} (b\theta_1 - b_m) \left(\frac{d\theta_1}{dt} + \gamma u_c e \right) \end{aligned}$$

With parameters updated as

$$\begin{aligned} \frac{d\theta_1}{dt} &= -\gamma u_c e \\ \frac{d\theta_2}{dt} &= \gamma y e \end{aligned}$$

the derivative becomes

$$\frac{dV}{dt} = -a_m e^2$$

The derivative of V with respect to time is thus negative semidefinite but not negative definite. This implies that $V(t) \leq V(0)$ and thus that e, θ_1 and θ_2 must be bounded. This implies that $y = e + y_m$ also is bounded. To use Theorem 6.4, the second derivative is determined

$$\frac{d^2V}{dt^2} = -2a_m e \frac{de}{dt} = -2a_m e (-a_m e - (b\theta_2 + a - a_m)y + (b\theta_1 - b_m)u_c)$$

Since u_c , e , and y are bounded, it follows that \ddot{V} is bounded and thus from earlier discussions dV/dt is uniformly continuous. From Theorem 6.4 it now follows that the error e will go to zero. Again, the parameters will not necessarily converge to their correct values; it is shown only that they are bounded. To have parameter convergence, it is necessary to impose conditions on the excitation of the system.

The adjustment rule from Lyapunov theory is straightforward and does not require filtering of the signals u_c and y , that is

$$\frac{d\theta}{dt} = \gamma \psi e$$

where θ is a vector of parameters and

$$\psi = (-u_c \ y)^T$$

for the Lyapunov rule. A block diagram of the system is shown in Figure 6.2.

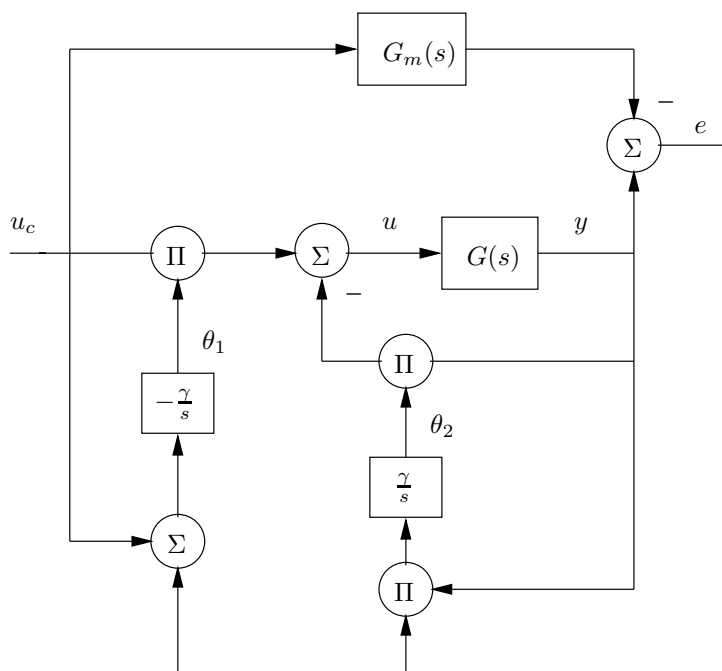


Figure 6.2. Block diagram of an MRAS based on Lyapunov theory for a first-order process.

6.2.4 State Feedback

In the next step, Lyapunov theory is used to derive stable MRASs for general linear systems with state feedback. The approach is the same as before

- Choose a controller structure.
- Derive the error equation.

- Choose a Lyapunov function. Use it to derive a parameter update mechanism such that the error goes to zero.

Consider a process model described by

$$\frac{dx}{dt} = Ax + Bu \quad (6.8)$$

Assume that for a given control law the response to command signals is given by

$$\frac{dx_m}{dt} = A_m x_m + B_m u_c \quad (6.9)$$

Let the controller be described by

$$u = M u_c - L x \quad (6.10)$$

The closed-loop system then becomes

$$\frac{dx}{dt} = (A - BL)x + B M u_c = A_c(\theta)x + B_c(\theta)u_c \quad (6.11)$$

Usually L and M are chosen to form the vector

$$\theta = \begin{pmatrix} L^T \\ M \end{pmatrix} \quad (6.12)$$

A good approach is to assume that the closed-loop system is described by (6.11), where matrices A_c and B_c depend on a parameter vector θ . Sometimes θ cannot be chosen such that (6.11) equals (6.9). According to (Wittenmark and Åström, 1995) a condition is that there exists a parameter θ^0 with

$$\begin{aligned} A_c(\theta^0) &= A_m \\ B_c(\theta^0) &= B_m \end{aligned} \quad (6.13)$$

Furthermore, when all control parameters can be chosen arbitrarily, it implies that

$$\begin{aligned} A - A_m &= BL \\ B_m &= BM \end{aligned}$$

Establish the error

$$e = x - x_m \quad (6.14)$$

Equation (6.9) subtracted from (6.8) gives

$$\frac{de}{dt} = \frac{dx}{dt} - \frac{dx_m}{dt} = Ax + Bu - A_m x_m - B_m u_c \quad (6.15)$$

According to (Wittenmark and Åström, 1995) it can be shown that (6.15) can be written as

$$\frac{de}{dt} = A_m e + \Psi(\theta - \theta^0) \quad (6.16)$$

Introduce the following quadratic function

$$V(e, \theta) = \frac{1}{2} \left(\gamma e^T P e + (\theta - \theta^0)^T (\theta - \theta^0) \right)$$

where P is a positive definite matrix and the function V is positive definite. To find out whether V is a Lyapunov function, its total time derivative is derived

$$\begin{aligned} \frac{dV}{dt} &= -\frac{\gamma}{2} e^T Q e + \gamma (\theta - \theta^0)^T \Psi^T P e + (\theta - \theta^0)^T \frac{d\theta}{dt} \\ &= -\frac{\gamma}{2} e^T Q e + (\theta - \theta^0)^T \left(\frac{d\theta}{dt} + \gamma \Psi^T P e \right) \end{aligned}$$

where the matrix Q is positive definite and fulfils (6.17)

$$A_m^T P + P A_m = -Q \quad (6.17)$$

If A_m is stable it follows from Theorem 6.2 that a pair of positive matrices P and Q exists. With the parameter adjustment law according to

$$\frac{d\theta}{dt} = -\gamma \Psi^T P e \quad (6.18)$$

the total time derivative becomes

$$\frac{dV}{dt} = -\frac{\gamma}{2} e^T Q e \quad (6.19)$$

The time derivative (6.19) is negative semidefinite. However, Barbalat's lemma can be used to show that the error e goes to zero. Notice that in order to derive the parameter update law it has been assumed that all states x are measurable.

6.2.5 Advantages with Lyapunov Stability Theory

It is possible to construct parameter adjustment rules based on Lyapunov's stability theory. The adaptive laws have guaranteed stability. The adjustment rules guarantee that the error goes to zero. Finally, arbitrarily high adaptation gains can be used.

6.3 Summary

Chapter 6 introduces the concept of MRAS. Lyapunov stability theory is introduced, and it is shown how Lyapunov theory can be used to construct stable MRAS. Essentially, the idea is to transform the existing problem to another where Lyapunov theory can be used. The major impact is that arbitrarily high adaptation gains can be used. This property depends on strong assumptions, such as: bounded signals, all states are measurable, and no input saturation.

Chapter 7

Adaptive Control

The study in this chapter will be based on the extended and complete system in Figure 7.1. It will be presented how adaptive control based upon Lyapunov stability theory can be applied to the complete system.

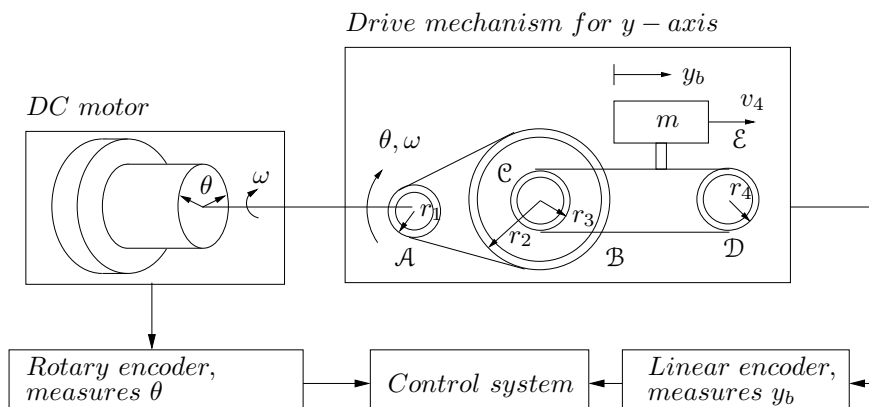


Figure 7.1. Block diagram for the total system.

7.1 System Description

According to the Figure 7.1, the total system consists of a DC motor connected to the drive mechanism introduced in Section 3.3.1. The input to the open-loop system is the armature current i_a , and the output is y_b , which is the bridge position. The motor shaft angle θ is derived from rotary encoder readings and the bridge position from linear encoder readings. Thus the system has one input and two outputs. The motor shaft angle θ and the bridge position y_b are sent to the controller in Figure 7.1. Since one of the goals from the problem description is to use a rotary

encoder, tachometer readings are neglected. The controller of the system is going to be implemented in two steps. The idea is to consider the system consisting of the DC motor initially and then connect that system in series with the drive mechanism.

7.1.1 DC Motor System

The DC motor system has the armature current i_a as input and motor shaft angle θ as output. In this system θ is measurable from rotary encoder readings. The transfer function is given by

$$G_{i_a, \theta}(s) = \frac{k_0}{s^2}$$

where k_0 depends on the rotor inertia of the motor. Notice that this transfer function is an approximation of

$$G(s) = \frac{k_0/\tau}{s(s + \frac{1}{\tau})}$$

To provide for both angle and velocity feedback; θ, ω , an observer is implemented. The estimates $\hat{\theta}$ and $\hat{\omega}$ are being fed back with a gain vector L_1 . The bandwidth of the closed-loop system is chosen to be 200 Hz.

7.1.2 The Total System

This system consists of the DC motor connected in series with the drive mechanism. The bandwidth of the closed-loop system around the DC motor is 200 Hz. The transfer function for the drive mechanism is given by

$$G_{\theta, y_b}(s) = \frac{k}{s^2 + as + b}$$

where $a = 28.65$ and $b = 8931$. To eliminate the observed oscillations (see Section 5.2) an MRAS is implemented. The resonance frequency of the derived and estimated model is 15 Hz with a damping of 0.11. The MRAS moves the poles of the closed-loop system to the desired location, a system with bandwidth 10 Hz and damping $\zeta_2 = 1$. Since the desired system has a bandwidth of 10 Hz, the inner loop around the motor with a bandwidth of 200 Hz can be neglected. Thus, the transfer function for the DC motor can be replaced by a static gain constant k . This implies that the reference model only has to be second order.

7.2 Control of the DC Motor

Consider the DC motor system in Figure 7.2, where the system has feedback from reconstructed states. The input signal i_a is being affected by non measurable noise w_{i_a} . In similar fashion, the process or the DC motor is being affected by non

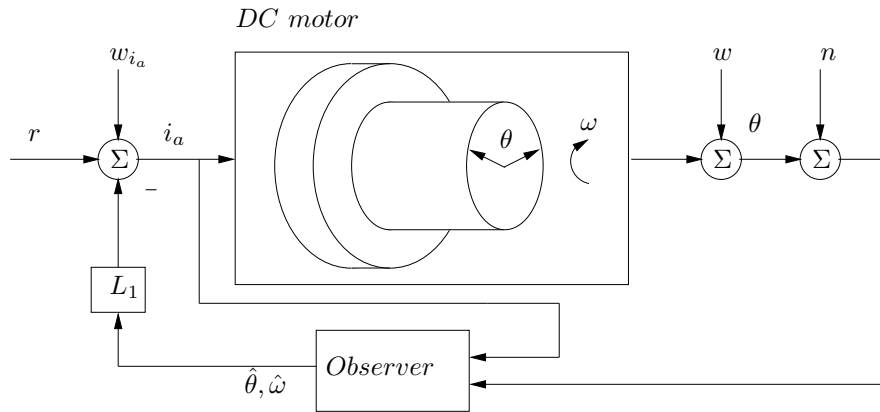


Figure 7.2. Block diagram for the DC motor system.

measurable process noise w . Finally, n denotes the measurable noise affecting the rotary encoder. The transfer function from input to output is given by

$$G_{i_a, \theta}(s) = \frac{k_0}{s^2}$$

where the numerator is

$$k_0 = \frac{k_T k_{VA}}{J}$$

Given and desired constants for the system are:

- $J = 5.86 \cdot 10^{-5} \text{ Nm s}^2$, rotor inertia of the DC motor.
- $k_T = 0.08 \text{ Nm/A}$, torque constant of the DC motor.
- $k_{VA} = 3$, conversion from Volt to Ampere.
- $\omega_1 = 2\pi \cdot 200 \text{ rad/s}$, desired bandwidth of the closed-loop system.
- $\zeta_1 = 1/\sqrt{2}$, desired damping of the closed-loop system.

Introduce the states

$$\begin{aligned} x_1 &= \theta \\ x_2 &= \omega \\ u &= i_a \end{aligned}$$

In state space form the system is written as

$$\begin{aligned} \frac{dx}{dt} &= A_1 x + B_1 u \\ \theta &= C_1 x \end{aligned}$$

where

$$A_1 = \begin{pmatrix} 0 & 1 \\ 0 & 0 \end{pmatrix} \quad (7.1)$$

$$B_1 = \begin{pmatrix} 0 \\ k_0 \end{pmatrix} \quad (7.2)$$

$$C_1 = \begin{pmatrix} 1 & 0 \end{pmatrix} \quad (7.3)$$

The following observer is chosen

$$\frac{d\hat{x}}{dt} = A_1\hat{x} + B_1u + K_1(y - C_1\hat{x})$$

where the observer gain is

$$K_1 = \begin{pmatrix} k_1 \\ k_2 \end{pmatrix} \quad (7.4)$$

Feedback is taken from the estimated states of the observer according to the control law

$$u = -L_1\hat{x} + r$$

where the feedback gain is

$$L_1 = \begin{pmatrix} l_{11} & l_{12} \end{pmatrix}$$

The transfer function of the closed-loop system is given by (Glad and Ljung, 1989)

$$G_c(s) = C_1(sI - A_1 + B_1L_1)^{-1}B_1 \quad (7.5)$$

If the feedback gain is chosen to be

$$L_1 = \begin{pmatrix} \frac{\omega_1^2}{k_0} & \frac{2\zeta_1\omega_1}{k_0} \end{pmatrix} \quad (7.6)$$

equations (7.1)-(7.3) and (7.6) in (7.5) give the following expression for the transfer function of the closed-loop system

$$G_{c_1}(s) = \frac{k_0}{s^2 + 2\zeta_1\omega_1s + \omega_1^2} \quad (7.7)$$

However, to simplify further stability and robustness investigation it is desired to rewrite the system. Introduce the following two transfer functions

$$\begin{aligned} F_r &= 1 - L_1(sI - A_1 + K_1C_1 + B_1L_1)^{-1}B_1 \\ F_\theta &= L_1(sI - A_1 + K_1C_1 + B_1L_1)^{-1}K_1 \end{aligned} \quad (7.8)$$

With (7.1)-(7.4) and (7.6) in (7.8), the transfer functions become

$$\begin{aligned} F_r &= \frac{s^2 + k_1s + k_2}{s^2 + (k_1 + 2\zeta_1\omega_1)s + k_2 + \omega_1^2 + 2k_1\zeta_1\omega_1} \\ F_\theta &= \frac{\omega_1}{k} \frac{(k_1\omega_1 + 2\zeta_1k_2)s + \omega_1k_2}{s^2 + (k_1 + 2\zeta_1\omega_1)s + k_2 + \omega_1^2 + 2k_1\zeta_1\omega_1} \end{aligned} \quad (7.9)$$

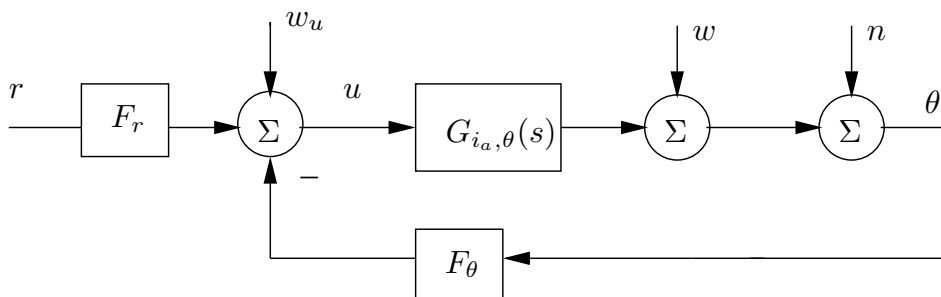


Figure 7.3. The modified block diagram for the DC motor system.

It follows that the system in Figure 7.2 is equivalent to the system given in Figure 7.3, with transfer functions according to (7.1) and (7.9) (Glad and Ljung, 1989).

Again, the input signal u is being affected by non measurable noise w_u . In similar fashion, the process $G_{i_a, \theta}(s)$ is being affected by non measurable process noise w . Finally, n denotes the measurable noise affecting the rotary encoder.

7.3 Control of the Total System

Consider to total system in Figure 7.4. It follows from earlier discussions that the inner loop with the DC motor system (the dotted box in Figure 7.4) can be ignored when the MRAS is constructed. In the derivations that follow, the DC motor system is replaced by a static gain with constant k . Thus, the goal is to determine a second-order MRAS for the drive mechanism.

Again, the transfer function corresponding to the drive mechanism is given by

$$G_{\theta, y_b}(s) = \frac{k}{s^2 + as + b}$$

To simplify further work, the numerator is chosen to be $k = 1$. Introduce the states

$$\begin{aligned} x_1 &= y_b \\ x_2 &= \dot{y}_b \end{aligned}$$

where y_b and \dot{y}_b are the position and speed of the bridge respectively. In state space form the system becomes

$$\frac{dx}{dt} = A_2x + B_2u \quad (7.10)$$

$$y_b = C_2x$$

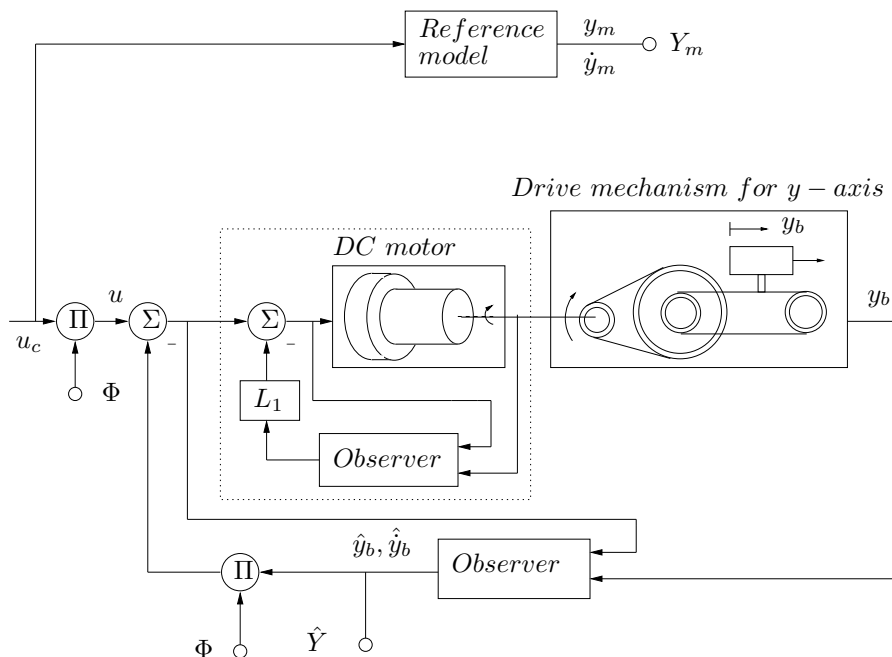


Figure 7.4. Block diagram of the total system. The bandwidth of the total closed-loop system is chosen to be 10Hz. The dotted box around the DC motor system implies it is a system with a bandwidth of 200 Hz. Since this bandwidth is so much higher than the outer closed-loop, the DC motor system is neglected in the MRAS construction.

where

$$A_2 = \begin{pmatrix} 0 & 1 \\ -b & -a \end{pmatrix} \quad (7.11)$$

$$B_2 = \begin{pmatrix} 0 \\ 1 \end{pmatrix} \quad (7.12)$$

$$C_2 = (1 \ 0) \quad (7.13)$$

Analogous with Example 6.2 the procedure to derive a stable MRAS for the system is summarized as follows:

- Choose a controller structure.
- Derive the error equation.
- Find a Lyapunov function and use it to derive a parameter updating law such that the error goes to zero.

Given and desired constants for the system are:

- $a = 28.65$, estimated parameter for the drive mechanism.
- $b = 8931$, estimated parameter for the drive mechanism.
- $\zeta_2 = 1$, desired damping of the total closed-loop system.
- $\omega_2 = 2\pi \cdot 10 \text{ rad/s}$, desired bandwidth of the closed-loop system.

The desired response to a command signal is given by the transfer function

$$G_m(s) = \frac{0.1\omega_2^2}{s^2 + 2\zeta_2\omega_2s + \omega_2^2} \quad (7.14)$$

The factor 0.1 in the numerator of (7.14) is chosen to give a reasonable metric displacement with respect to an input signal. Introduce the states

$$\begin{aligned} x_{m1} &= y_m \\ x_{m2} &= \dot{y}_m \end{aligned}$$

where y_m , and \dot{y}_m are the desired position and speed of the bridge respectively. In state space form the system becomes

$$\frac{dx_m}{dt} = A_m x_m + B_m u_c \quad (7.15)$$

$$y = C_m x_m$$

where

$$A_m = \begin{pmatrix} 0 & 1 \\ -\omega_2^2 & -2\zeta_2\omega_2 \end{pmatrix} \quad (7.16)$$

$$B_m = \begin{pmatrix} 0 \\ 0.1\omega_2^2 \end{pmatrix} \quad (7.17)$$

$$C_m = (1 \quad 0) \quad (7.18)$$

Choose the control law

$$u = M u_c - L_2 x \quad (7.19)$$

where

$$M = \phi_3 \quad (7.20)$$

$$L_2 = \begin{pmatrix} \phi_1 \\ \phi_2 \end{pmatrix} \quad (7.21)$$

The closed-loop system then becomes

$$\frac{dx}{dt} = (A_2 - B_2 L_2)x + B_2 M u_c = A_c(\Phi)x + B_c(\Phi)u_c \quad (7.22)$$

with

$$A_c(\Phi) = \begin{pmatrix} 0 & 1 \\ -b - \phi_1 & -a - \phi_2 \end{pmatrix} \quad (7.23)$$

$$B_c(\Phi) = \begin{pmatrix} 0 \\ \phi_3 \end{pmatrix} \quad (7.24)$$

Introduce the error equation

$$e = x - x_m = \begin{pmatrix} x_1 - x_{m1} \\ x_2 - x_{m2} \end{pmatrix} = \begin{pmatrix} e_1 \\ e_2 \end{pmatrix} \quad (7.25)$$

Subtracting (7.15) from (7.10) gives

$$\frac{de}{dt} = \frac{dx}{dt} - \frac{dx_m}{dt} \quad (7.26)$$

Analogous with the discussions in Chapter 6 and (6.15)-(6.16), (7.26) can be written as

$$\frac{de}{dt} = A_m e + \Psi(\Phi - \Phi^0) \quad (7.27)$$

where

$$\Psi = \begin{pmatrix} 0 & 0 & 0 \\ -x_1 & -x_2 & u_c \end{pmatrix} \quad (7.28)$$

$$\Phi = \begin{pmatrix} \phi_1 \\ \phi_2 \\ \phi_3 \end{pmatrix}$$

$$\Phi^0 = \begin{pmatrix} \omega_2^2 - b \\ 2\zeta_2\omega_2 - a \\ 0.1\omega_2^2 \end{pmatrix}$$

The same quadratic function as in Chapter 6 and (6.17) is chosen, that is

$$V(e, \Phi) = \frac{1}{2}(\gamma e^T P e + (\Phi - \Phi^0)^T (\Phi - \Phi^0))$$

where P is a positive definite matrix of the form

$$P = \begin{pmatrix} p_1 & p_2 \\ p_2 & p_3 \end{pmatrix} \quad (7.29)$$

and the function V is positive definite. To find out whether V is a Lyapunov function, its total time derivative is derived

$$\begin{aligned} \frac{dV}{dt} &= -\frac{\gamma}{2} e^T Q e + \gamma(\Phi - \Phi^0)^T \Psi^T P e + (\Phi - \Phi^0)^T \frac{d\Phi}{dt} \\ &= -\frac{\gamma}{2} e^T Q e + (\Phi - \Phi^0)^T \left(\frac{d\Phi}{dt} + \gamma \Psi^T P e \right) \end{aligned}$$

where Q is positive definite and such that

$$A_m^T P + P A_m = -Q$$

Since A_m is stable for the desired model, it follows from Theorem 6.2 that a pair of positive definite matrices P and Q with this property always exists. With the parameter adjustment law according to

$$\frac{d\Phi}{dt} = -\gamma\Psi^T P e \quad (7.30)$$

the total time derivative becomes

$$\frac{dV}{dt} = -\frac{\gamma}{2} e^T Q e \quad (7.31)$$

The time derivative of the Lyapunov function is negative semidefinite. By using Barbalat's lemma in the same way as in Example 6.2 it can be shown that the error e goes to zero. With (7.25), (7.28), (7.29) in (7.30) the parameter adjustment law takes the form

$$\frac{d\Phi}{dt} = \begin{pmatrix} \gamma x_1(p_2 e_1 + p_3 e_2) \\ \gamma x_2(p_2 e_1 + p_3 e_2) \\ -\gamma u_c(p_2 e_1 + p_3 e_2) \end{pmatrix} \quad (7.32)$$

Since it is assumed that all states x are measurable, one observer is derived for the process; see Figure 7.4.

7.3.1 Process Observer

The following observer is chosen for the process

$$\frac{d\hat{x}}{dt} = A_2 \hat{x} + B_2 u + K_2 (y_b - C_2 \hat{x})$$

where the observer gain is

$$K_2 = \begin{pmatrix} k_3 \\ k_4 \end{pmatrix} \quad (7.33)$$

Feedback is taken from the estimated states of the observer according to the control law

$$u = -L_2 \hat{x} + M u_c$$

The transfer function of the closed-loop system for the process is given by

$$G_{c_{tot}}(s) = C_2 (sI - A_2 + B_2 L_2)^{-1} B_2 M \quad (7.34)$$

The expression is derived from a minor manipulation of what is given in (Glad and Ljung, 1989). With (7.11)-(7.13) and (7.20), (7.21) in (7.34) the transfer function becomes

$$G_{c_{tot}}(s) = \frac{\phi_3}{s^2 + (\phi_2 + a)s + \phi_1 + b} \quad (7.35)$$

When the command signal u_c has continuous excitation, the controller parameters will converge to their desired values, that is

$$\Phi = \begin{pmatrix} \omega_2^2 - b \\ 2\zeta_2 \omega_2 - a \\ 0.1 \omega_2^2 \end{pmatrix} \quad (7.36)$$

To verify that the closed-loop system will have its desired behavior, (7.36) in (7.35) gives

$$G_{c_{tot}}(s) = \frac{0.1\omega_2^2}{s^2 + 2\zeta_2\omega_2s + \omega_2^2} \quad (7.37)$$

which is the desired response to a command signal. To simplify further stability and robustness investigation it is desired to rewrite the system. Introduce the following two transfer functions

$$\begin{aligned} F_{u_c} &= (1 - L_2(sI - A_2 + K_2C_2 + B_2L_2)^{-1}B_2)M \\ F_{y_b} &= L_2(sI - A_2 + K_2C_2 + B_2L_2)^{-1}K_2 \end{aligned} \quad (7.38)$$

With (7.11)-(7.13), (7.21) and (7.33) in (7.38), the transfer functions become

$$\begin{aligned} F_{u_c} &= \frac{(s^2 + (k_3 + a)s + b + k_4 + k_3a)\phi_3}{s^2 + (a + \phi_2 + k_3)s + k_3a + k_3\phi_2 + b + k_4 + \phi_1} \\ F_{y_b} &= \frac{(k_3\phi_1 + k_4\phi_2)s + (k_3a + k_4)\phi_1 - k_3\phi_2b}{s^2 + (a + \phi_2 + k_3)s + k_3a + k_3\phi_2 + b + k_4 + \phi_1} \end{aligned} \quad (7.39)$$

It follows that the system in Figure 7.4 is equivalent to the system given in Figure 7.5, with transfer functions according to (7.10) and (7.39) (Glad and Ljung, 1989). For simplicity, the reference model is not included in Figure 7.5.

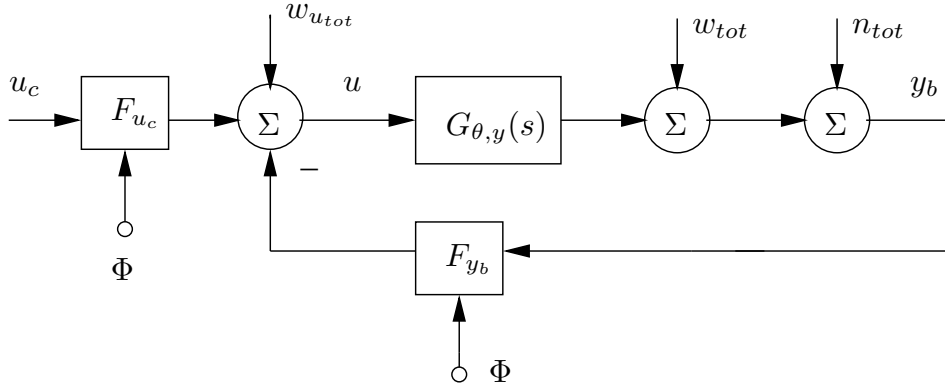


Figure 7.5. The modified block diagram for the total system. The reference model and the adjustment mechanism are not included.

The input signal u is being affected by non measurable noise $w_{u_{tot}}$. In similar fashion, the process $G_{\theta,y}(s)$ is being affected by non measurable process noise w_{tot} . Finally, n_{tot} denotes the measurable noise affecting the linear encoder.

7.4 Simulations

In this section simulations of the DC motor system and the total adaptive system are shown and discussed.

7.4.1 Simulation of the DC Motor System

Figure 7.6 shows the result of a step response of the DC motor system in Figure 7.2. To have unity gain of the closed-loop system, the numerator of the transfer function in (7.7) is chosen to be $k_0 = \omega_1^2$. Further, the observer gain is chosen to be

$$K_1 = \begin{pmatrix} 2\xi_1 \\ 2\xi_1^2 \end{pmatrix}$$

where $\xi_1 = 2\pi \cdot 400$, which is found to give good results. The input signal to the system is the reference signal r and the output signal is the motor shaft angle θ . As desired, the step response has a small overshoot; the DC motor system has damping $\zeta_1 = 1/\sqrt{2}$. Furthermore, the system has a short rise-time.

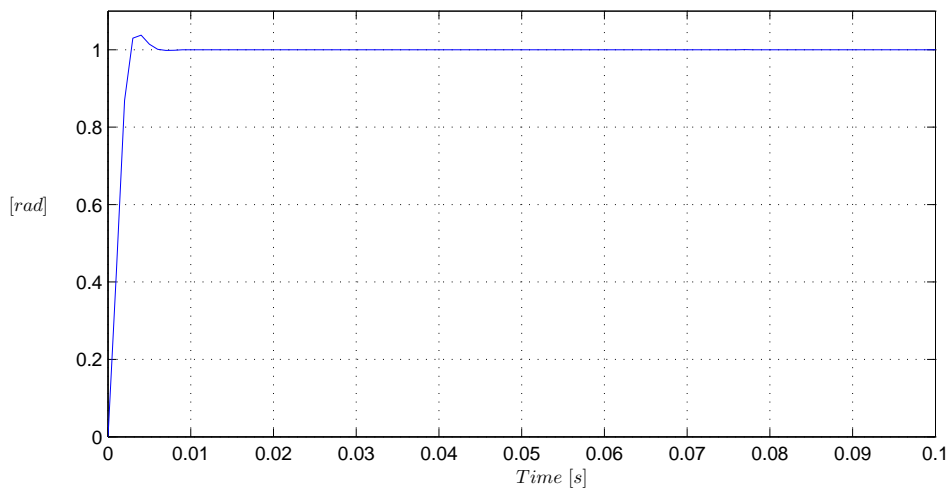


Figure 7.6. Result of a step response for the DC motor system. Notation: the motor shaft angle θ is plotted in radians.

7.4.2 Simulation of the Total System

Figure 7.7 shows the result of a simulation of the total system in in Figure 7.4. The observer gains are chosen to be

$$K_1 = \begin{pmatrix} 2\xi_1 \\ 2\xi_1^2 \end{pmatrix}$$

$$K_2 = \begin{pmatrix} 2\xi_2 - a \\ 2\xi_2^2 - a(2\xi_2 - a) - b \end{pmatrix}$$

where $\xi_1 = 2\pi \cdot 400$, $\xi_2 = 2\pi \cdot 50$. These choices are found to give good results. The output signal is the position of the bridge y_b . The reference signal u_c is a square wave with amplitude 1 and frequency 0.5 Hz. The adaptation gain is $\gamma = 10000$. The system adapts rather fast, and there is almost no difference between process and model output at time $t = 15$ s. Furthermore, the adaptation gain γ can be chosen even higher. The idea of the simulation is to prove that the adaptation mechanism works.

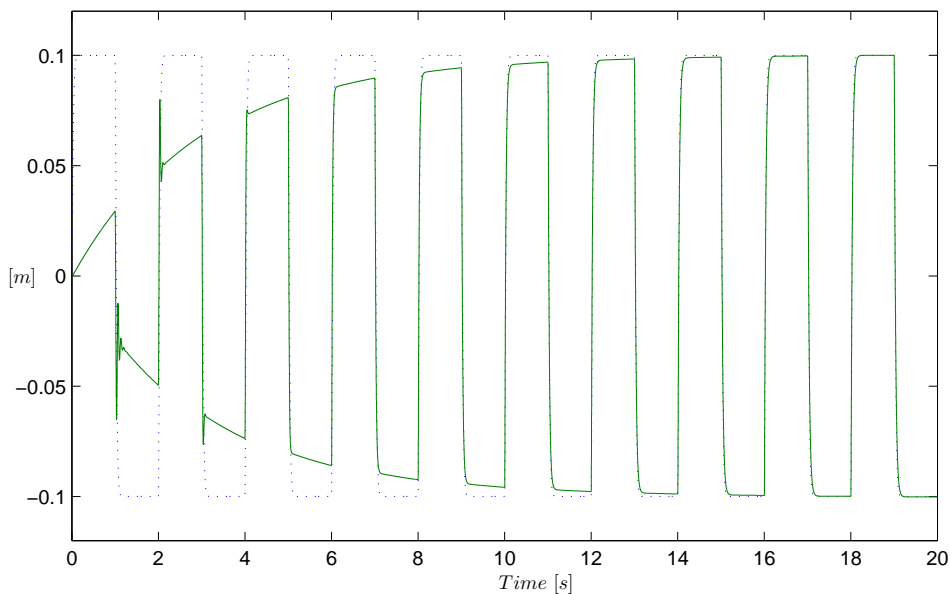


Figure 7.7. Simulation result of the total system. Notation: process output y_b (solid), model output y_m (dotted).

7.5 Stability of the Closed-loop System

Consider the system in Figure 7.8. The *Nyquist Stability Criterion* can be used to determine whether the closed-loop system is stable or not.

Theorem 7.1 *The number of poles in the right half plane of the closed-loop system in Figure 7.8, is equal to the number of poles in the right half plane for $G_0 = GF_y$, plus the amount of revolutions the curve in the Nyquist diagram encircles the point -1 .*

If G_0 does not have poles in the right half plane, the stability criterion for the closed-loop system states that the point -1 must not be encircled by the curve in the Nyquist diagram.

□

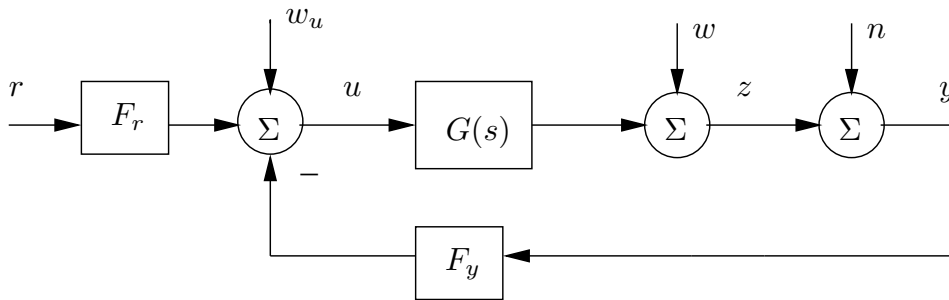


Figure 7.8. The closed-loop system.

The Nyquist criterion is investigated for the closed-loop systems of the DC motor system and finally to the total system.

7.5.1 Closed-loop System of the DC Motor

Consider the system in Figure 7.3. To be able to use the Nyquist criterion G_0 is determined numerically

$$G_0 = G_{i_a, \theta} F_{\theta} = \frac{4.799 \cdot 10^{16} s + 3.15 \cdot 10^{19}}{1.579 \cdot 10^6 s^4 + 1.074 \cdot 10^{10} s^3 + 3.655 \cdot 10^{13} s^2} \quad (7.40)$$

Figure 7.9 shows the Nyquist diagram for (7.40). The Nyquist curve does not encircle the point -1 and hence the closed-loop system of the DC motor is stable.

7.5.2 Total Closed-loop System

Consider the system in Figure 7.5. To be able to use the Nyquist criterion G_0 is determined numerically

$$G_0 = G_{\theta, y} F_{y_b} = \frac{1.013 \cdot 10^7 s - 1.156 \cdot 10^9}{s^4 + 657 s^3 + 2.243 \cdot 10^5 s^2 + 1.127 \cdot 10^7 s + 1.763 \cdot 10^9} \quad (7.41)$$

Figure 7.10 shows the Nyquist diagram for (7.41). The Nyquist curve does not encircle the point -1 and hence the closed-loop system of the total system is stable.

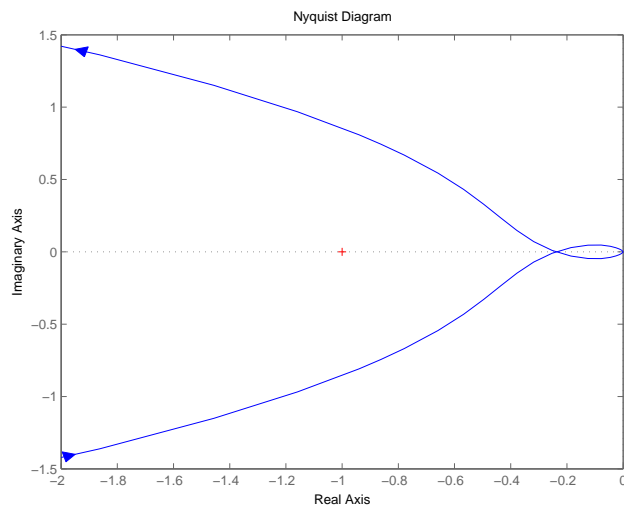


Figure 7.9. The Nyquist diagram of G_0 in (7.40).

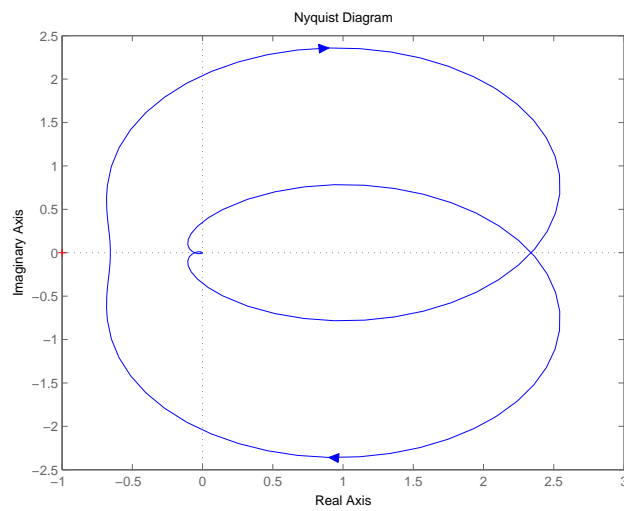


Figure 7.10. The Nyquist diagram of G_0 in (7.41).

7.6 Sensitivity and Robustness

In practice a system can not be known exactly. The real system is most likely far more complex than the model being used, and it is affected by different disturbances. Different model errors imply that the real closed-loop system differs

from the derived one. It is important that the control system can complete its task even when disturbances affect the system, and when the real system differs from the model the regulator calculations are based on. The concept of *sensitivity* and *robustness* is used to describe and measure these properties of the control system.

7.6.1 Sensitivity

Consider the system in Figure 7.8. The sensitivity function S in (7.42) describes how disturbances w affect the output signal y . Another way of interpreting the sensitivity function is that it describes disturbance rejection. The function also describes how model errors are handled. It can be shown that a main goal is to make $|S(i\omega)|$ small for frequencies where disturbance and model error is expected (Glad and Ljung, 1989).

$$w \mapsto y, \quad S = G_{wy} = (I + GF_y)^{-1} \quad (7.42)$$

Sensitivity of the DC Motor System

Consider the DC motor system in Figure 7.3. The corresponding sensitivity function for the DC motor system numerically becomes

$$S = \frac{s^4 + 6804s^3 + 2.315 \cdot 10^7 s^2}{s^4 + 6804s^3 + 2.315 \cdot 10^7 s^2 + 3.039 \cdot 10^{10} s + 1.995 \cdot 10^{13}} \quad (7.43)$$

Figure 7.11 shows a Bode magnitude plot of the sensitivity function in (7.43). It is clear that the sensitivity function is small for low frequencies, disturbances are well damped for frequencies between 0-1000 rad/s.

Sensitivity of the Total System

Consider the total system in Figure 7.5. The corresponding sensitivity function for the total system numerically becomes

$$S = \frac{s^4 + 657s^3 + 2.243 \cdot 10^5 s^2 + 1.127 \cdot 10^7 s + 1.763 \cdot 10^9}{s^4 + 657s^3 + 2.243 \cdot 10^5 s^2 + 2.14 \cdot 10^7 s + 6.064 \cdot 10^8} \quad (7.44)$$

Figure 7.12 shows a Bode magnitude plot of the sensitivity function in (7.44). It is clear that the sensitivity function has a strange behavior and looks far from the idealized case. Normally, the sensitivity function is small for low frequencies which implies that disturbances are well damped for low frequencies. Compare with Figure 7.11. However, the sensitivity function is small for some low frequencies, and hence, disturbances are well damped for frequencies between 60-250 rad/s.

7.6.2 Robustness

A very important issue is robustness of a system, that is, how severe the model errors are allowed to be without risking the stability of the closed-loop system.

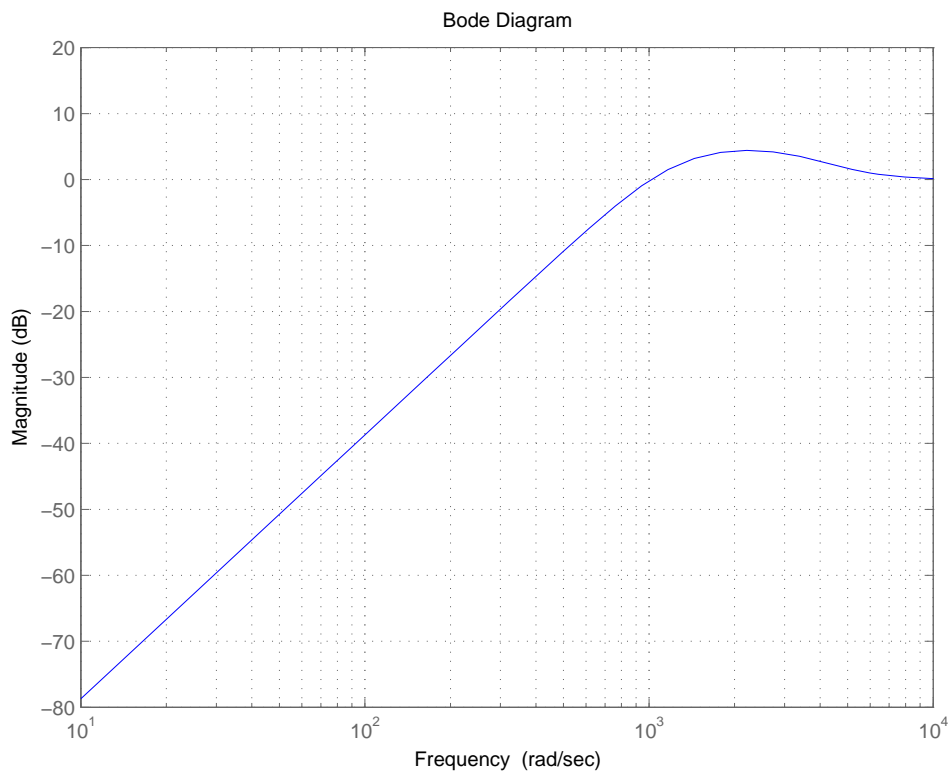


Figure 7.11. Bode magnitude plot of the sensitivity function S in (7.43) of the DC motor system.

Especially, uncertainty of a system's real properties at high frequencies may be significant. The robustness of the system may be dependent upon assumptions made concerning dynamics of the physical plant, such as:

- all hardware components are assumed to be ideal, that is, there are no (short) time-delays when hardware becomes active (initial adjustment).
- the approximated model of the DC motor system is correct.
- the estimated transfer function between the motor shaft angle θ to the bridge position y_b is perfect.

Hence, it is important that the control system has a built-in robustness so desired results are met even when the real system differs from the model being used. The concept of *stability robustness* is used to describe that the stability of the closed-loop system is not being jeopardized with certain model errors.

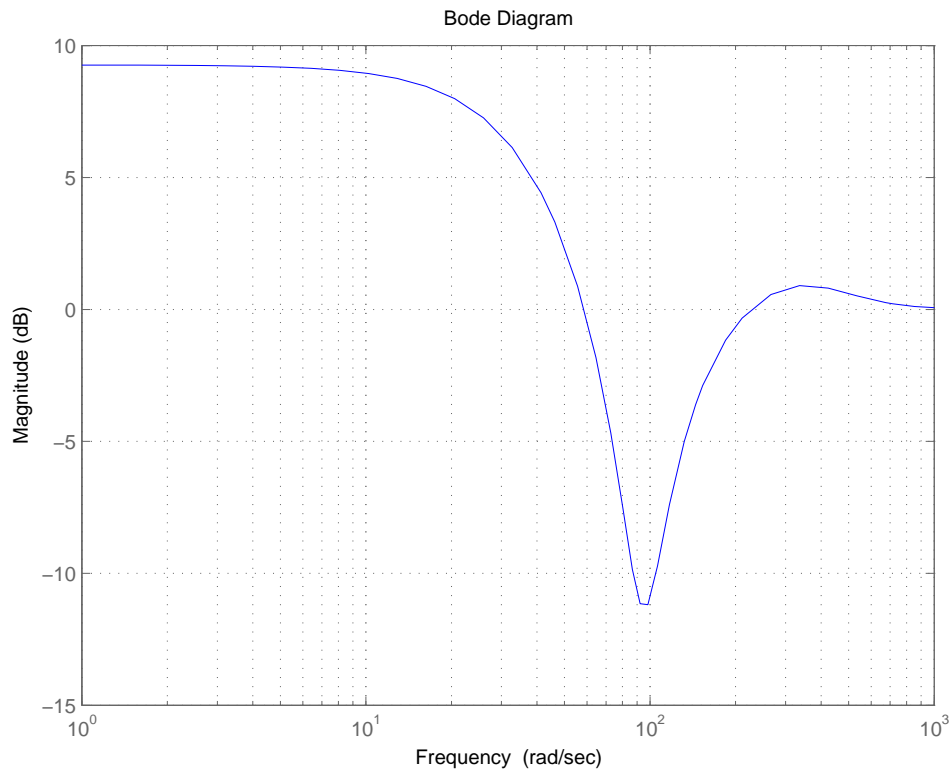


Figure 7.12. Bode magnitude plot of the sensitivity function S in (7.44) of the total system.

It can be shown that the complementary sensitivity function T in (7.45) describes the robustness properties of a closed-loop system according to Figure 7.8, see (Glad and Ljung, 1989).

$$T = (I + GF_y)^{-1}GF_y \quad (7.45)$$

It is desired to make the complementary sensitivity T small, this prevents measurement errors n (see Figure 7.8), from affecting the system; making T small also makes the system less sensitive to model errors. Typically, $|T(i\omega)|$ is chosen to be small for high frequencies, because measurement errors and relative model errors often have high frequency characteristics (Glad and Ljung, 1997).

Robustness of the DC Motor System

Consider the system in Figure 7.8. The corresponding complementary sensitivity function T for the DC motor system numerically becomes

$$T = \frac{3.039 \cdot 10^{10}s + 1.995 \cdot 10^{13}}{s^4 + 6804s^3 + 2.315 \cdot 10^7s^2 + 3.039 \cdot 10^{10}s + 1.995 \cdot 10^{13}} \quad (7.46)$$

Figure 7.13 shows the complementary sensitivity function for the DC motor system. It is clear that T is small for high frequencies, from 2000 rad/s and above, model errors or measurement noise will have minor impact on the system. Figure 7.14

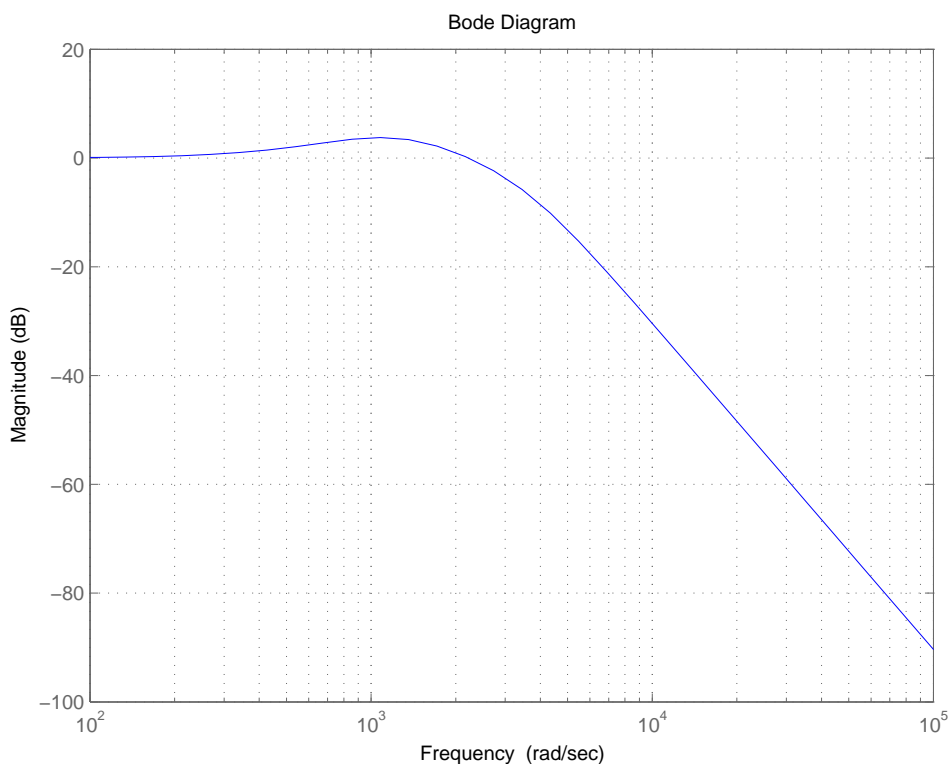


Figure 7.13. Bode magnitude plot of the complementary sensitivity function T in (7.46) for the DC motor system.

shows a simulation of the DC motor system when additive measurement noise n is included according to Figure 7.3. The output signal θ is plotted with different choice of noise frequency. The noise is chosen to be $n = 0.1 \sin(\omega t)$, where $\omega = 10, 500, 1000$ rad/s. The plot shows the expected behavior to disturbance according to discussions of the Bode magnitude plot of T above. Noise with frequency around 1000 rad/s is clearly amplified. In the simulation the amplitude is kept fixed.

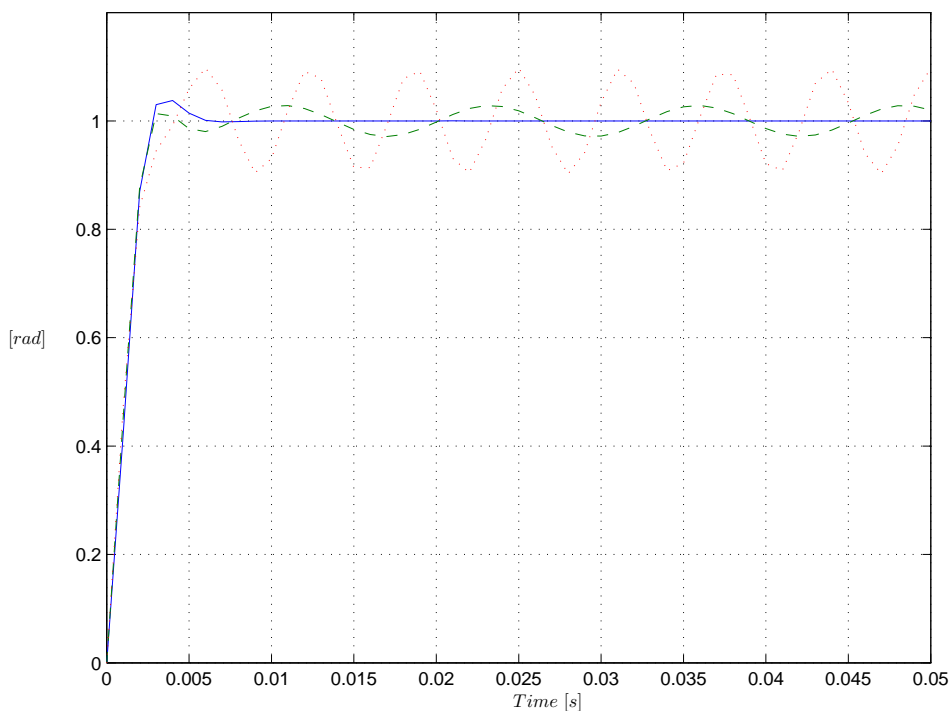


Figure 7.14. Results when the DC motor system is influenced by noise n , the output signal θ is plotted. Notation: $\omega = 10$ rad/s (solid), $\omega = 500$ rad/s (dashed), $\omega = 1000$ rad/s (dotted).

Robustness of the Total System

Consider the total system in Figure 7.5. The corresponding complementary sensitivity function T for the total system numerically becomes

$$T = \frac{1.013 \cdot 10^7 s - 1.156 \cdot 10^9}{s^4 + 657s^3 + 2.243 \cdot 10^5 s^2 + 2.14 \cdot 10^7 s + 6.064 \cdot 10^8} \quad (7.47)$$

Figure 7.15 shows the complementary sensitivity function T of the total system. It is clear that high frequencies are well damped, frequencies from 100 rad/s and higher will have minor impact on the closed-loop system. Figure 7.16 shows a simulation of the total system when additive measurement noise n_{tot} is included according to Figure 7.5. The output signal y_b is plotted with different choice of noise frequency. The noise is chosen to be $n_{tot} = 0.01 \sin(\omega t)$, where $\omega = 10, 100$ rad/s. The plot shows the expected behavior to disturbance according to discussions of the Bode magnitude plot of T above. The noise is amplified for very low frequencies. Noise with frequencies between 60-250 rad/s is well damped. When the noise

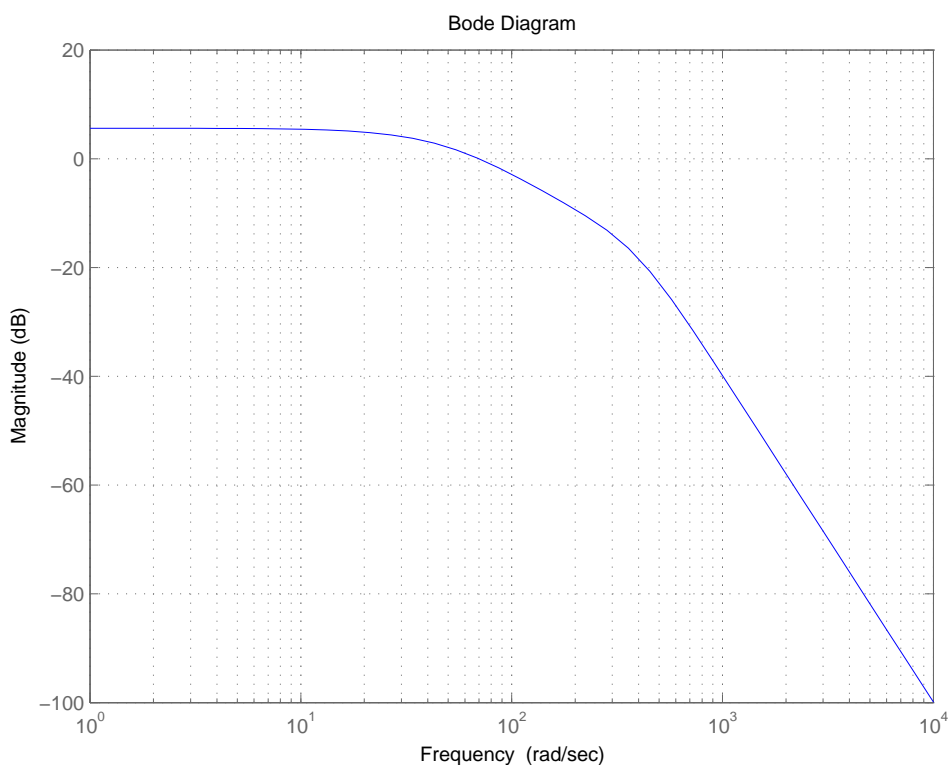


Figure 7.15. Bode magnitude plot of the complementary sensitivity function T in (7.47) for the total system.

frequency increases, the amplitude decreases naturally and thus high frequencies have minor effect on the system. Assume that the estimated model changes with time, that is, the existing model

$$\frac{dx}{dt} = A_2x + B_2u$$

changes to

$$\frac{dx}{dt} = \Delta A_2x + B_2u \quad (7.48)$$

where

$$A_2 = \begin{pmatrix} 0 & 1 \\ -b & -a \end{pmatrix}$$

$$\Delta A_2 = \begin{pmatrix} 0 & 1 \\ -(b \pm 20\%) & -(a \pm 20\%) \end{pmatrix}$$

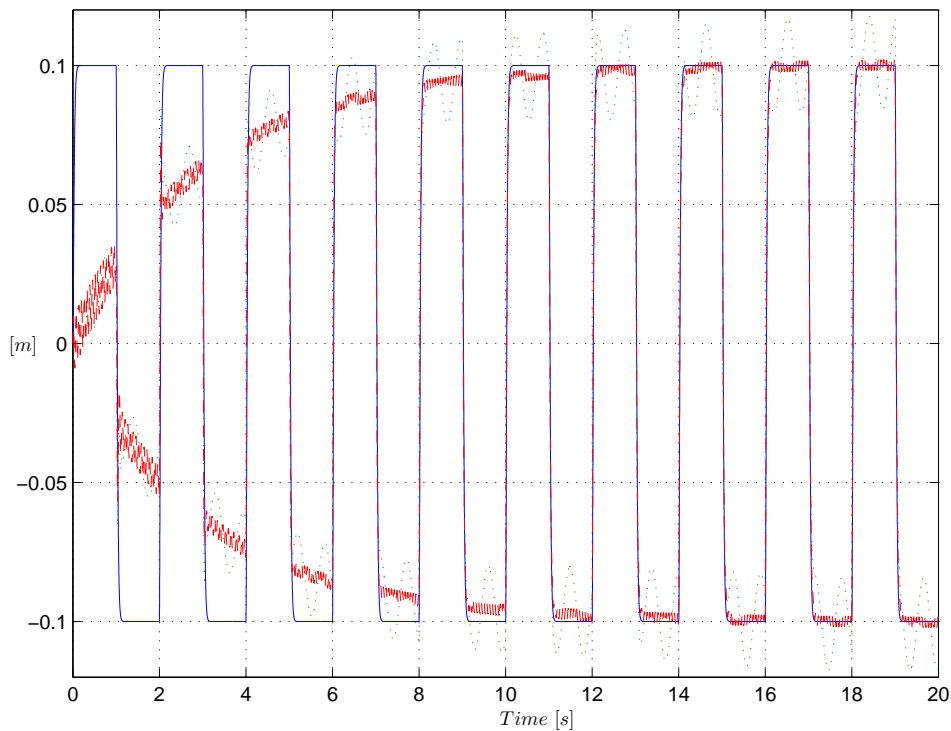


Figure 7.16. Results when the total system is influenced by noise n_{tot} . Notation: model output y_m (solid), process output y_b with $\omega = 10$ rad/s (dotted), process output y_b with $\omega = 100$ rad/s (dashed).

This can be interpreted as a change of the belt tension by $\pm 20\%$ and a change of the damping by $\pm 20\%$. Figure 7.17 shows a simulation of the total system, when the estimated model changes according to (7.48) at time $t = 1$ s. Notice that the process has already converged to the reference model at time $t = 0$ s and thus that the initial adaptation is not shown in the plot. The adaptive algorithm has its desired behavior and works very well, at time $t = 8$ s there is almost no difference between process and model output.

7.7 Summary

In this chapter, the use of adaptive control on the total system is discussed. An inner closed-loop system is created for the DC motor system with a bandwidth of 200 Hz. The inner loop uses an observer which estimates two states, θ and ω . Initially, only one state is measurable from rotary encoder readings, θ .

An MRAS is created for the total system, however its reference model is only

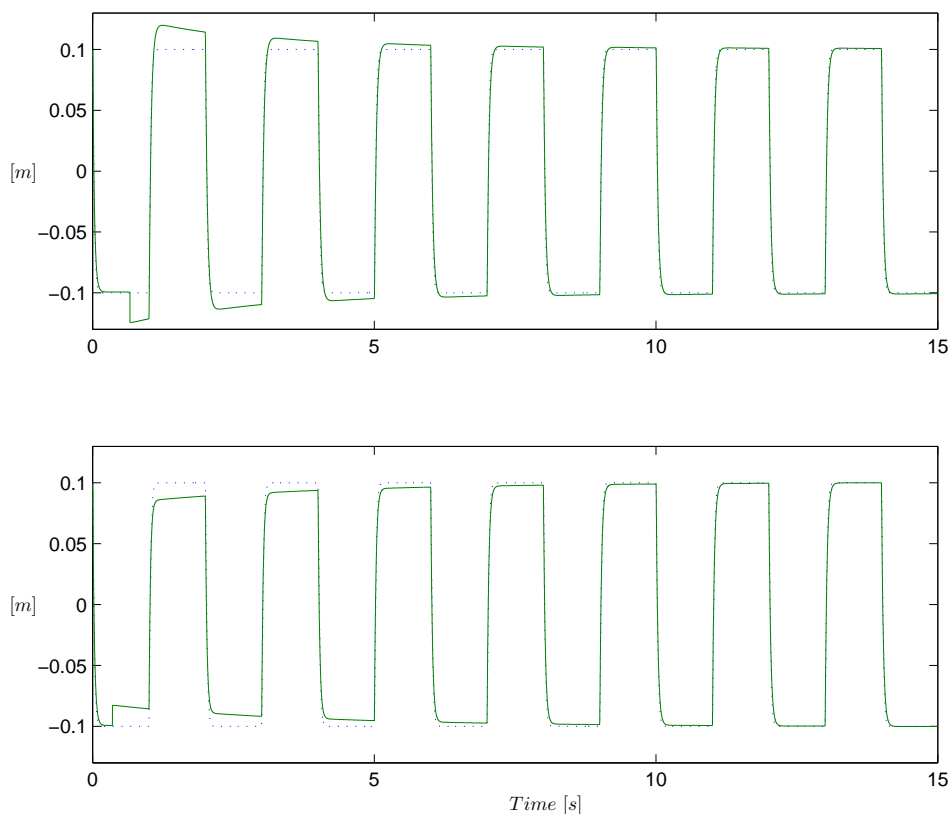


Figure 7.17. Simulation of the total system when the estimated process changes at time $t = 1$ s. Notation: model output y_m (dotted), process output y_b with (a-20%), (b-20%) (up, solid), process output y_b with (a+20%), (b+20%) (down, solid).

second order and reflects the estimated model for the drive mechanism. This depends on the inner loop bandwidth being made so much higher than the outer loop. In other words, the dynamics of the DC motor system are ignored. The MRAS creates a closed-loop system with a bandwidth of 10 Hz and a damping of $\zeta_2 = 1$.

A Nyquist diagram of G_0 shows that the closed-loop system of the DC motor is stable. Likewise, a Nyquist diagram shows that the total closed-loop system is also stable.

The concept of sensitivity and robustness is discussed. The sensitivity function S for the DC motor system shows that noise with frequencies between 0-400 rad/s is well damped and thus has minor impact. Noise with frequencies around 1000 rad/s is amplified. The sensitivity function for the total system shows that noise with very low frequencies is not so well damped. Noise with frequencies between

60-250 rad/s does not affect the closed-loop system. Noise disturbance signals with frequencies from 500 rad/s and up have minor impact to the total closed-loop system.

The complementary sensitivity function T describes the robustness of a system. Typically, it is chosen to be small for frequencies where measurement noise and model errors are expected. The complementary sensitivity function for the closed-loop DC motor system, shows that the system will not be affected by measurement errors or model errors in a major way; T is small for frequencies around 2000 rad/s and higher. In the same way, the T function for total system shows that noise with frequencies from 100 rad/s is well rejected.

Finally, the estimated drive mechanism is due to a change. The existing model is changed from the estimated model to a new process. This can be seen as, for example, a change of the belt tension or, a change of damping or a change of inertia. It is shown that the adaptive mechanism handles such changes rather well. This shows the advantage of adaptive control versus traditional, where controller parameters are time-invariant and thus fixed. If there is a major change in the process, a new model may have to be estimated, and the controller parameters have to be tuned in to give good results.

Chapter 8

Conclusions

In this chapter a summary and a reflection of the results and conclusions in the thesis are given. Some parts that will need further work are also pointed out.

8.1 Summary

It is clear that position damping of drive mechanisms in CMM's is critical, thus such drive mechanisms must be controlled by very precise regulators. The use of encoders has obvious benefits, since all outputs are digital and can easily be processed by a data acquisition card. Another advantage is that encoder readings generally are very accurate. The encoders in the existing system have a noise variance in the order of 10^{-13} . Tachometers on the other hand, have very noisy analog outputs. Hence, it is understandable that a rotary encoder will have more potential than a tachometer when good control of the DC motor system is desired. Since the rotary encoder output is an angle (position), it is easy to estimate angular velocity for instance with an observer. The accuracy of such a velocity estimate can be made much better than the accuracy of tachometer readings.

It is possible to estimate the transfer function from motor shaft angle θ to bridge position y_b with use of a rotary and a linear encoder. These digital outputs can be used in the System Identification Toolbox in MATLAB™ to estimate a black-box model, in this case an ARX-model. The estimated ARX-model can easily be validated by investigating properties such as: model order, prediction compared with validation data, value of loss function, standard deviation of estimated model parameters, auto correlation of residuals for the output, cross correlation for input and output residuals. It is also possible to derive physical models with use of the bond graph concept. The models can be compared with the chosen ARX-model. In this case, when there is a match between the chosen arx2 model and one of the physical models, two unknown parameters can be identified; a spring constant and a damping constant. These parameters have a physical interpretation. The impact

is that the knowledge of these parameters allows for deeper comprehension of the physical system.

The DC motor system can be controlled separately from the total system. The rotary encoder output can be sent to an observer that estimates angle $\hat{\theta}$ and angular velocity $\hat{\omega}$. With these estimated states and a static control gain, the bandwidth of the closed-loop system of the DC motor can be chosen to give desirable properties. In this study it is chosen to be 200 Hz. Essentially the bandwidth can be chosen arbitrarily, however one must take into account that the DC motor has its own mechanical resonance frequency. This frequency has to be avoided at any time to give the system good performance. Hence, this is one of the reasons the 200 Hz bandwidth is chosen for the DC motor system.

It is possible to develop a stable MRAS with use of Lyapunov stability theory. The other reason for making the bandwidth of the DC motor system 200 Hz is that its dynamics can be neglected and replaced by a static gain if the bandwidth of the total closed-loop system is made much smaller. In other words, making the desired bandwidth of the reference model small the model order of the MRAS can be reduced. In the actual system, this approximation leads to a second-order MRAS with a bandwidth of 10 Hz. One condition that needs to be fulfilled when Lyapunov stability theory is applied to a system, is that all states must be measurable. As a result, one observer is implemented. The linear encoder output that measures the bridge position y_b , is sent to a process observer which estimates \hat{y}_b and $\hat{\dot{y}}_b$. Now when all states are estimated, Lyapunov stability theory can be used. The designed adaptive mechanism drives the bandwidth of the total closed-loop system to 10 Hz. Simulations show that the MRAS has its desired behavior. The system adapts rather fast to a square-wave reference signal. However, the adaptation rate can be made even faster. Notice also that in the physical system, it is not very likely that a reference signal ever would have the shape of a square wave, but rather a saw-tooth shape. A saw-tooth shape or in other words a triangle-waveform is even easier for the MRAS to follow. The use of a square-waveform more represents a worst-case scenario. Furthermore, the MRAS is not going to be implemented and run in real-time but at a tune-up procedure where settling time is not so critical.

Robustness analysis shows that the total system performs very well when additive measurement noise affects the process output. At very low frequencies the noise is amplified, but at higher frequencies the effect is small. Moreover, measurement errors are typically high frequency. The simulations are based upon a worst case choice of the additive noise. In the physical system such a disturbance signal will most probably have a smaller amplitude. Furthermore, robustness analysis also shows that the total system handles model errors very well. The complementary sensitivity function is very small for frequencies higher than 100 rad/s. Hence, the total closed-loop system is very robust. Simulations also show that the adaptive mechanism performs very well if the system changes with time, for instance a change like $a \pm 20\%$, $b \pm 20\%$. In the simulations it only takes the adaptive

mechanism 8s to correct for such a model error. However, the adaptive mechanism handles much worse changes. Simulations show that the algorithm has its desired behavior even for a $\pm 300\%$ change, but of course the adaptation takes much longer. On the other hand, such an extreme change would indicate a major failure in the system; like a broken belt. Furthermore, it is also clear that the MRAS increases the damping with at least a factor of nine. However, higher damping can be achieved with a higher adaptation gain. Thus the goal to increase position damping of the drive mechanism of the y-axis is reached, and the damping increases by a factor of nine.

8.2 Further Work

It would be interesting to develop an off-line automatic routine for estimating the transfer function from motor shaft angle θ to position of the bridge y_b . The implication would be that the routine could be used on arbitrary and larger CMM's, assuming there is a rotary encoder attached to the DC motor. The routine could also be used on the two other drive mechanisms for the x and z-axes. However, since the largest inertia (the bridge) affects the y-axis, the algorithm would be implemented for the y-axis first. It would also be interesting to implement the off-line adaptive mechanism for a CMM. In order to implement the model-reference adaptive system for the studied system, the procedure can be divided into steps:

- All transfer functions and observers must be transformed into a discrete time representation. This is done either analytically with bilinear transformation (Söderkvist, 1998) or with the MATLAB™ command `c2d` which transforms a continuous transfer function into a discrete one.
- All continuous transfer functions must be transformed into the discrete time domain. However, it may be easier to initially consider the discrete form of the MRAS instead of the continuous version, thus only one transformation will be needed.
- A sampling time must be chosen, for instance $T = 0.001s$ will be fast enough for the adaptive system.
- The time discrete version of the MRAS must be implemented in a program language, preferably C/C++. This is the most challenging part of the procedure. Again, the easiest way to go is to consider the MRAS in the time discrete domain. Derivatives and integrations will be represented by time shifts, the accuracy of such derivatives and integrations will depend on the step size, or in other words, the sampling frequency T . Differential equations can either be implemented to support one dimensional update of one state or preferably to support n dimensional update on n states, a discrete state space representation. Hence, systems would be described by matrices which also allows for easier future modifications of the adaptive system; it is straight forward to extend systems in the state space representation. Even

more elegant would be to implement a representation of transfer functions in the Z -domain and then implement routines for inverse Z -transformation. In many cases it is preferred to study the impact of transfer functions and regulators in the frequency domain, hence a Z -domain representation could be useful.

- The executable code for the adaptive system must be tested and run on a micro processor, preferably on a DSP card. The DSP card must support digital input and output signals, thus the rotary and linear encoder readings can be utilized. The adaptive controller or the adaptive routine can be run on the micro processor in the DSP card. The idea of controlling the DC motor system separately from the total adaptive system can be used. In the micro processor, the two control systems can be run on different processes. Hence, these processes can use different sampling frequencies which may be desirable.

Another interesting idea is to implement either an on-line routine for model estimation and an on-line MRAS for the CMM. This would be far more challenging than the suggested implementations above. Also, a sufficient amount of micro processor power would be needed. However, on-line algorithms could be run in different ways. For instance, the algorithms could take small samples of the process every n th second and use them to update parameters. Thus the implementation would be a compromise between control and needed micro processor power.

Bibliography

B&S (2000). *Testsoft*. Brown & Sharpe Inc.

Glad, T. and Ljung, L. (1989). *Reglerteknik
Grundläggande teori*. Studentlitteratur, second edition.

Glad, T. and Ljung, L. (1997). *Reglerteori - Flervariabla och olinjära metoder*. Studentlitteratur.

Glad, T. and Ljung, L. (2002). *Modellbygge och Simulering*. Studentlitteratur.

Gustafsson, F., Ljung, L., and Millnert, M. (2001). *Signalbehandling*. Studentlitteratur, Lund.

Ljung, L. (1987). *System Identification , Theory For The User*. Prentice-Hall Inc.

Ljung, L. (2000). *System Identification Toolbox - User's Guide*. The MathWorks, Inc., Sherborn, MA USA.

Maplesoft (2003). *Maple 9 Student Edition*. Waterloo Maple Inc., Waterloo, Ontario, Canada.

MathWorks (2003). *MATLAB 6.5 Student Version*. The MathWorks, Inc., Sherborn, MA USA.

NI (2002). *LabVIEW 6.0*. National Instruments Corporation, Austin, TX, USA.

Söderkvist, S. (1998). *Formler & Tabeller*. Erik Larsson AB.

Wilcox (2001). *PC-DIMIS 3.5*. Wilcox.

Wittenmark, B. and Åström, K. J. (1995). *Adaptive Control*. Addison-Wesley, second edition.

Appendix A

Physical Models

A.1 One-spring Model

The following equations can be found with use of the bond graph concept and the bond graph in Section 3.3.1.

$$S_1 : F_3 - F_k - F_d = 0 \quad (\text{A.1})$$

$$C : \frac{1}{k} : F_k = k \int (v_3 - v_4) d\tau \quad (\text{A.2})$$

$$R : d : F_d = d(v_3 - v_4) \quad (\text{A.3})$$

$$S_2 : F_3 - F_m - F_R = 0 \quad (\text{A.4})$$

$$I : m : v_4 = \frac{1}{m} \int F_m d\tau \quad (\text{A.5})$$

$$R : \phi : F_R = \phi v_4 \quad (\text{A.6})$$

$$TF : \frac{r_2}{r_1 r_3} : v_3 = \frac{r_1 r_3}{r_2} \omega_1 \quad (\text{A.7})$$

Introduce

$$u = \omega_1 \quad (\text{A.8})$$

and the states

$$x_1 = F_k \quad (\text{A.9})$$

$$x_2 = v_4 \quad (\text{A.10})$$

With (A.2) the derivative of (A.9) is given by

$$\dot{x}_1 = k(v_3 - v_4) \quad (\text{A.11})$$

Equations (A.7), (A.8) and (A.10) in (A.11) give

$$\dot{x}_1 = -kx_2 + \frac{kr_1 r_3}{r_2} u \quad (\text{A.12})$$

Analogously, with (A.5) the derivative of (A.10) is given by

$$\dot{x}_2 = \frac{1}{m}F_m \quad (\text{A.13})$$

Equation (A.4) in (A.13) gives

$$\dot{x}_2 = \frac{1}{m}(F_3 - F_R) \quad (\text{A.14})$$

Equations (A.1), (A.10) and (A.6) in (A.14) give

$$\dot{x}_2 = \frac{1}{m}(F_k + F_d - \phi x_2) \quad (\text{A.15})$$

Equations (A.9) and (A.3) in (A.15) give

$$\dot{x}_2 = \frac{1}{m}(x_1 + d(v_3 - v_4) - \phi x_2) \quad (\text{A.16})$$

Finally (A.7), (A.8) and (A.10) in (A.16) give

$$\dot{x}_2 = \frac{1}{m}x_1 - \frac{d + \phi}{m}x_2 + \frac{dr_1r_3}{mr_2}u \quad (\text{A.17})$$

From (A.12),(A.17) the state space form is written as

$$\dot{\mathbf{x}} = \begin{pmatrix} 0 & -k \\ \frac{1}{m} & -\frac{d+\phi}{m} \end{pmatrix} \mathbf{x} + \begin{pmatrix} \frac{kr_1r_3}{r_2} \\ \frac{dr_1r_3}{mr_2} \end{pmatrix} \mathbf{u} \quad (\text{A.18})$$

Let us now extend the system with the new state y_b , denoting bridge position. To summarize, the extended system consists of the following states:

$$\begin{aligned} x_1 &= F_k \\ x_2 &= y_b \\ x_3 &= v_4 = \dot{y}_b \end{aligned}$$

The extended state space form of (A.18) becomes

$$\dot{\mathbf{x}} = \begin{pmatrix} 0 & 0 & -k \\ 0 & 0 & 1 \\ \frac{1}{m} & 0 & -\frac{d+\phi}{m} \end{pmatrix} \mathbf{x} + \begin{pmatrix} \frac{kr_1r_3}{r_2} \\ 0 \\ \frac{dr_1r_3}{mr_2} \end{pmatrix} \mathbf{u}$$

The transfer function from angular velocity ω_1 of the DC motor to position of the bridge y_b is given by the equation

$$G_{\omega_1, y_b}(s) = C(sI - A)^{-1}B \quad (\text{A.19})$$

where

$$\begin{aligned} A &= \begin{pmatrix} 0 & 0 & -k \\ 0 & 0 & 1 \\ \frac{1}{m} & 0 & -\frac{d+\phi}{m} \end{pmatrix} \\ B &= \begin{pmatrix} \frac{kr_1r_3}{r_2} \\ 0 \\ \frac{dr_1r_3}{mr_2} \end{pmatrix} \\ C &= (0 \quad 1 \quad 0) \end{aligned} \tag{A.20}$$

With (A.20) the transfer function in (A.19) becomes

$$G_{\omega_1, y_b}(s) = \frac{r_1 r_3 (ds + k)}{r_2 s (ms^2 + (d + \phi)s + k)}$$

The following relationship is stated for the system

$$Y_b(s) = G_{\omega_1, y_b}(s) \Omega_1(s)$$

However, the following relationship is also true

$$\Omega_1(s) = s \Theta_1(s)$$

and hence the transfer function from motor shaft angle θ_1 to position of the bridge y_b is given by

$$Y_b(s) = G_{\omega_1, y_b}(s) s \Theta_1(s)$$

Finally the searched transfer function becomes

$$G_{\theta_1, y_b}(s) = \frac{r_1 r_3 (ds + k)}{r_2 (ms^2 + (d + \phi)s + k)}$$

A.2 Three-spring Model

The following equations can be found with use of the bond graph concept and the bond graph in Section 3.3.2.

$$TF : T_1 = r_1 F_1, v_1 = r_1 \omega_1 =: r_1 u \tag{A.21}$$

$$s_1 : F_1 - F_{k_1} - F_{d_1} = 0 \tag{A.22}$$

$$C : \frac{1}{k_1} : F_{k_1} = k_1 \int (v_1 - v_2) d\tau \tag{A.23}$$

$$R : d_1 : F_{d_1} = d_1 (v_1 - v_2) \tag{A.24}$$

$$TF : F_3 = \frac{r_2}{r_3} F_1, v_3 = \frac{r_3}{r_2} v_2 \tag{A.25}$$

$$s_2 : F_3 - F_{k_2} - F_{d_2} = 0 \quad (\text{A.26})$$

$$C : \frac{1}{k_2} : F_{k_2} = k_2 \int (v_3 - v_4) d\tau \quad (\text{A.27})$$

$$R : d_2 : F_{d_2} = d_2(v_3 - v_4) \quad (\text{A.28})$$

$$s_3 : F_3 - F_m - F_R - F_{k_3} = 0 \quad (\text{A.29})$$

$$I : m : v_4 = \frac{1}{m} \int F_m d\tau \quad (\text{A.30})$$

$$R : \phi + d_3 : F_R = (\phi + d_3)v_4 \quad (\text{A.31})$$

$$C : \frac{1}{k_3} : F_{k_3} = k_3 \int v_4 d\tau \quad (\text{A.32})$$

Introduce the states

$$\begin{aligned} x_1 &= F_{k_1} \\ x_2 &= F_{k_2} \\ x_3 &= v_4 \\ x_4 &= F_{k_3} \end{aligned} \quad (\text{A.33})$$

Equations (A.24) and (A.21) in (A.22) give

$$F_1 = x_1 + d_1(r_1 u - v_2) \quad (\text{A.34})$$

Equations (A.28) and (A.25) in (A.26) give

$$F_3 = x_2 + d_2 \left(\frac{r_3}{r_2} v_2 - x_3 \right) \quad (\text{A.35})$$

Equations (A.34) and (A.35) in (A.25) give

$$v_2 = \frac{r_2 r_3}{d_1 r_2^2 + d_2 r_3^2} \left(\frac{r_2}{r_3} x_1 - x_2 + d_2 x_3 + \frac{d_1 r_1 r_2}{r_3} u \right) \quad (\text{A.36})$$

Differentiation of (A.23) gives

$$\dot{x}_1 = k_1(v_1 - v_2) \quad (\text{A.37})$$

and with (A.21), (A.37) becomes

$$\dot{x}_1 = k_1(r_1 u - v_2) \quad (\text{A.38})$$

Finally with (A.36), (A.38) becomes

$$\begin{aligned} \dot{x}_1 &= - \frac{k_1 r_2^2}{d_1 r_2^2 + d_2 r_3^2} x_1 + \frac{k_1 r_2 r_3}{d_1 r_2^2 + d_2 r_3^2} x_2 - \\ &\quad \frac{k_1 d_2 r_2 r_3}{d_1 r_2^2 + d_2 r_3^2} x_3 + \frac{k_1 r_1 d_2 r_3^2}{d_1 r_2^2 + d_2 r_3^2} u \end{aligned} \quad (\text{A.39})$$

Differentiation of (A.27) gives

$$\dot{x}_2 = k_2(v_3 - v_4) \quad (\text{A.40})$$

With (A.25), (A.40) becomes

$$\dot{x}_2 = \frac{k_2 r_3}{r_2} v_2 - k_2 x_3 \quad (\text{A.41})$$

Finally with (A.36), (A.41) becomes

$$\begin{aligned} \dot{x}_2 = & \frac{k_2 r_2 r_3}{d_1 r_2^2 + d_2 r_3^2} x_1 - \frac{k_2 r_3^2}{d_1 r_2^2 + d_2 r_3^2} x_2 - \\ & \frac{d_1 k_2 r_2^2}{d_1 r_2^2 + d_2 r_3^2} x_3 + \frac{d_1 r_1 k_2 r_2 r_3}{d_1 r_2^2 + d_2 r_3^2} u \end{aligned} \quad (\text{A.42})$$

Differentiation of (A.30) gives

$$\dot{x}_3 = \frac{1}{m} F_m \quad (\text{A.43})$$

With (A.29), (A.43) becomes

$$\dot{x}_3 = \frac{1}{m} (F_3 - F_R - F_{k_3}) \quad (\text{A.44})$$

Equations (A.26) and (A.31) inserted in (A.44) give

$$\dot{x}_3 = \frac{1}{m} (F_{k_2} + F_{d_2} - (\phi + d_3)v_4 - F_{k_3}) \quad (\text{A.45})$$

With (A.33) and (A.28), (A.45) becomes

$$\dot{x}_3 = \frac{1}{m} (x_2 + d_2(v_3 - x_3) - (\phi + d_3)x_3 - x_4) \quad (\text{A.46})$$

Equation (A.25) inserted in (A.46) gives

$$\dot{x}_3 = \frac{1}{m} (x_2 + d_2(\frac{r_3}{r_2}v_2 - x_3) - (\phi + d_3)x_3 - x_4) \quad (\text{A.47})$$

Finally (A.36) inserted in (A.47) gives

$$\begin{aligned} \dot{x}_3 = & \frac{d_2 r_2 r_3}{m(d_1 r_2^2 + d_2 r_3^2)} x_1 + \frac{d_1 r_2^2}{m(d_1 r_2^2 + d_2 r_3^2)} x_2 + \\ & \left(\frac{d_2^2 r_3^2}{m(d_1 r_2^2 + d_2 r_3^2)} - \frac{d_2 + d_3 + \phi}{m} \right) x_3 - \\ & \frac{1}{m} x_4 + \frac{d_1 r_1 d_2 r_2 r_3}{m(d_1 r_2^2 + d_2 r_3^2)} u \end{aligned} \quad (\text{A.48})$$

Differentiation of (A.32) gives

$$\dot{x}_4 = k_3 v_4 \quad (\text{A.49})$$

With (A.33), (A.49) becomes

$$\dot{x}_4 = k_3 x_3 \quad (\text{A.50})$$

In state space form the system becomes

$$\begin{aligned} \dot{\mathbf{x}} = & \begin{pmatrix} -\frac{k_1 r_2^2}{d_1 r_2^2 + d_2 r_3^2} & \frac{k_1 r_2 r_3}{d_1 r_2^2 + d_2 r_3^2} & -\frac{k_1 d_2 r_2 r_3}{d_1 r_2^2 + d_2 r_3^2} & 0 \\ \frac{k_2 r_2 r_3}{d_1 r_2^2 + d_2 r_3^2} & -\frac{k_2 r_3^2}{d_1 r_2^2 + d_2 r_3^2} & -\frac{d_1 k_2 r_2^2}{d_1 r_2^2 + d_2 r_3^2} & 0 \\ \frac{d_2 r_2 r_3}{m(d_1 r_2^2 + d_2 r_3^2)} & \frac{d_1 r_2^2}{m(d_1 r_2^2 + d_2 r_3^2)} & \frac{d_2^2 r_3^2}{m(d_1 r_2^2 + d_2 r_3^2)} - \frac{d_2 + d_3 + \phi}{m} & -\frac{1}{m} \\ 0 & 0 & k_3 & 0 \end{pmatrix} \mathbf{x} + \\ & \begin{pmatrix} \frac{k_1 r_1 d_2 r_3^2}{d_1 r_2^2 + d_2 r_3^2} \\ \frac{d_1 r_1 k_2 r_2 r_3}{d_1 r_2^2 + d_2 r_3^2} \\ \frac{d_1 r_1 d_2 r_2 r_3}{m(d_1 r_2^2 + d_2 r_3^2)} \\ 0 \end{pmatrix} \mathbf{u} \end{aligned} \quad (\text{A.51})$$

We now extend the system with a new state y_b , denoting bridge position. To summarize, the states of the systems are now

$$\begin{aligned} x_1 &= F_{k_1} \\ x_2 &= F_{k_2} \\ x_3 &= y_b \\ x_4 &= v_4 \\ x_5 &= F_{k_3} \end{aligned} \quad (\text{A.52})$$

The extended state space form of (A.51) becomes

$$\begin{aligned} \dot{\mathbf{x}} = & \begin{pmatrix} -\frac{k_1 r_2^2}{d_1 r_2^2 + d_2 r_3^2} & \frac{k_1 r_2 r_3}{d_1 r_2^2 + d_2 r_3^2} & 0 & -\frac{k_1 d_2 r_2 r_3}{d_1 r_2^2 + d_2 r_3^2} & 0 \\ \frac{k_2 r_2 r_3}{d_1 r_2^2 + d_2 r_3^2} & -\frac{k_2 r_3^2}{d_1 r_2^2 + d_2 r_3^2} & 0 & -\frac{d_1 k_2 r_2^2}{d_1 r_2^2 + d_2 r_3^2} & 0 \\ 0 & 0 & 0 & 1 & 0 \\ \frac{d_2 r_2 r_3}{m(d_1 r_2^2 + d_2 r_3^2)} & \frac{d_1 r_2^2}{m(d_1 r_2^2 + d_2 r_3^2)} & 0 & \frac{d_2^2 r_3^2}{m(d_1 r_2^2 + d_2 r_3^2)} - \frac{d_2 + d_3 + \phi}{m} & -\frac{1}{m} \\ 0 & 0 & 0 & k_3 & 0 \end{pmatrix} \mathbf{x} + \\ & \begin{pmatrix} \frac{k_1 r_1 d_2 r_3^2}{d_1 r_2^2 + d_2 r_3^2} \\ \frac{d_1 r_1 k_2 r_2 r_3}{d_1 r_2^2 + d_2 r_3^2} \\ 0 \\ \frac{d_1 r_1 d_2 r_2 r_3}{m(d_1 r_2^2 + d_2 r_3^2)} \\ 0 \end{pmatrix} \mathbf{u} \end{aligned} \quad (\text{A.53})$$

The transfer function from motor angular velocity ω_1 to bridge position y_b is given by the equation

$$G_{\omega_1, y_b}(s) = C(sI - A)^{-1} B + D \quad (\text{A.54})$$

where

$$\begin{aligned}
 A &= \begin{pmatrix} -\frac{k_1 r_2^2}{d_1 r_2^2 + d_2 r_3^2} & \frac{k_1 r_2 r_3}{d_1 r_2^2 + d_2 r_3^2} & 0 & -\frac{k_1 d_2 r_2 r_3}{d_1 r_2^2 + d_2 r_3^2} & 0 \\ \frac{k_2 r_2 r_3}{d_1 r_2^2 + d_2 r_3^2} & -\frac{k_2 r_3^2}{d_1 r_2^2 + d_2 r_3^2} & 0 & -\frac{d_1 k_2 r_2^2}{d_1 r_2^2 + d_2 r_3^2} & 0 \\ 0 & 0 & 0 & 1 & 0 \\ \frac{d_2 r_2 r_3}{m(d_1 r_2^2 + d_2 r_3^2)} & \frac{d_1 r_2^2}{m(d_1 r_2^2 + d_2 r_3^2)} & 0 & \frac{d_2^2 r_3^2}{m(d_1 r_2^2 + d_2 r_3^2)} - \frac{d_2 + d_3 + \phi}{m} & -\frac{1}{m} \\ 0 & 0 & 0 & k_3 & 0 \end{pmatrix} \\
 B &= \begin{pmatrix} \frac{k_1 r_1 d_2 r_3^2}{d_1 r_2^2 + d_2 r_3^2} \\ \frac{d_1 r_1 k_2 r_2 r_3}{d_1 r_2^2 + d_2 r_3^2} \\ 0 \\ \frac{d_1 r_1 d_2 r_2 r_3}{m(d_1 r_2^2 + d_2 r_3^2)} \\ 0 \end{pmatrix} \\
 C &= (0 \ 0 \ 1 \ 0 \ 0) \\
 D &= 0
 \end{aligned} \tag{A.55}$$

With (A.55) the transfer function in (A.54) becomes

$$\begin{aligned}
 G_{\omega_1, y_b}(s) &= \left(\left(d_1 d_2 s^2 + (d_1 k_2 + k_1 d_2) s + k_1 k_2 \right) r_1 r_2 r_3 \right) / \\
 &\quad \left(s \left((m d_1 r_2^2 + m d_2 r_3^2) s^3 + ((d_1 \phi + d_1 d_3 + d_1 d_2 + m k_1) r_2^2 + \right. \right. \\
 &\quad \left. \left. (m k_2 + d_2 d_3 + \phi d_2) r_3^2 \right) s^2 + \right. \\
 &\quad \left. ((d_1 k_2 + k_1 d_2 + k_1 d_3 + k_1 \phi + d_1 k_3) r_2^2 + \right. \\
 &\quad \left. (k_2 d_3 + \phi k_2 + d_2 k_3) r_3^2 \right) s + (k_1 k_2 + k_1 k_3) r_2^2 + k_2 k_3 r_3^2 \Big) \Big)
 \end{aligned} \tag{A.56}$$

Equation (A.54) is solved with Maple™ (Maplesoft, 2003). The following relationship is valid for the system.

$$Y_b(s) = G_{\omega_1, y_b}(s) \Omega_1(s) \tag{A.57}$$

However, the following relationship is also true

$$\Omega_1(s) = s \Theta_1(s) \tag{A.58}$$

and hence the transfer function from motor angle θ_1 to position of the bridge y_b is given by

$$Y_b(s) = G_{\omega_1, y_b}(s) s \Theta_1(s) \tag{A.59}$$

Finally the searched transfer function becomes

$$\begin{aligned}
 G_{\theta_1 y_b}(s) = & r_1 r_2 r_3 \left(d_1 d_2 s^2 + (d_1 k_2 + k_1 d_2) s + k_1 k_2 \right) / \\
 & \left((d_1 r_2^2 + d_2 r_3^2) m s^3 + \right. \\
 & \left((d_2 d_3 + m k_2 + d_2 \phi) r_3^2 + (\phi d_1 + m k_1 + d_1 d_2 + d_1 d_3) r_2^2 \right) s^2 + \\
 & \left((d_1 k_2 + d_1 k_3 + k_1 d_3 + \phi k_1 + k_1 d_2) r_2^2 + (d_2 k_3 + k_2 d_3 + \phi k_2) r_3^2 \right) s + \\
 & \left. (k_1 k_2 + k_1 k_3) r_2^2 + k_2 k_3 r_3^2 \right)
 \end{aligned} \tag{A.60}$$

På svenska

Detta dokument hålls tillgängligt på Internet – eller dess framtida ersättare – under en längre tid från publiceringsdatum under förutsättning att inga extraordinära omständigheter uppstår.

Tillgång till dokumentet innebär tillstånd för var och en att läsa, ladda ner, skriva ut enstaka kopior för enskilt bruk och att använda det oförändrat för ickekommersiell forskning och för undervisning. Överföring av upphovsrätten vid en senare tidpunkt kan inte upphäva detta tillstånd. All annan användning av dokumentet kräver upphovsmannens medgivande. För att garantera äktheten, säkerheten och tillgängligheten finns det lösningar av teknisk och administrativ art.

Upphovsmannens ideella rätt innefattar rätt att bli nämnd som upphovsman i den omfattning som god sed kräver vid användning av dokumentet på ovan beskrivna sätt samt skydd mot att dokumentet ändras eller presenteras i sådan form eller i sådant sammanhang som är kränkande för upphovsmannens litterära eller konstnärliga anseende eller egenart.

För ytterligare information om Linköping University Electronic Press se förlagets hemsida <http://www.ep.liu.se/>

In English

The publishers will keep this document online on the Internet - or its possible replacement - for a considerable time from the date of publication barring exceptional circumstances.

The online availability of the document implies a permanent permission for anyone to read, to download, to print out single copies for your own use and to use it unchanged for any non-commercial research and educational purpose. Subsequent transfers of copyright cannot revoke this permission. All other uses of the document are conditional on the consent of the copyright owner. The publisher has taken technical and administrative measures to assure authenticity, security and accessibility.

According to intellectual property law the author has the right to be mentioned when his/her work is accessed as described above and to be protected against infringement.

For additional information about the Linköping University Electronic Press and its procedures for publication and for assurance of document integrity, please refer to its WWW home page: <http://www.ep.liu.se/>